Design of Synthetic Cell Division System

（人工細胞分裂システムの設計）

Fei Hao

June 2014

Graduate School of Materials Science

Nara Institute of Science and Technology (NAIST)

Contents

Chapter 1: General introduction

1.1 Biomembranes

Biomembranes mainly composed with various kinds of lipids as the boundary separates life from the non-living enviroments, but allows materials or energy exchange between them as a permeable barrier. Biomembranes are created by the lipid self-assemby through noncovalent interactions and form bilayer structures. In the membranes, lipid molecules relocate themselves in a various ways as shown in Figure 1-1.[1]

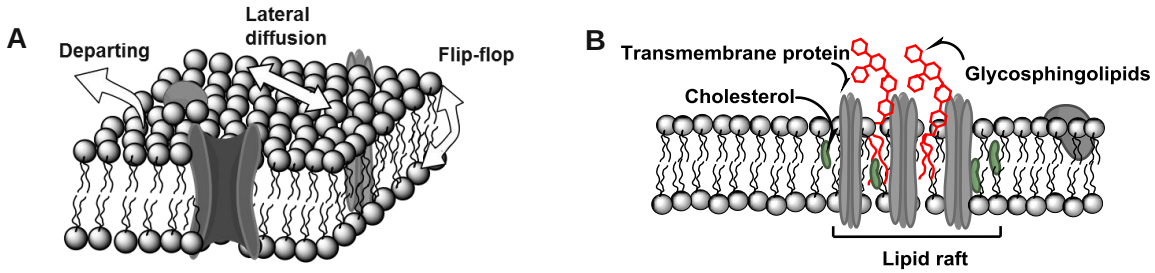

Figure 1-1. (A) Biomembrane composed of lipids and the lipids movemts in different way;[1] (B) Lipids raft structure in biomembrane.[2]

Lipid molecules with amphiphilic structures expose their polar head groups to the aqueous phase and orient their hydrophobic chains inwardly adjacent to each other. Lipids can lateraly drift in the bilayer, or flip-flop from one layer to another layer, or might depart from the bilayer altogether depending on lipid structure and conditions (Figure 1-1 (A)). If membranes are composed of two or more kinds of lipids, it is possible that one kind of lipids will segregate into a domain. In biomembranes including various kinds of lipids, there are domains enriched in cholesterol, sphingolipids and a kind of proteins named caveolins that play a role inducing budding formation. Such a domain so-called lipid raft[2] has been implicated in signal transduction and membrane trafficking pathways (Figure 1-1 (B)).[3]

1.1.1 Cellular membrane trafficking

In a biological system, the inter- and intra-cellular transport of important bioactive molecules and signals are performed through incupsulating into the vesicles. This is the basic communication mechanism between a cell and another cell or in intracellular enviroments. The vesicles transport, which is a main pathway of memebrane trafficking, supplies various organelles with appropriate proteins and lipid composition. Thus the transport of proteins, lipids and signaling molecules to plasma membrane and cytosol is achieved.[4] Importance of intracellular transport at the level of organ physiology is also highlighted, because numerous mutations in components of vesicular machinery lead to disease in humans.[5]

One of the representations in the steps of membrane trafficking is illustrated in Figure 1-2.[6] The trafficking process can be divided into four essential stages as follows; (1) budding, (2) movement, (3) tethering and (4) fusion (Figure 1-2).[6] These stages regulated by protein ensure that a daughter vesicle with information was delivered from the donor compartment into the acceptor membrane. Then the information is transferred into the acceptor compartment by fusion of daughter vesicles with acceptor membrane. At the initial stage, a kind of membrane coat protein is immobilized in a special region on the membrane surface through specific reconginition interactions. Secondly, transmembrane cargo protein and cargo receptor protein in the membrane assemble into the region enriched with the coat proteins. After that, a budding structure grows through the interactions among some kinds of coat proteins. A daughter vesicle is peeled off from the donor membrane, when the neck between the budding vesicle and the donor membrane is severed either by direct action of coat proteins or by accessory proteins. Then the generated vesicle moves towards the receptor membrane by diffusion, or by

the aid of a cytoskeletal track. Finally the vesicle becomes tethered to the acceptor membrane by the combination of a GTP bound Rab and a tethering factor. The fusion of the vesicle with the acceptor membrane is associated with vesicle-associated SNARE (v-SNARE). The v-SNARE on the acceptor membrane assembles into a four-helix bundle (trans-SNARE complex) to drive the membrane fusion and delivery of the cargo.

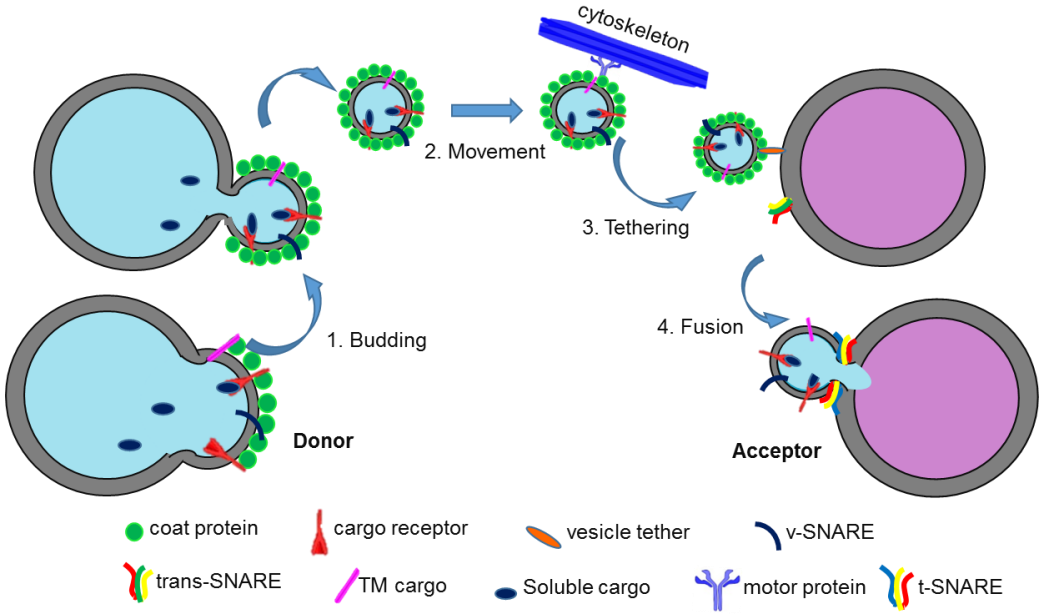

Figure 1-2. The four essential steps in vesicle transport. (1) Budding: coat proteins are recruited onto the donor membrane to induce the formation of a vesicle. (2) Movement: the vesicle moves toward the acceptor compartment by diffusion or at the aid of a cytoskeletal track. (3) Tethering: tethering factors work in conjunction with Rab GTPases to tether the vesicle to their acceptor membrane. (4) Fusion: due to the formation of a four-helix bundle (trans-SNARE complex) vesicle-associated SNARE on the acceptor membrane.[6]

1.1.2 Biomembrane division induced by membrane coat proteins

To illustrate the mechanism of biomembrane division, a kind of biomembrane models was introduced in Figure 1-3. During the formation of new vesicles from the donor membrane, coat protein complexes (CPC) mediated membrane budding and selective incorporation of soluble cargo into the generated vesicles.[7] Those CPC that are

supermolecular assemblies of proteins change the flat membrane patches into round budding structure, leading to the transport vesicles peel off from the donor membrane. There are two protein heterodimers that form the coat complex. These proteins are Sec23p-Sec24p heterodimer and Sec13p-Sec31p heterotetramer. They are proposed as coat protein complex-II (COPII).[9] Identification and characterization of COPII have been a greatest achievement in understanding budding process.[8] The core COPII components are the small Ras-like GTPhase Sar1p, the Sec23p-Sec24p subcomplex and Sec13p-Sec31p subcomplex.[9] In Figure 1-3, a guanine nucleotide activates the Sar1-GDP into Sar1-GTP and results in the Sar1-GTP anchored into the membrane bilayer.[10] This causes the immobilization of adaptor protein complex Sec23-Sec24 through interactions between Sar1-GTP and Sec23. Sec24 interacts with soluble cargo through the cargo receptors as a bridge or transmembrane cargo. Then the Sar1—Sec23-Sec24-cargo complex binds to a Sec13-Sec31 complex, and the self-assembly of Sec13-Sec31 complexes connects the two Sar1—Sec23-Sec24-cargo complexes. Finally a coat oligomerization cargo is formed due to the self-assembly of Sec13-Sec31 complexes. Sar1 was displaced by both cargo- and Sec31-mediated stimulation of GTP-activating-protein activity of Sec23. The budding structure is formed through the activity of Sar1 that is bound to the concave face of Sec23-Sec24. Finally, fission can be achieved by the ring of newly recruited Sar1-GTP molecules due to the formation of a kind of rigidity scaffolds with high curvature.[11]

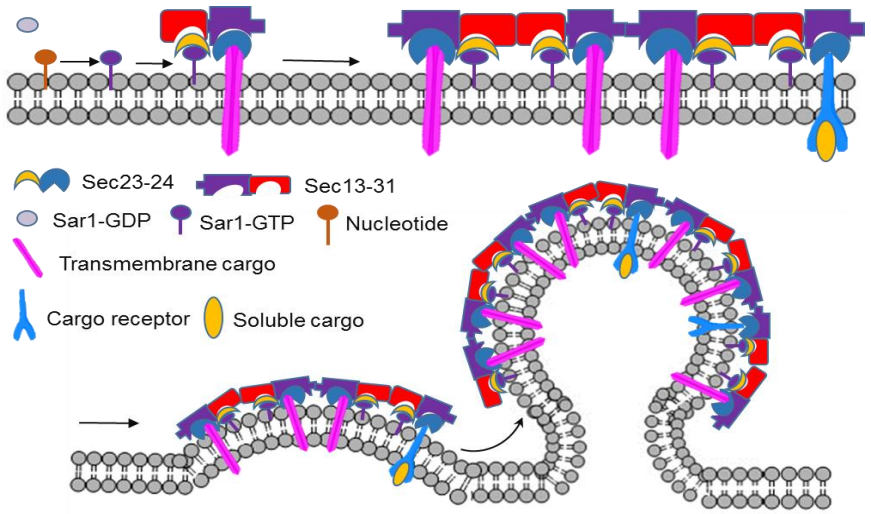

Figure 1-3. Unifying model for COPII cage assembly and budding and selective incroporation of soluble cargo was mediated by the COPII.[8]

1.2 Artificial biomembranes

1.2.1 Liposomes

Lipid vesicles called liposomes with shells composed with bilayer membranes are closed, hollow spheres as shown in Figure 1-4. Since the structure of liposomes has first clarified by transmission electron microscopy in 1965 by Bangham and his coworkers,[12] their discovery led to extensive researches on biomembrane mimics using liposomes. Recently, liposome-related researches have expanded to chemical, biochemical, physicochemical and biophysical fields.[13] However, until 1976, it is believed that lipid bilayer vesicles can be only prepared by natural lipids, such as phospholipids and glycolipids. In 1977, however, Kunitake and Okahata demonstrated that a synthetic lipid, didodecyldimethylammonium bromide, forms lipid bilayer vesicles like liposome.[14] Up to the present time, huge numbers of bilayer forming synthetic lipids have been prepared, and many kinds of functional lipids have been developed.

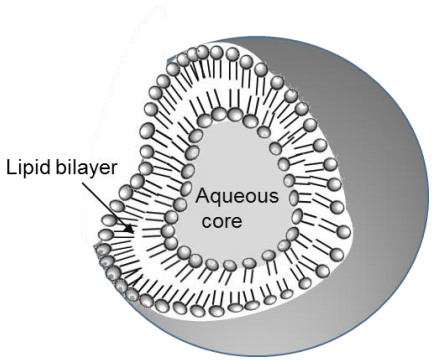

Figure 1-4. Schematic image of liposome structure.

The following vesicle types are commonly described depending on the size; small unilamellar vesicles (SUVs) with diameters of 30–100 nm, large unilamellar vesicles (LUVs) with diameters of 100–200 nm, and giant unilamellar vesicles (GUVs) ranging from 1 to 100 μm. Now liposomal membranes formed by natural lipids or synthetic lipids are widely employed as biomembrane models in order to simulate biomembrane process or to construct artificial cells.

1.2.2 Phase transition behavior of liposomes

Liposomal membranes exhibit thermotropic phase transition behavior. When temperature is lowered, the lipid bilayer undergoes a highly cooperative disorder-to-order transition of lipids packing (Figure 1-5). Such transition temperature is called phase transition temperature (T_m). The disordered bilayer, called liquid crystalline state, expands laterally with diverse gauche conformations of carbon chains packing above T_m. When temperature is below T_m, the diverse gauche conformations of carbon chains undergo transition of rigid linear all-trans chains packing to give ordered structure called gel state, in which carbon chains are in fully extended.[16]

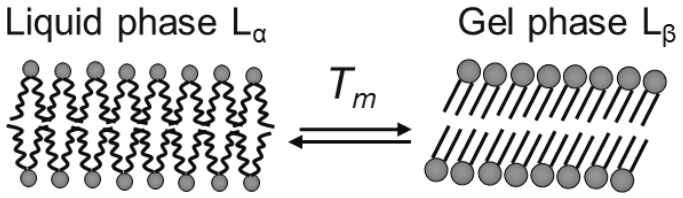

Figure 1-5. Thermotropic phase transition of bilayer membrane formed by phospholipid.[15]

A kind of thermal analysis methods, differential scanning calorimetry (DSC), is well established in the liposomes researches, and is most frequently used to evaluate the phase behavior of lipids membranes. From the DSC measurements, information on lipid packing, membrane fluidity, and drug-liposome interactions can be obtained.[17]

1.2.3 Phase separation behavior of liposomes

Liposomes composed of more than two kinds of lipids experience phase separation due to assembly of lipid domains with different lipid composition. Phase separation is induced by external stimuli such as temperature change,[18] electrostatic interactions,[19] or interaction of macromolecules such as polymers[20] and membrane proteins[21]. Figure 1-6 shows that phase separation of liposomes formed by binary lipids is triggered by diverse stimuli.[1] Phase separation of lipids membrane usually mentions membrane functions, such as membrane deformation, and membrane division and fusion.[22] Therefore, much attention has been paid for phase separation behavior of liposomal membranes to understand dynamic membrane processes.

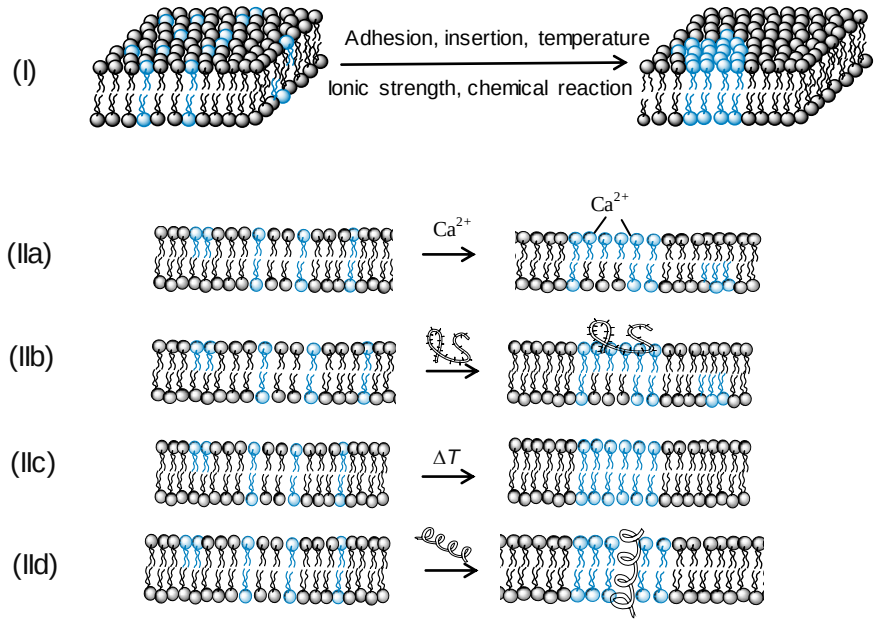

Figure 1-6. Types of phase separation in binary lipid membrane. I) Phase separation of two lipids in a lateral manner; II) various external effects leading to different modes of phase separation: a) lateral phase separation induced by ion complexation, b) vertical phase separation induced by the adsorption of hydrophilic polymers, c) lateral phase separation induced by temperature, and d) lateral phase separation induced by incorporation of hydrophobic polymers.[1]

1.2.4 Application of liposomes to artificial membrane division

Up to the present time, there are several published works on artificial membrane division systems. These studies can be divided into two categories depending on triggers for budding and fission (Table 1-1). In the former category, the membrane fission was initiated by changing physical conditions around vesicles, such as ionic strength affecting osmotic pressure[23] and temperature.[24] Such physical conditional changes induced the fission mainly through increasing surface area of external monolayer or reducing the volume of vesicles. The second category uses external molecules as triggers for the budding/fission. The triggers include metal ions,[25] detergents,[26] membrane lipid precursor,[27] peptide,[28] membrane protein.[29]

Table 1-1. Artificial membrane division systems reported previously.

Category	Trigger	Brief description
Physical conditional change	Osmotic pressure increase: addition of sorbitol outside vesicles[23b]	Area-to-volume ratio of vesicles is changed by water loss, reducing the inner volume and providing excess external membrane area, which leads to budding of vesicles.
	Temperature increase [24d]	Increasing of temperature expands the outer surface area of vesicles. The difference in surface area between outer and inner layer of vesicles causes the budding and fission
External molecule as a trigger	Metal ions: La^{3+} and Gd^{3+} [25a]	La^{3+} and Gd^{3+} located around the outer layer of vesicles change the lateral compression pressure of membrane. Such change induces formation of spontaneous curvature for fission.
	Detergents: Triton X-100 and Brij 98[26a]	Detergent molecules destabilize the bilayer membrane by inserting into the vesicles through hydrophobic interactions. Such destabilization of membrane causes budding and fission.
	Membrane lipid precursor: lysophos-phatidylcholine (lyso-PC)[27]	Lyso-PC insertes into the outer layer membrane to decrease the Gibbs free energy of the system. Then, shape change of the vesicles occurs until the elastic energy of vesicles became to minimum.
	Peptide: positively charged peptide WLFLLKKK (peptide-1)[28b]	Peptide-1 binds to the surface of membrane which increases the area of outer layer membrane. The difference in surface area between outer and inner layer induces budding and fission.
	Membrane protein: Phospholipase A2[29b]	Accumulation of enzymatic hydrolysis products perturbs lipid packing around the protein bound domain, and leads to an increase in free energy. To decrease the energy, the budding and fission of membrane happen.

1.3 Nonbilayer structures

The ability of hydrated lipids to adopt a variety of phases in addition to the bilayer phase is well known, and the behavior is called lipid porymorphism.[30] In other words, lipid membrane structures are governed by the concept of lipid shape−aggregate structure relationship,[33] as schematically illustrated in Figure 1-7.[34] The class A lipids with inverted conical shape forms a structure with high positive curvature such as micelles. The class B lipids with cylindrical shape such as phosphatidylcholine preferentially form bilayer structures. On the other hand, The class C lipids with conical shape such as phosphatidylethanolamine favors to construct nonbilayer structures with high negative curvature, such as the inverted hexagonal (H_{II}) phase composed of extended inverted micelles. Another nonlamellar structure is the inverted cubic (Q_{II}) phase as shown in Figure 1-8,[35] which is considered to locate between lipid bilayer and H_{II} phase.[36]

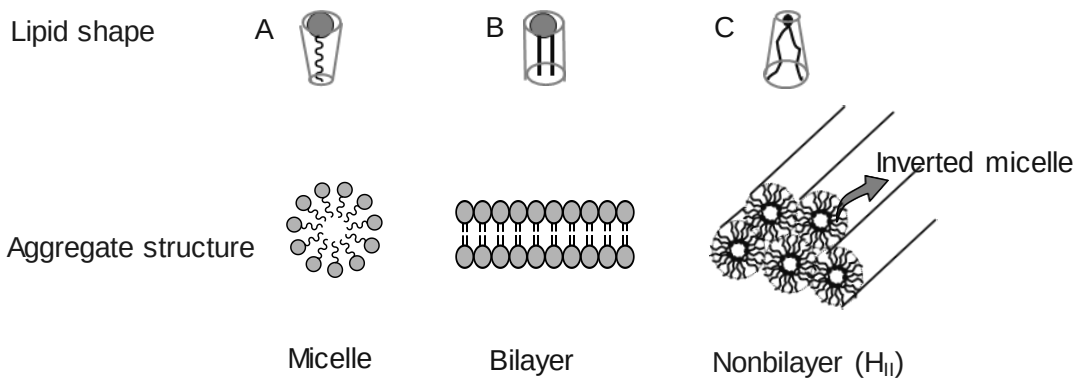

Figure 1-7. Concept of lipid shape−aggregate structure relationship.[34]

The nonbilayer structures are not so familiar as compared with bilayer structures, however the formaer structures have been recognized to be of functional importance in biomembrane system.[31] Earlier studies found that the mciroorganisms, such as *Acholeplasma laidlawii* and *Clostn'dium butyricum*, adopted bilayer or nonbilayer structures by changing the amounts of bilayer and nonbilayer forming lipids in their membranes in response to the environments.[32]

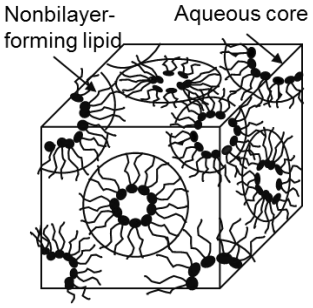

Figure 1-8. Inverted cubic phase (Q_{II}).[35]

1.3.1 Roles of nonbilayer structures in biological system

A lot of biological membranes contain a substantial amount of nonbilayer forming lipids. The findings, that the nonbilayer forming lipids extracted from biomembranes form the nonbilayer aggregates such as lipidic particles under physiological conditions, strongly suggest significant roles of nonblilayer structures in dynamic biomembrane processes.[37]

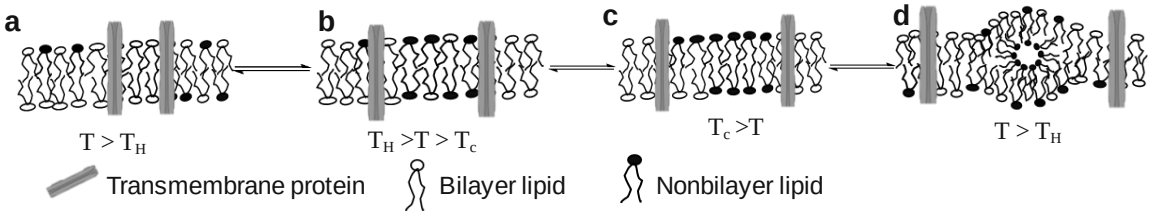

Figure 1-9. Schematic representation of the phase separation in biomembranes accompanying with formation of nonbilayer structure during cooling process.[38]

One of the examples of nonbilayer structures formed in biomembrane ststem was shown in Figure 1-9.[38] The transmembrane protein molecules were inserted in the bilayer membrane formed by the mixture of bilayer and nonbilayer forming lipid. Above the the transition temperature from liquid crystalline phase to inverted hexagonal

phase for pure nonbilayer forming lipid (T_H), there is no specific interactions between the proteins and lipids, and two kinds of lipids diffuse homogeneously to form a fluid bilayern (Figure 1-9 a). Upon cooling to the temperature between T_H and the phase transition temperature of mixed lipids membrane from liquid-crystalline to gel phase (T_c), the nonbilayer forming lipid molecules segregate to form lipid domains (Figure 1-9 b). Below T_c, the intrisic proteins and lipids are excluded from the gel phase (Figure 1-9 c). When the temperature is increased above T_H , the domain enriched with the nonblilayer forming lipid has a tendency to form the nonbilayer structures, such as inverted micelles or extended H_{II} phase, leading to increase in permeability of bilayer membrane.

Another good example on the roles of nonbliayer structure in biological activity is relative to cell division.[39] In this study, a kind of cyclic peptide coupled with fluoresence-labled streptavidin was employed to stain nonbilayer forming lipid, phosphatidylethanolamine, to mointor the localization of nonbilayer forming lipid molecules in the division of Chinese hamster ovary cells. They found that nonbilayer forming lipid extremely aggregated at the cleavage furrow during the late telophase of cytokinesis. The results suggest that the redistribution of membrane phospholipids is a crucial step for cytokinesis, and redistribution of nonbilayer forming lipid at the cleavage furrow especially plays key roles in successful cell division.

1.3.2 Nonbilayer structures in artificial biomembranes

It is well known that naturally occuring nonbilayer forming lipids play important roles in cell fusion.[40] To clarify the biofunctional significance of nonbilayres in biomembranes, liposomes containing nonbilayer forming lipids have been used as biomembrane models. It has been confirmed by ^{31}P-NMR measurements that nonbilayer

structures appeared at jointing points connecting two bilayer membranes as intermediates in membrane fusion.[42] In this study oleic acid and glycerol monooleate were incorporated into phospholipid bilayers. These lipids induced fusion of biomembrane, and showed a well-definded transition from bilayer phase to inverted hexagonal phase in the presence of Ca^{2+} ions. On these grounds, it has been proposed that the fusion event proceeds through the following stages as shown in Figure 1-10;[41] aggregation of proteins to produce areas of protein free lipid bilayer, which subsequently make contact (step 1), formation of intermediate nonbilayer structrue with inverted micelles derived from the outer monolayers contacting region (step 2) and transformation of the nonblilaer structure to bilayers structure to complete the fusion process (step 3). The presence of Ca^{2+} ions was significant for each stage, because Ca^{2+} ions induced the aggregation of proteins and membrane-membrane contact.[43]

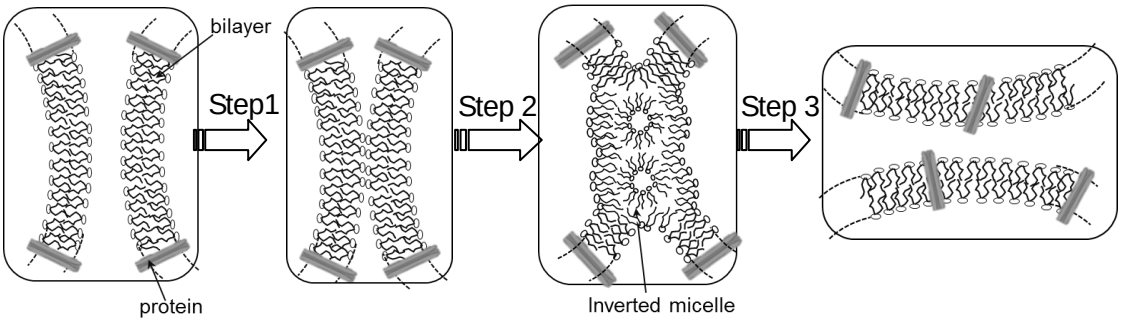

Figure 1-10. Proposed mechanism of membrane fusion.[41]

According to the concept of lipid s hape−aggregate structure relationship, lipid packing shape is not only determined by the chemical structure of lipid molecule but also by environmental factors, such as bound divalent cations[44] and hydration.[45] For example, binding of Ca^{2+} ions to negatively charged lipids with a large cross-sectional area of head group leads to decrease in headgroup area through charge nutrarization and followed dehydration. As a result, the lipid packing shape in the membrane changes

from sylindorical to conical shape to stabilize nonbilayer phase.[42]

Design of nonbilayer structures using synthetic peptide lipids has been reported by our group. The peptide lipids are biomimetic materials hybridizing the structural characteristics of bilayer forming lipids with those of peptides, having the following tripartite structure; a polar head moiety, a hydrophobic double-chain segment, and an amino acid residue interposed between them.[46] In general, peptide lipids having ionic head moiety form morphologically stable bilayer membrane due to formation of hydrogen-belt domain among the amino acid residues. However, nonionic peptide lipid having a quinoyl moiety, QC_5Ala2C_{14}, forms nonbilayer structure as schematically shown in Figure 1-11.[47] In this lipid, the headgroup area is decreased through hydrogen bonding interactions among the hydroxyl groups on the head moieties. The nonbilayer stucture composed of inverted micellar aggregate with inner aqueous compartments was visualized by negative stainning electron microscopy.[47] The nonbilayer structure was further analized by small angle X-ray diffraction measurements to belong to face-centered cubic phase.[48]

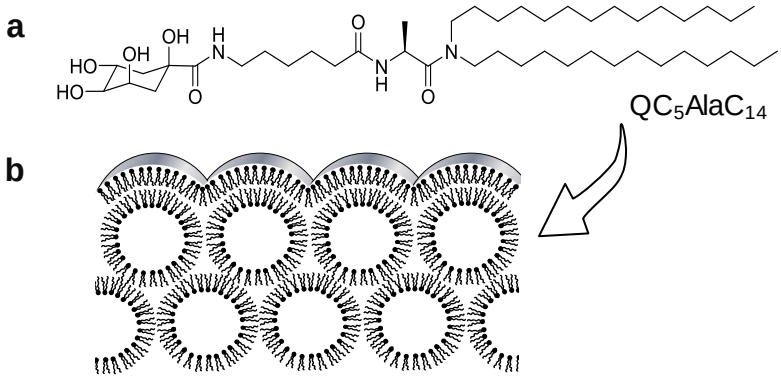

Figure 1-11. Structure of nonbilayer forming peptide lipid (a) and schematic illustration of nonbilayer aggregate (b).[47]

1.4 **Purpose of this study**

Several interesting systems on the division of artificial cell membranes have been reported as mentioned above. Most of the reports mainly focus on understanding the dynamic behavior from physical viewpoints, however the membrane division mechanism has not been clarified at molecular level.

In this study, I firstly investigated on step-by-step analysis of dynamic membrane division process induced by a hydrophilic chemical signal in order to clarify the mechanism at molecular level. Secondly, I focused on the participation of nonbilayer forming lipid, or a hydrophobic chemical signal, on synthetic cell division. Nonbilayer structures play important roles in biomembrane process as memtioned above. While the participation of various nonbilayer-forming lipids in membrane fusion processes has been clarified,[49] there are few reports of reverse-division behavior induced by such lipids. So I evaluated the potential of nonbilayer forming peptide lipid having quinoyl moiety as a trigger of liposomal membrane division. These approaches would provide us a useful guidepost how to control the dynamic membrane process in general.

This doctoral thesis consists of the following four chapters. Chapter 1 is the general introduction. In this chapter, research backgrounds and propose were discribed.

In Chapter 2, division behavior of liposomal membrane formed by a phospholipid and a synthetic cationic lipid induced by a hydrophilic chemical signal, pyranine, was evaluated in detail. The membrane division process in this system was able to analyze by separating into the following three stages; binding of anionic chemical signal onto the positively charged membrane surface, the signal binding induced phase separation of liposomal membrane, and budding and followed fission. In the initial stage, signal binding to the polar head moiety of cationic lipids in the membrane was

thermodynamically and kenetically analyzed by fluorescence spectroscopy, and formation of 1:4 complex of chemical signal with cationic lipids through electrostatic interactions was confirmed. The formation of signal–lipid complex gave a perturbation of lipid distribution in liposomal membrane to induce phase separation forming lipid domains as evaluated by differential scanning calorimetry and fluorescence microscopy. Then the membrane budding selectively happened from the lipid domain, in which the chemical signal bound to the cationic lipids to form the ion cluster developed on the membrane surface. Control of lipid phase separation and membrane budding was successfully achieved by tuning ionic strength of aqueous solution. Finally, fission of liposomal membrane was observed from the budded vesicles in moderate probability. The present dynamic membrane process was monitored by fluorescence microscopy in both static and video mode. The physicochemical factors which influence in the membrane dynamics were clarified.

In Chapter 3, division behavior of liposomal membrane formed by a phospholipid and a nonbilayer forming peptide lipid was investigated. Firstly, the nonbilayer structure formed by the nonionic peptide lipid having quinoyl moiety was characterized in detail by cryogenic transmission electron microscopy (TEM) and TEM tomography. In the presence of the nonbilayer forming lipid in liposomal membrane, dynamic membrane division was specifically observed by optical microscopy in phase contrast and fluorescence mode. The membrane division was induced by formation of phase separated domains in membrane, probably nonbilayer forming lipid-rich and phosphorlipid-rich domain, as confirmed by differential scanning calorimetric measurements. In addition, I found that the membrane division behavior was sensitive to temperature, which influenced in the phase state of lipid membrane. On these ground,

the mechanism of present membrane division system concerning nonbilayer forming lipid was proposed.

Chapter 4 is the general conclusions. I summarized the results of this research and discussed future perspectives especially focusing on possibilities of synthetic cell division for application to molecular communication, a new communication paradigm in information and communication technology.

1.5 References

(1) Binder, W. H.; Barragan, V.; Menger, F. *Angew. Chem. Int. Ed.* **2003,** *42*, 5802-5827.

(2) Pike L. J. *J. Lipid Res.* **2006,** *47*, 1597-1598.

(3) Anderson, R. G. W.; Jacobson K. *Science* **2002,** *296*, 182-12825.

(4) Spang, A. *Cell. Mol. Life Sci.* **2008,** *65*, 2781-2789.

(5) Ohno, H. *J. Biochem.* **2006**, *139*, 941-942.

(6) Boyd, C.; Hughes, T.; Pypaert, M.; Novick, P. *J. Cell Biol.* **2004,** *167*, 889-901.

(7) Kirchhausen, T. *Nat. Rev. Mol. Cell Biol.* **2000,** *1*, 187-198.

(8) Gurkan, C.; Stagg, S. M.; LaPointe, P.; Balch, W. E. *Nature Rev. Mol. Cell Biol.*, **2006,** *7*, 727-738.

(9) Bonifacino, J. S.; Glick, B. S. *Cell* **1994,** *116*, 153-166.

(10) Barlowe, C.; Schekman, R. *Nature* **1993,** *365*, 347-349.

(11) (a) Edeling, M. A.; Smith, C.; Owen, D. *Nature Rev. Mol. Cell Biol.* **2006,** *7*, 32-44; (b) Conner, S. D.; Schmid, S. L. *Nature* **2003,** *422*, 37-44.

(12) Bangham, A. D.; Standish, M. M.; Watkins, J. C. *J. Mol. Biol.* **1965**, *13*, 238-252.

(13) (a) Baumgart, T. S.; Hess, T.; Webb, W. W. *Nature* **2003**, *425*, 821-824; (b) Veatch, S. L.; Keller, S. L. *Phys. Rev. Lett.* **2005**, *94*, 148101-148105; (c) Lasic, D. D.; Joannic, R. B.; Keller, C.; Frederik, P. M.; Auvray, L. *Adv. Colloid Interface Sci.* **2001**, *89*, 337-349.

(14) Kunitake, T.; Okahata, Y. *J. Am. Chem. Soc.* **1977**, *99*, 3860-3861.

(15) Pentak, D.; Sulkowski, W. W.; Sulkowska, A. *J. Therm. Anal. Cal.* **2008,** *93*, 471-477.

(16) Wolf, D. E. *Curr. Top. Membr.* **1994,** *40*, 143-165.

(17) Kevin, M. G.; Duncan, T.; Craig, Q. Q. M. in *Liposomes,* eds. by Torchilin, V. P.;

Weissig, V. Oxford University Press, Oxford, **2002,** pp 79-103.

(18) Veatch, S.; Keller, S. *Biophys. J*. **2003**, *85*, 3074-3083.

(19) Agafonov, A. V.; Gritsenko, E. N.; Shlyapnikova, E. A.; Kharakoz, D. P.; Belosludtseva, N. V.; Lezhnev, E. I.; Saris, N. L.; Mironova, G. D. *J. Membrane Biol*. **2007,** *215*, 57–68.

(20) Tsafrir, I.; Sagi, D.; Arzi, T.; Guedeau-Boudeville, M. A.; Frette, V.; Kandel, D.; Stavans, J. *Phys. Rev. Lett.* **2001**, *86*, 1138-1141.

(21) Takahashi, H. *Mol. Mem. Biol*. **1996**, *13*, 233-240.

(22) (a) Baumgart, T. S.; Hess, T.; Webb, W. W. *Nature* **2003**, *425*, 821-824; (b) Hui, S. W.; Stewart, T. P.; Boni, L. T.; Yeagke, P. L. *Scince***, 1981,** *212*, 921-923.

(23) (a) Ohnishi, S. I.; Ito, T. *Biochem.* **1974,** *13*, 881-887; (b) Yanagisawa, M.; Imai, M.; Taniguchi, T. *Phys. Rev. Lett.* **2008**, *100*, 148102-148106; (c) Meghan Andes-Koback, M.; Keating, C. D. *J. Am. Chem. Soc.* **2011**, *133*, 9545-9555.

(24) (a) Leirer, C.; Wunderlich, B.; Myles, V. M.; Schneider, M. F. *Biophys. Chem.* **2009,** *143*, 106-109; (b) Veatch, S. L.; Keller, S. L. *Biophys. J*. **2003,** *85*, 3074-3083; (c) Baumgart, T.; Hess, S. T. Webb, W. W. *Nature* **2003,** *425*, 821-824; (d) Kas, J.; Sackmann, E. *Biophys. J*. **1991,** *60*, 825-844.

(25) (a) Tanaka, T.; Tamba, Y. Masum, S. M.; Yamashita, Y.; Yamazaki, M. *Biochim. Biophys. Acta* **2002,** *1564*, 173-182; (b) Menger, F. M.; Balachander, N. *J. Am. Chem. Soc.* **1992-12***4*, 5862-5863.

(26) (a) Staneva, G.; Angelova, M. I.; Koumanov, K. *Chem. Phys. Lipids*, **2004**, *129*, 53-62; (b) Nomura, F.; Nagata, M.; Inaba, T.; Hiramatsu, H.; Hotani, H.; Takiguchi, K., *Proc. Natl. Acad. Sci. U.S.A.* **2001,** *98*, 2340-2345. (c) Sato, Y.; Yasuhara, K.; Kikuchi, J.; Sato, T. N. *Sci. Rep*. **2013,** *3*, 3475-3480.

(27) Takakura, K.; Sugawara, T. *Langmuir* **2004,** *20*, 3832–3834.

(28) (a) Hanczyc, M. M.; Fujikawa, S. M.; Szostak, J. W. *Science* **2003,** *302*, 618-622; (b) Yamashita, Y.; Masum, S. M. Tanaka, T.; Yamazaki, M. *Langmuir* **2002,** *18*, 9638-9641.

(29) (a) Jeanne, C.; Stachowiak, J. C.; Hayden, C. C.; Sasaki, D. Y. *Proc. Natl. Acad. Sci. USA*, **2010,** *107*, 7781-7786; (b) Staneva, G.; Angelova, M. I.; Koumanov, K. *Chem. Phys. Lipids* **2004,** *129*, 53-62.

(30) de Kruijff, B. D. *Curr. Opin. Chem. Biol.* **1997,** *1*, 564-569.

(31) (a) Etienne, F.; Spector, D.; Brot, N.; Weissbach, H. *Biochem. Biophys. Res. Commun.* **2003,** *300*, 378-382; (b) Cornell, R. B.; Arnold, R.S. *Chem. Phys. Lipids* **1996,** *81*, 215-227.

(32) de Kruijff, B. D. *Nature* **1987,** *329*, 587-588.

(33) Cullis, P. R.; de Kruijff, B. D. *Biochim. Biophys. Acta* **1979,** *559*, 399-420.

(34) Laan, E. B.; Killian, J. A.; de Kruijff, B. D. *Biochim. Biophys. Acta* **2004,** *1666*, 275-288.

(35) Kirk, G. L.; Gruner, S. M.; Stein, D. L. *Biochemistry* **1984,** *23*, 1093-1102.

(36) Grune, S. *J. Phys. Chem.***1989,** *93*, 7562-7570.

(37) (a) Burnell, E.; Alphen, V. L.; Verkleij, A.; de Kruijff, B. D. *Biochim. Biophys. Acta* **1980,** *597*, 492-501; (b) Cullis, P. R.; de Kruijff, B. D.; Hope, M. J.; Nayar, R.; Rietveld, A.; Verkleij, A. J. *Biochim. Biophys. Acta* **1980,** *600*, 625-63.

(38) Quinn, P. J.; Williams, W. P. *Biochim. Biophys. Acta* **1983,** *737*, 223-266.

(39) Emoto. K.; Kobayashi, T.; Yamaji A.; Aizawa, H.; Yahara, I.; Inoue, K.; Masato, Umeda, M. *Proc. Natl. Acad. Sci. USA,* **1996,** *93*, 12867-12872.

(40) (a) Cullis, P. R.; Hope, M. J. *Nature*, **1978**, *271*,672-674; (b) Verkleij, A. J. *Biochim.*

Biophys. Acta **1984**, *779*, 43-63; (c) Mueller, A.; O'Brien, D. F. *Chem. Rev.*, **2002**, *102*, 727-757; (d) Tenchov, B.; Koynova, R. *Eur. Biophys. J.*, **2012**, *41*, 841-850.

(41) Cullis, P. R.; Hope, M. J. *Nature* **1978,** *271*, 672-674.

(42) (a) Verkleij, A. J.; Mombers, C.; Gerritsen, W. J.; Leunissen, L.; Cullis, P. R. *Biochim. Biophys. Acta* **1979,** *555*, 358-361; (b) Kuzmin, P. I.; Zimmerberg, J.; Chizmadzhev, Y. A.; Cohen, F. S. *Proc. Natl. Acad. Sci. USA***, 2001,** *98*, 7235-7240.

(43) Poste, G.; llison, A. C. *Biochim. Biophys. Acta*. **1973,** *300*, 421-465.

(44) Cullis, P. R.; de Kruijff, B. D. *Biochim. Biophys. Acta* **1979,** *559*, 399-420.

(45) Tate, M. W.; Eikenberry, E. F.; Turner, D. C.; Shyamsunder, E.; Gruner, S. M. *Chem. Phys. Lipids* **1991,** *57*, 147-164.

(46) Murakami, Y.; Kikuchi, J. in *Bioorganic Chemistry Frontiers*, ed. by Dugas, H. Springer-Verlag, Berlin, **1991**, *Vol. 2*, pp. 73-113.

(47) Murakami, Y.; Nakano, A.; Kikuchi, J.; Takaki, T. *Chem. Lett*. **1983,** 1891-1894.

(48) Murakami, Y.; Kikuchi, J.; Takaki T.; Uchimura, K. *Bull. Chem. Soc. Jpn*. **1987,** *60*, 1469-1479.

(49) (a) Murakami, Y.; Kikuchi, J.; Takaki, T. *Chem. Lett.*, **1985**, 1899-1902. (b) Murakami, Y.; Kikuchi, J.; Takaki, T. *Bull. Chem. Soc. Jpn.*, **1986**, *59*, 515-523. (c) Pécheur, E. I.; Sainte-Marie, J.; Bienvenüe, A.; Hoekstra, D. *J. Membr. Biol.*, **1999**, *167*, 1-17; (d) Hafez, I. M.; Cullis, P. R. *Adv. Drug Delivery Rev.*, **2001**, *47*, 139-148.

Chapter 2: Synthetic cell division system: Roles of chemical signal which induce division of lipid bilayer vesicles

2.1 Introduction

In biological systems, inter- and intra-cellular communications involving membrane vesiculation are related to cellular transport and membrane components trafficking between donor and acceptor membrane.[1] A popular membrane phenomenon, budding and fission, represents the initial stage of transport vesicle formation in cellular trafficking process.[2] The membrane division mechanism has been molecularly detailed, which is initiated by the unique molecular and structural properties of coat protein complexes (CPCs) anchored on a patch in the donor membrane. These complexes include the clathrin, coat protein complex-I (COPI) and coat protein complex-II (COPII). CPCs formed a polymeric scaffold on the vesicle surface with the generation of membrane curvature and finally lead to the budding and fission.[2,3] Inspired by the dynamic membrane behavior in biological system, artificial membrane division has been widely investigated to simulate the membrane trafficking.

Since the deformation of artificial vesicles induced by a kind of chemical signal was observed by Menger and his colleagues in 1992,[4] the membrane division behavior has been demonstrated to occur under various conditions. In most of cases, giant vesicles, artificial cells with micrometer size, were widely used owing to their biologically relevant morphological properties, such as membrane division and fusion.[5] The morphological changes of giant vesicles are driven by addition of chemical signals such as membrane forming molecules,[6] membrane precursors,[7] surfactants,[8] or by changing physical conditions around the vesicles such as osmotic pressure.[9]

In order to provide a guiding principle for designing synthetic cell division systems, we need to clarify the general mechanism of membrane division at molecular level. However, most of the previous works, in which membrane division behavior was observed using giant vesicles formed by phospholipids, paid attention to explain the dynamic membrane behavior from physical viewpoints. This is very important to understand the dynamic behavior, however it seems to be difficult to answer how to design the synthetic cell division systems at a molecular level.

Recently, Dr. Zhonghua Wang in our group has found that a membrane division behavior induced by a chemical signal, pyranine.[10] She prepared giant vesicles formed by a phospholipid (DMPC) and a cationic synthetic lipid ($N^+C_3U2C_{16}$) in a molar ratio of 7:3 in aqueous media. Upon addition of fluorescent water-soluble molecule, pyranine, to the giant vesicles, she observed the membrane division via phase separation by means of differential scanning calorimetry and optical microscopic observation. However, detail mechanism of this system was unrevealed up to the present time, because of rather limited experimental data in the previous researches.

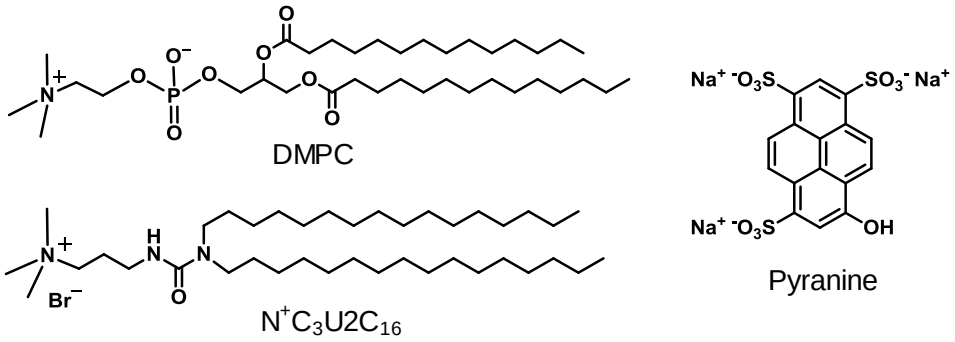

Chart 2-1. Srtuctures of liposomal membrane forming lipids and chemical signal.

So, in the present work, I picked up this division system to clarify the detail mechanism of membrane dynamics and to find a guidepost how to design artificial membrane division systems in general. Herein, I systematically analyzed the present dynamic membrane behavior by separating the following four steps; (1) the quantitative analysis for the interactions of pyranine with membrane surface, (2) the phase separation behavior induced by the signal-binding, (3) the budding of liposomal membrane, and (4) the followed fission from a mother vesicle to daughter vesicles as schematically shown in Figure 2-1.

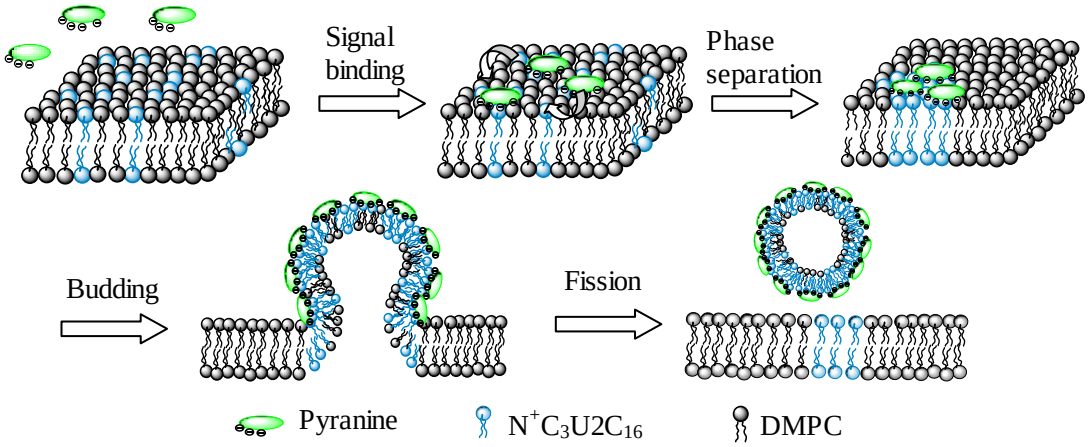

Figure 2-1. Schematic representation of the dynamic morphological changes of liposomal membrane composed of DMPC and $N^{+}C_3U2C_{16}$ as induced by pyranine.

In addition, the structures of daughter vesicles formed from the mother vesicles were not clear in the Wang's work. I thought that the reason probably comes from the preparation procedure of giant vesicles. While simple hydration method was employed in her work, an electroformation method was introduced in my work to prepare many giant vesicles that were big enough for optical microscopic observation. I herein provided clear microscopic images of daughter vesicles, and systematic experimental analysis.

Furthermore, only static microscopic images have been reported in the Wang's work.

In my work, I observed the dynamic processes by optical microscopy in both static and movie mode. As a result, the patient microscopic observation clearly revealed the whole membrane dynamics in the present membrane division system.

2.2 Experimental section

2.2.1 Materials and methods

Materials

1,2-Dimyristoyl-*sn*-glycero-3-phosphocholine (DMPC, lyophilized powder), 1,2-dipalmitoyl-*sn*-glycero-3-phosphocholine (DPPC), 1,2-dilauroyl-*sn*-glycero-3-phosphocholine (DLPC) were purchased from Avanti Polar Lipids. Trisodium 8-hydroxypyrene-1,3,6-trisulfonate (pyranine) was obtained from Tokyo Chemical Industry CO., Ltd. and the other chemicals were obtained from Wako Pure Chemical Industries, Ltd. Dihexadecylamine was synthesized by the reaction of hexadecylamine with 1-bromohexadecane in the presence of sodium carbonate and purified by recrystallization from hexane. *N*,*N*-Dihxadecyl-*N*'-(3-triemethylammoniopropyl)urea bromide ($N^{+}C_3U2C_{16}$) was prepared according to the synthetic route as shown in Scheme 2-1. Ultrapure water purified by MilliQ apparatus was used in all measurements.

Measurements

High performance liquid chromatography (HPLC) for purification of compounds was done by using a JAI Model instrument (Japan Analytical Instruments) equipped with JAIGEL-H-P columns. Nuclear magnetic resonance (NMR) spectra were taken on a JNM-ECP400 spectrometer (JEOL, Tokyo) with tetramethylsilane (TMS) as an internal standard. Fluorescence spectra were recorded on a HITACHI F-7000 spectrofluorometer. The temperature of samples was maintained using a thermoelectric

cell holder equipped with a water recycling system. The optical microscopic observations were carried out using an Olympus IX71 in phase contrast or fluorescence mode. Fluorescence images were recorded on a digital camera C11440 using a mirror filter (U-MWBV2, excitation wavelength 400-440 nm).

Phase transition behavior of liposomal membranes was evaluated by an ultra high sensitive differential scanning calorimeter (VP-DSC, MicroCal Inc.). The measurement was performed in a temperature range from 15 to 45 ℃ with a scanning rate of 0.5 ℃/min. The enthalpy change for phase transition (ΔH) from the gel to liquid-crystalline phase was determined by integrating the area of endothermic peak. The van't Hoff enthalpy (ΔH_{VH}) was also evaluated, which is equal to the amount of heat required for the cooperative units undergoing gel to liquid-crystalline phase transition. The ratio of $\Delta H_{VH} / \Delta H$ gives the cooperative unit (C.U.), which indicates the number of cooperative molecules concerning to the phase transition.

2.2.2 Synthesis of bilayer forming cationic lipid

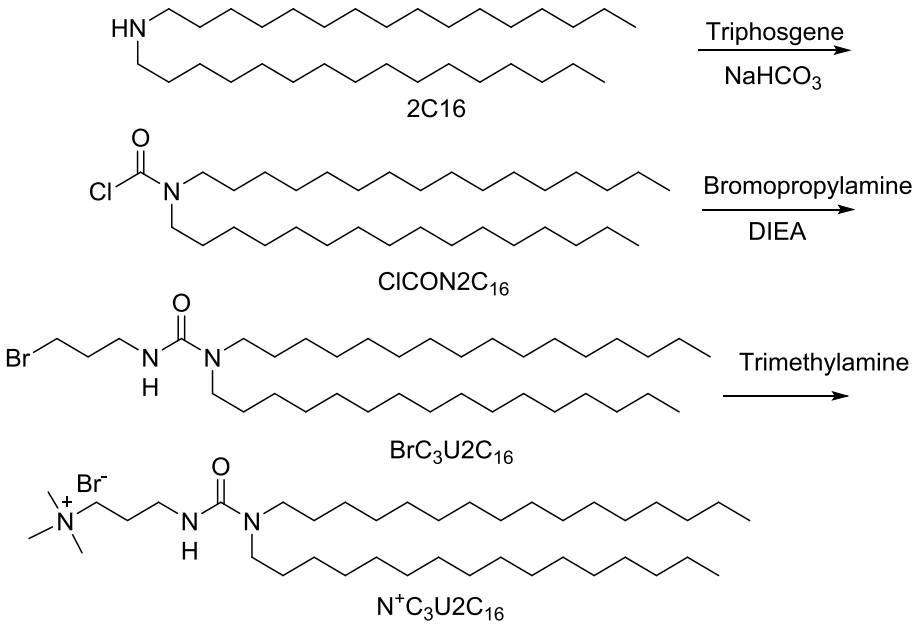

Scheme 2-1

Synthesis of N,N-dihxadecyl-1-chloroformamide (ClCON2C_{16})

Dihexadecylamine ($2C_{16}$) (2.0 g, 4.3 mmol) in dry chloroform (10 ml) was slowly dropped into dry chloroform solution (25 ml) containing triphosgene (840 mg, 2.8 mmol) and sodium hydrogencarbonate (800 mg, 9.5 mmol) on an ice bath for 1 h. The mixture was stirred for 20 h at room temperature. Then the insoluble material was filtered off and the solvent was evaporated to give the product. Yield: 190 mg (83%). This product was immediately used in the next step without purification.

Synthesis of N,N-Dihxadecyl-*N*'-(3-bromopropyl)urea *(BrC_3U2C_{16})*

Cl$CON2C_{16}$ (1.0 g, 1.9 mmol) was dissolved in dry 1,2-dichloroethane (16 ml). To the mixture was added 3-bromopropylamine (0.5 g, 2.3 mmol) in dry 1,2-dichloroethane (10 ml) including *N,N*-diisopropylethylamine (DIEA) (1.3 ml, 7.6 mmol). The solution was stirred for 30 h at 75 ℃. Then, the reaction mixture was washed with saturated aqueous NaCl, 10% aqueous citric acid, and saturated aqueous NaCl in this sequence. After evaporation of solvent, the crude product was purified by silica gel chromatography with column size of 20 mmϕ x 20 cm using ethyl acetate-hexane (1:5 v/v) as eluant. Yield: 200.0 mg (17%). TLC: R_f = 0.37 (ethyl acetate-hexane (1:5 v/v)). ^{1}H-NMR (400 MHz, $CDCl_3$, TMS): δ/ppm 0.88 [6H, t, *J*=6.6 Hz, C*H*$_3$], 1.25–1.43 [52H, m, (C*H*$_2$)$_{13}$CH$_3$], 1.52 [2H, t, NCH$_2$C*H*$_2$], 1.62 [2H, m, NCH2C*H*$_2$], 2.12 [2H, m, BrCH$_2$C*H*$_2$], 3.23 [2H, m, NC*H*$_2$], 3.68 [4H, m, NC*H*$_2$, BrCH$_2$CH$_2$C*H*$_2$], 4.47 [2H, m, BrC*H*$_2$].

Synthesis of N,N-dihxadecyl-N'-(3-triemethylammoniopropyl)urea bromide (N$^+$$C_3$U2$C_{16}$)

Gaseous trimethylamine was generated by heating of aqueous trimethylamine (30%, 150 ml) at 70 ℃, and introduced into a solution of BrC_3U2C_{16} (400 mg, 0.63 mmol) in

dry tetrahydrofuran (50 ml). After saturation of trimethylamine gas into the solution, the mixture was stirred for 6 days at 50 ℃. The crude product was purified by HPLC using chloroform as eluant. Yield: 60 mg (15%). ^{1}H-NMR (400 MHz, $CDCl_3$, TMS): δ/ppm 0.88 [6H, t, J=6.4 Hz, C*H*3], 1.25 [52H, m, $(CH_2)_{13}CH_3$], 1.51 [4H, m, $NHCH_2CH_2$], 2.15-2.09 [2H, m, CH_2CH_2NHCO], 3.23 [4H, t, J=7.5 Hz, NCH_2], 3.32 [9H, s, NCH_3], 3.39 [2H, dd, J=7.7 Hz, 5.1 Hz, CH_2NHCO], 3.89 [2H, t, J=7.7 Hz, N^+CH_2] and 5.72 [1H, t, J=5.1 Hz, N*H*]. HR-MS (TFA-Na^+, *m*/*z*, matrix: m-NBA): calcd for $C_{29}H_{82}N_3O$ ($[M]^+$), 608.6452; found, 608.6458.

2.2.3 Preparation of bilayer vesicles

Giant unilamellar vesicles (GUVs) formed with DMPC and $N^+C_3U2C_{16}$ in a molar ratio of 7:3 was prepared by electroformation method described in the reference.[11] Lipid mixture in 1 mM chloroform (10 μl) was spread and dried on a conductive indium-tin oxide (ITO) coated glass slide at room temperature to give a lipid film. Then the film was kept under reduced pressure for 1 h to remove the solvent completely. The lipid film was rehydrated in 12 mM sucrose solution (200 μl) in a chamber as shown in Figure 2-2. GUVs were allowed to grow on a temperature-controlled microscope stage for 20 min at 40 ℃ under a sine voltage (850 mV, 10 Hz).

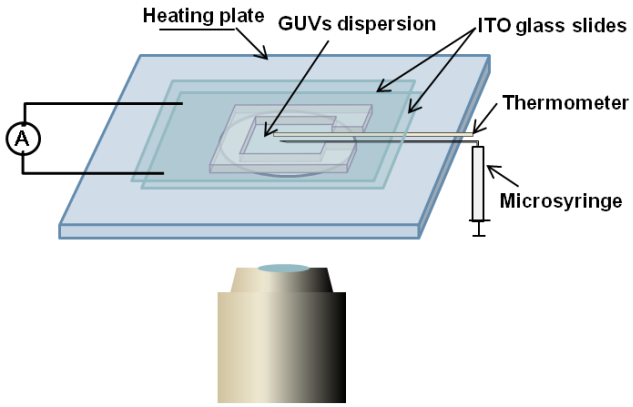

Figure 2-2. Schematic illustration of equipment for electorformation of GUVs. The chamber containing GUVs dispersion locates at the center of stage for microscopic observation.

Large unilamellar vesicles (LUVs) used for fluorescence spectroscopy were prepared as follows. Stock solutions of 10 mM DMPC in chloroform (70 μl) and 10 mM $N^{+}C_3U2C_{16}$ in chloroform (30 μl) were placed in a round-bottom flask and the solvent was evaporated and dried under reduced pressure for 3 h to give a thin lipid film. 12 mM aqueous sucrose (1 ml) was gently added to the lipid film, and the mixture was incubated on a water bath for 30 min at 40 ℃ for swelling the lipid layer. Then the mixtute was shaken by vortex mixing for 5 min to afford multi-walled vesicles. After 5 times repeating of freeze-and-thaw cycle at -196 and 40 ℃ for aqueous dispersion, the resulting aqueous vesicles were passed through the lipid vesicle extruder (LiposoFast miniextruder from Avestin) with a membrane having 100 nm diameter pore size for 20 times to form LUVs.

2.3 **Results and discussion**

2.3.1. Signal binding behavior

2.3.1.1 Thermodynamic analysis of signal binding

(a) Fluorescence spectroscopic properties of pyranine

In this work, pyranine was used as the chemical signal which induced the division of liposomal membranes. In this section, I evaluated the interactions of chemical signal with liposomal membranes by fluorescence spectroscopy.

Pyranine has been used as a pH-sensitive fluorescent molecular probe for steady-state measurements of inner aqueous phase of vesicular systems[12] and gradient proton concentration across the membranes[13] owing to its fluorescence intensity depending on the ionization of 8-hydroxyl group. Pyranine undergoes acid dissociation with pK_a of 7.40 at 25 ℃. Protonated pyranine (POH) shows an absorption maximum at 402 nm, while the conjugate base, deprotonated pyranine (PO^-), has an absorption maximum at 450 nm (Figure 2-3). When these species are excited by light at their individual absorption maxima, they give strong fluorescence at 510 nm in aqueous solutions at pH above 2. When excitation spectra are taken with emission at 510 nm, these species give the spectra very close to their individual absorption spectra.

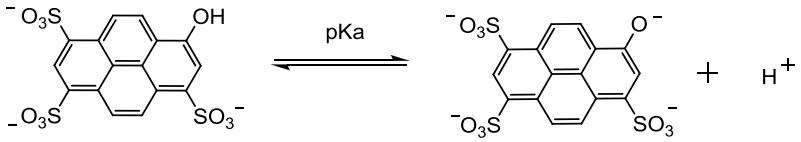

Figure 2-3: Structures of protonated and deprotonated pyranine and their absorption maxima.[13]

Since it has been reported that the pK_a^* value of pyranine in the excited state is lowered to 0.40,[15] the fluorescence with a maximum at 510 nm for POH must arise from the lowest excited state for the conjugate base of pyranine (PO^{-*}) shown as spectra d in

Figure 2-4. When the fluorescence spectra measure at pH 1.0, the emission maximum shifts to 440 nm (specra c in Figure 2-4). This emission is considered arising from the lowest excited state for the protonated species (POH*). The pertinent prototropic equilibria in an aqueous solution are shown in Figure 2-5.

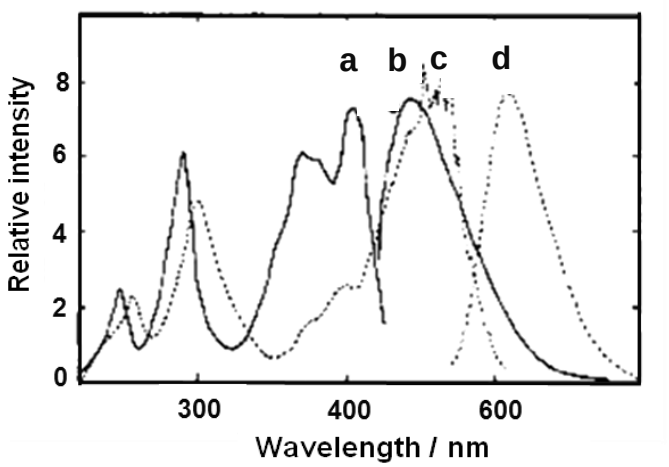

Figure 2-4. Excitation and emission spectra of 1 μM pyranine in aqueous solutions. Excitation spectra, a and c, and emission spectra, b and d, are for POH at pH 1.0 and for PO^- at pH 10.0 respectively.[14]

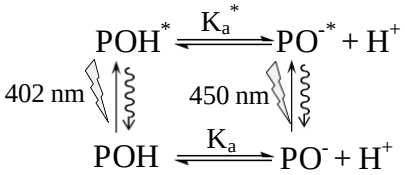

Figure 2-4. Prototropic equilibra of pyranine in aquesous solution. Excitated states are marked with asterik.

Pyranine molecules bound tightly with cationic vesicles due to the multivalent property.[10] Herein, I studied the fluorescence spectroscopy of pyranine in detail. Upon addition of liposomal membrane formed by DMPC and $N^+C_3U2C_{16}$ in a molar ratio of 7:3 at pH 6.5 and 26 ℃, the peak maximum of excitation spectra showed a drastic red shift from 402 to 450 nm, and the fluorescence intensity of protonated pyranine was

decreased (Figure 2-5). The red shift of excitation spectra indicates that protonated pyranine gradually becomes to be deprotonated species through the liposomal membrane. Fendler and his co-workers proposed that the apparent pK_a value on the cationic membrane surface was higher than that of bulk aqueous phase.[13] Thus the red shift in the excitation spectra can be attributed to the anionic pyranine species bound to the cationic lipids through the electrostatic interactions.

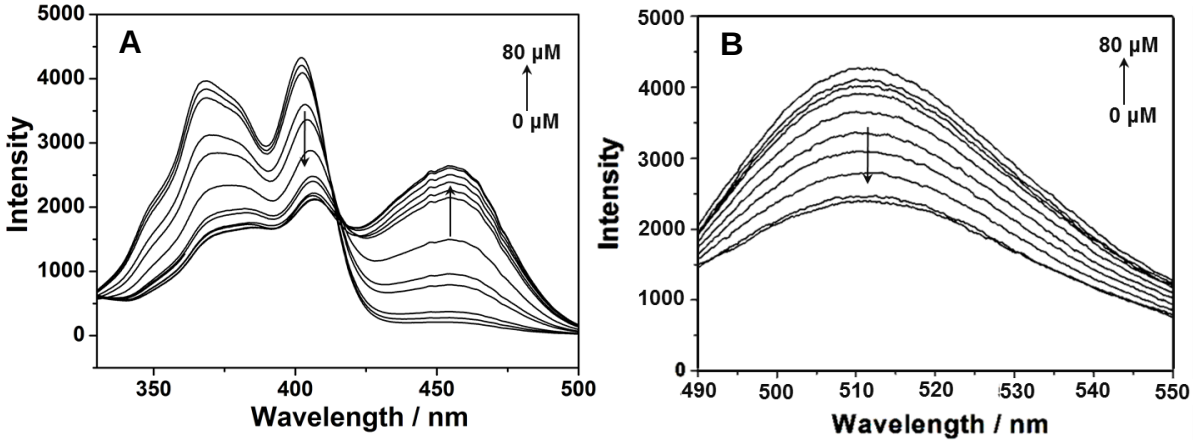

Figure 2-5. Excitation (A) and emission spectra (B) of 1 μM pyranine upon addition of LUVs formed by DMPC/$N^+C_3U2C_{16}$ (7:3) from 0 to 80 μM in 12 mM sucrose solution at pH 6.5 and 26 ℃. λ_{ex}, 402 nm; λ_{em}, 510 nm.

In order to clarify the interactions between the chemical signal and the cationic lipid on the membrane surface quantitatively, stoichiometry and binding constant for the signal-lipid complex were evaluated as follows.

(b) Fluorescence behavior of pyranine in the absence of liposomal membrane

Firstly, acid dissociation behavior of hydroxyl group of pyranine was observed by measuring the pH dependence of fluorescence intensity in water. As shown in Figure 2-6, the intensity of excitation spectra at 402 nm was decreased with an increase in pH in a sigmoidal manner, with concomitant increase in the intensity of excitation spectra at 450 nm. The results indicate that pyranine is completely in the protonated and the

deprotonated state at pH below 5 and above 10, respectively.

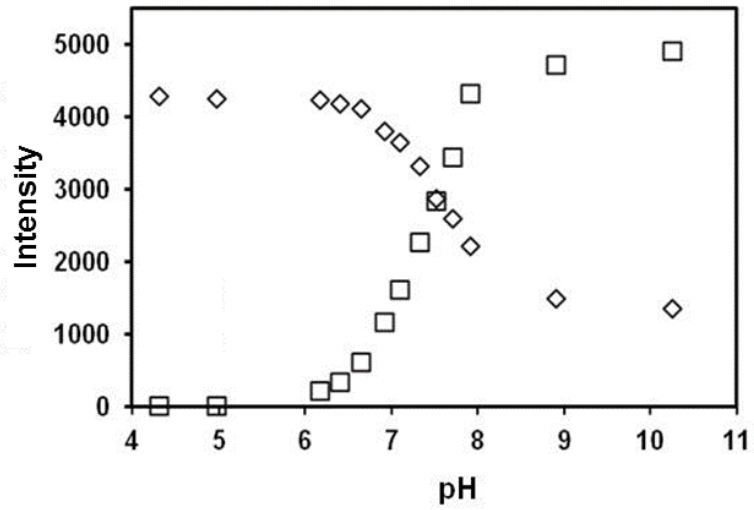

Figure 2-6. pH dependences of fluorescence intensity for 1.5 μM pyranine in water at 26 ℃. Excitation intensities at 402 and 450 nm were shown as rhombus and square, respectively. λ_{em}, 510 nm. pH was adjusted by HCl or NaOH.

The intensities of excitation spectra at 402 and 450 nm, I_{402} and I_{450}, have a linear relationship to the concentrations of pyranine under aqueous diluted conditions, as shown in equations 2-1 and 2-2, respectively.

$$I_{402} = K_{402}^{POH}[POH] + K_{402}^{PO^-}[PO^-] \quad (2\text{-}1)$$

$$I_{450} = K_{450}^{PO^-}[PO^-] \quad (2\text{-}2)$$

Where, [POH] and [PO^-] are concentrations of protonated and deprotonated pyranine in equilibrium state, respectively, and K_{402}^{POH}, $K_{402}^{PO^-}$, and $K_{450}^{PO^-}$ are the corresponding coefficients. [POH] and [PO^-] are correlated with the initial concentration of pyranine, $[POH]_0$, as equation 2-3.

$$[POH]_0 = [POH] + [PO^-] \quad (2\text{-}3)$$

The acid dissociation equilibrium constant K_a in equation 2-4, is defined as equation 2-5.

$$POH \overset{K_a}{\rightleftharpoons} PO^- + H^+ \quad (2\text{-}4)$$

$$K_a = ([PO^-]\,[H^+]) / [POH] \quad (2\text{-}5)$$

The equation 2-5 is converted to equation 2-6.

$$pK_a = -\log K_a = \log([POH]/[PO^-]) + pH \quad (2\text{-}6)$$

The pK_a value of pyranine in water has been reported to be 7.4. Thus, pyranine exists as nearly completely protonated or deprotonated species under the pH conditions far from the pK_a value by two pH units.

The correlation between emission intensity of excitation spectra at 402 nm and concentration of pyranine at pH 3.1 was shown in Figure 2-7. Under this pH condition, pyranine is in protonated form completely. A good linear relationship was observed in a concentration range less than 2 μM. Similar behavior was also observed at pH 6.5 for the plots of emission intensity of excitation spectra at 402 and 450 nm versus concentration of pyranine (Figure 2-8). These results indicate that fluorescence intensity has a good linearity with pyranine concentration below 2 μM under various aqueous pH conditions.

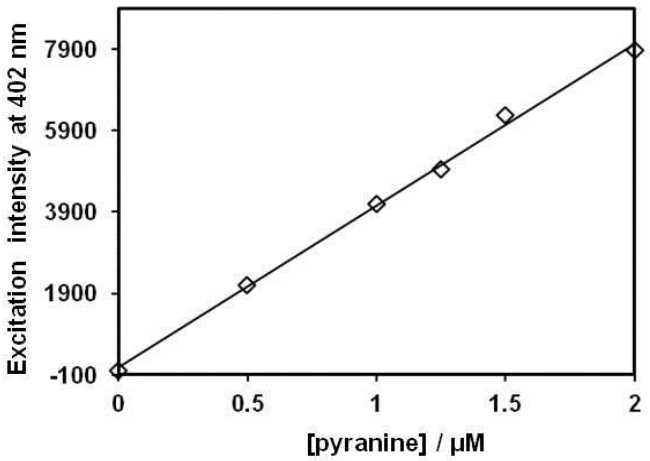

Figure 2-7. Correlation of intensity of excitation spectra at 402 nm with pyranine concentration in aqueous solution at pH 3.1 and 26 ℃. λ_{em}, 510 nm. Linear correlation constant (R^2), 0.9976.

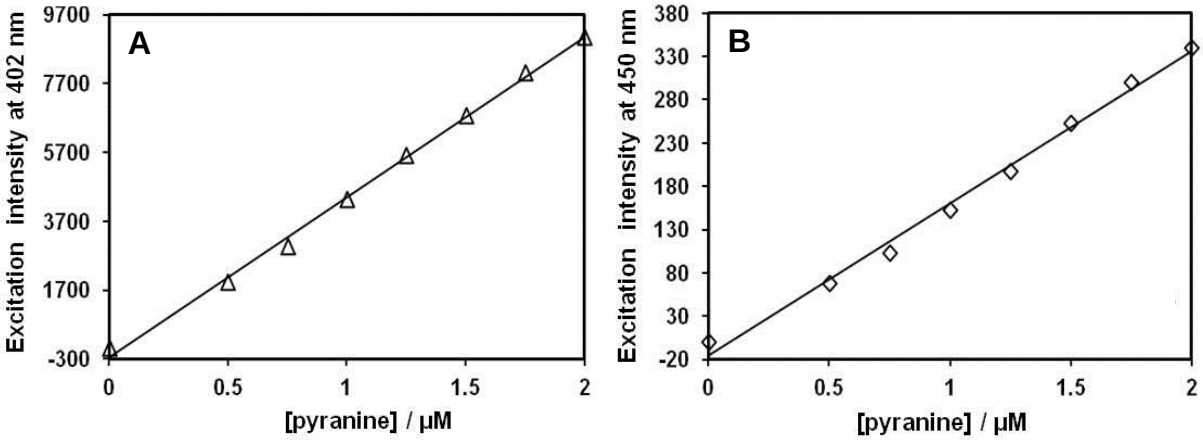

Figure 2-8. Correlations of intensity of excitation spectra at 402 (A) and 450 nm (B) with pyranine concentration in aqueous solution at pH 6.5 and 26 ℃. λ_{em}, 510 nm. Linear correlation constants (R^2), 0.9973 and 0.9933 for A and B, respectively.

(c) Fluorescence behavior of pyranine in the presence of liposomal membrane

Correlations of emission intensity of excitation spectra at 402 and 450 nm with pyranine concentration were examined in liposomal membrane formed by DMPC and $N^+C_3U2C_{16}$ in a molar ratio of 7:3 at pH 6.5 and 26 ℃. As shown in Figure 2-9, a good linear relationship was observed in a concentration range less than 1.5 μM. The results indicate that fluorescence intensity versus pyranine concentration has a good linearity in the presence of liposomal membrane.

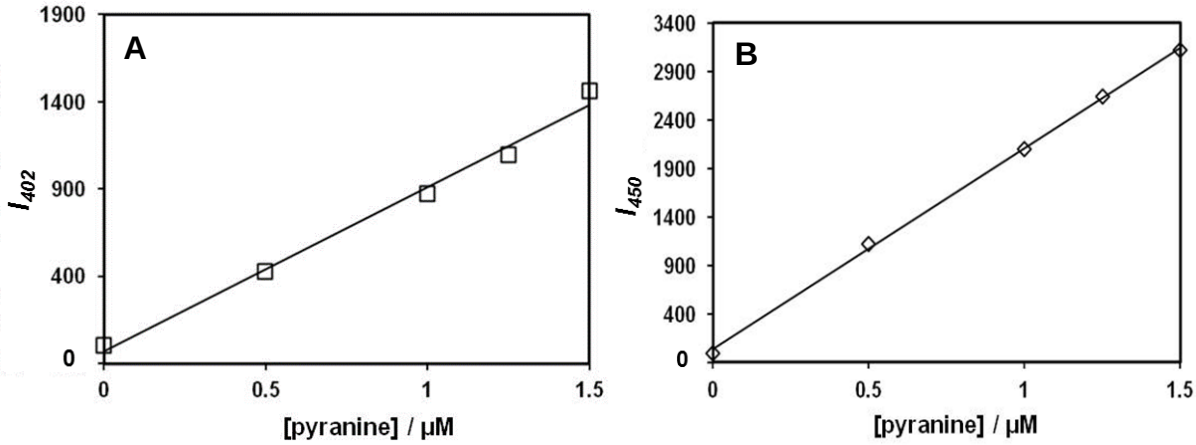

Figure 2-9. Correlations of intensity of excitation spectra at 402 (A) and 450 nm (B) with pyranine concentration in the presence of liposomal membrane formed by DMPC and $N^+C_3U2C_{16}$ in a molar ratio of 7:3 in 12 mM sucrose solution at pH 6.5 and 26 ℃. Total lipid concentration, 200 μM. λ_{em}, 510 nm. Linear correlation constants (R^2), 0.9911 and 0.9991 for A and B, respectively.

(d) Job's plot analysis

In order to determine the stoichiometry of complex formed by pyranine and $N^+C_3U2C_{16}$, Job's plot analysis was performed. This is one of the most reliable methods to evaluate the stoichiometry for complex formation in solutions. When a quantity reflecting the amount of complex is plotted by changing the molar ratio of two chemical species, under the conditions that total concentration of species keeps constant, the stoichiometry of complex is obtained from the vending point of plot. In the present system, fluorescence intensity change has linear relationship to the amount of complex as mentioned above. In addition, pyranine is very hydrophilic molecule incapable of permeation across the bilayer membrane. Thus, the emission intensity of excitation spectra at 450 nm (I_{450}) relative to that at 402 nm (I_{450}), which reflects the concentration of complex, was plotted against $[POH]_0$ / ($[POH]_0$ + $[L]_0^{ex}$) (Figure 2-10). Where, $[POH]_0$ and $[L]_0^{ex}$ are initial concentrations of pyranine and $N^+C_3U2C_{16}$ locating in the external layer of membrane. $[L]_0^{ex}$ was calculated from the lipid distribution in outer

and inner lipid layer of vesicles (50:50), which was derived from the hydrodynamic diameter of vesicles (116 nm) with polydispersity index (0.085) by means of dynamic light scattering measurements and the bilayer thickness (5 nm) estimated by molecular model.

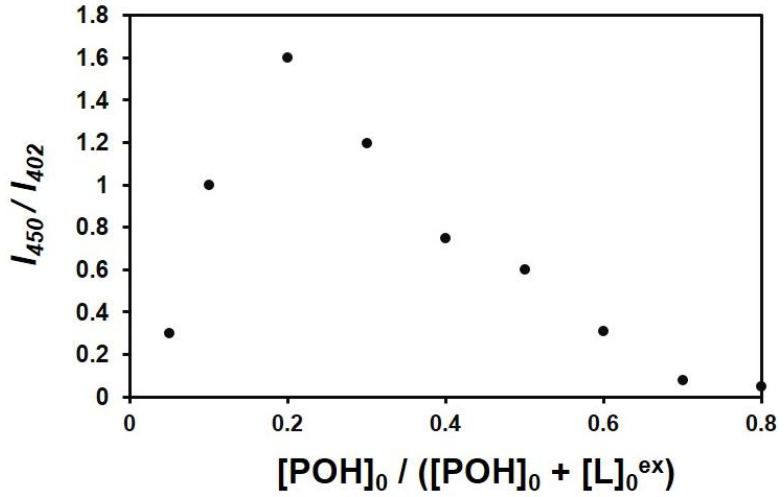

Figure 2-10. Job's plot for complex formation between pyranine and $N^+C_3U2C_{16}$ in the presence of liposomal membrane formed by DMPC and $N^+C_3U2C_{16}$ in a molar ratio of 7:3 in 12 mM sucrose solution at pH 6.5 and 26 ℃. $[POH]_0$ and $[L]_0^{ex}$ are initial concentrations of pyranine and $N^+C_3U2C_{16}$ locating in the outer layer of membrane, or 50% of cationic lipid molecules. Total concentration of $[POH]_0$ and $[L]_0^{ex}$ was maintained at 2.0 μM.

The Job's plot showed the maximum vending point at the value that $[POH]_0$ / ($[POH]_0$ + $[L]_0^{ex}$) was 0.2. Thus, it became apparent that one pyranine molecule interacted with four $N^+C_3U2C_{16}$ to form a complex in a stoichiometry of 1:4. Judging from the excitation spectral change shown in Figure 2-5, each tetraanionic deprotonated pyranine formed an ionic cluster with four cationic polar heads of lipids through the multipoint electrostatic interactions.

(e) Binding constant for the pyranine-$N^+C_3U2C_{16}$ complex

The equilibrium of complex formation between pyranine and $N^+C_3U2C_{16}$ in the present liposomal membrane is expressed as follows.

$$[POH] + 4\,[L]^{ex} \underset{}{\overset{K}{\rightleftharpoons}} [C] \qquad (2\text{-}7)$$

Where, K and C are binding constant and concentration for the 1:4 complex of pyranine with the cationic lipid molecules, respectively. The binding constant is defined as equation 2-8.

$$K = [C] / ([POH]\,([L]^{ex})^4) \qquad (2\text{-}8)$$

By considering the mass balance for pyranine and the cationic lipid,

$$[POH]_0 = [POH] + [C] \qquad (2\text{-}9)$$

$$[L]_0{}^{ex} = [L]^{ex} + 4[C] \qquad (2\text{-}10)$$

the equation 2-8 is converted to equation 2-11.

$$K = [C] / (([POH]_0 - [C])\,([L]_0{}^{ex} - 4[C])^4) \qquad (2\text{-}11)$$

On the other hand, the intensity of excitation spectra at 450 nm (I_{450}) shown in Figure 2-5 (A) has a linear relationship with [C]. Accordingly, the binding constant can be calculated from the nonlinear curve fitting for the plot of I_{450} vs $[L]_0^{ex}$ as shown in Figure 2-11. In conclusion, the binding constant for the 1:4 complex of pyranine with $N^+C_3U2C_{16}$ was calculated to be $3.8 \times 10^{22}\ M^{-4}$.

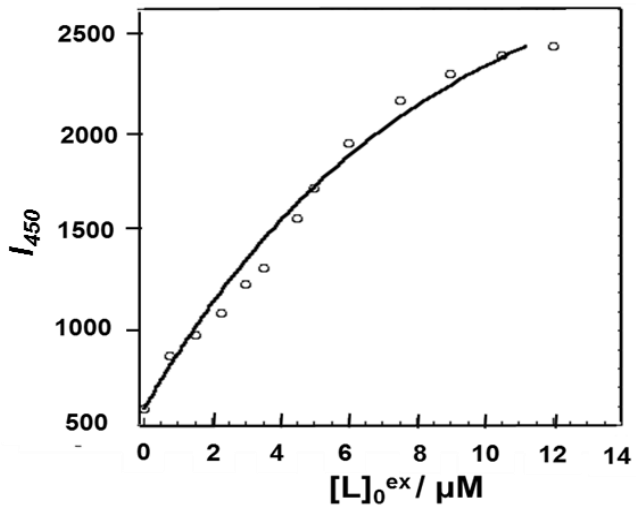

Figure 2-11. Relationship between the intensity of excitation spectra at 450 nm and $[L]_0^{ex}$. The data were taken from Figure 2-5 (A). Solid line indicates the calculated curve.

2.3.1.2 Kinetic analysis of signal binding

The dynamic process of signal binding to the cationic liposome was evaluated by monitoring th0065 time-dependence of fluorescence spectra. Figure 2-12 shows the time courses of fluorescence intensity of pyranine at various temperatures upon addition of the aqueous liposome formed by DMPC and $N^{+}C_3U2C_{16}$ in a molar ratio of 7:3 at pH 10.3. Under the present pH condition, pyranine is in the deprotonated form before and after interaction with the liposomal membrane. The gradual increase in fluorescence intensity at 510 nm was observed specifically at the temperatures of 24, 26, and 28 ℃ (Figure 2-12 (A)), which are in the phase transition temperature range of liposomal membrane between the gel and the liquid crystalline phase (vide infra). On the other hand, there was no transient in the fluorescence intensity in the temperature range corresponding to a gel (Figure 2-12 (B)) and a liquid crystalline phase (Figure 2-12 (C)).

As for electronic spectral properties of pyranine, theoretical characterization on the molecular orbitals of pyranine has been done to explain the solvatochromism.[16,17] The absorption and emission spectra of pyranine is shaped by coupling of pyranine with the solvent molecules depending on the ability of solvent to donate a hydrogen bond. Accordingly, pyranine has been used as a sensitive probe to monitor real-time polymerization of monomers[18] and polymer gelation process.[19] The time-dependent fluorescence intensity changes of pyranine have also been used for monitoring the dehydration process of polymer.[20]

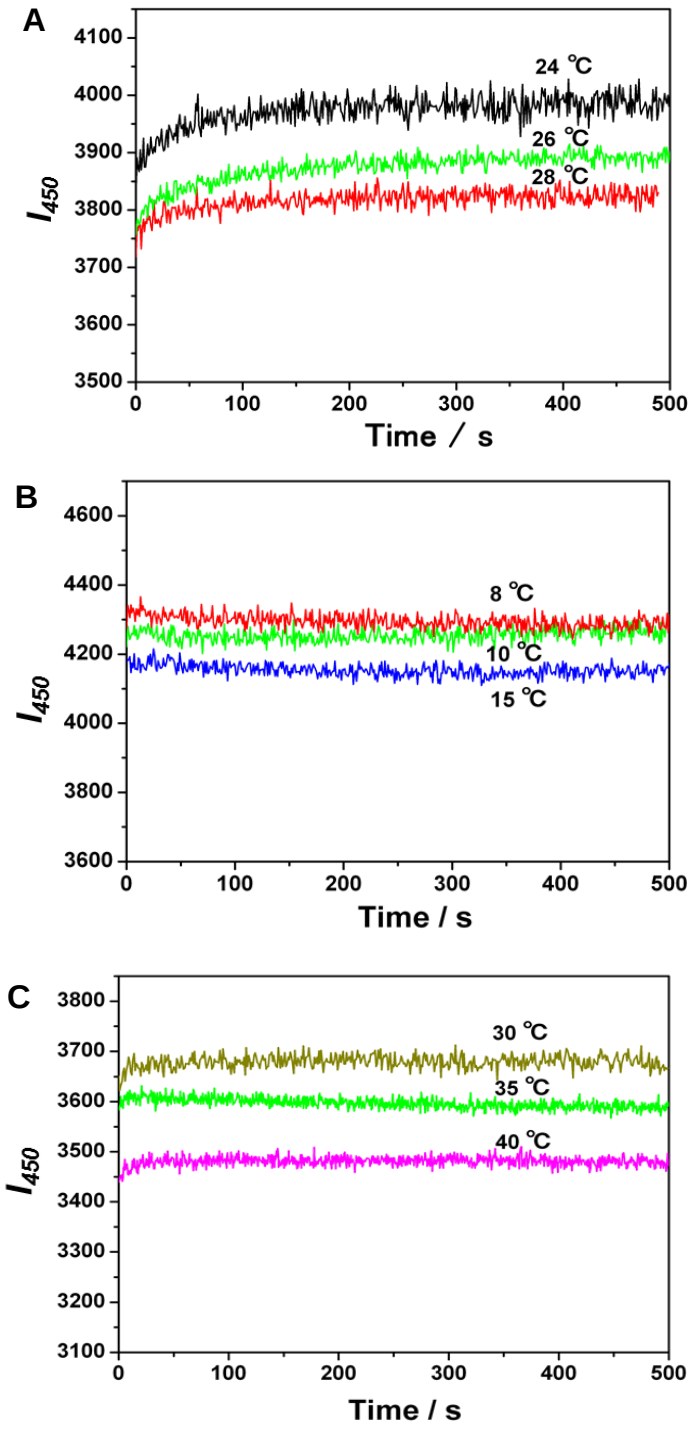

Figure 2-12. Time courses of fluorescence intensity of 1μM pyranine at various temperatures upon addition of liposomal membrane formed by DMPC and $N^{+}C_3U2C_{16}$ in a molar ratio of 7:3 in aqueous solution at pH 10.3. Total lipid concentration, 40 μM. λ_{ex}, 450 nm; λ_{em}, 510 nm.

On these grounds, the gradual increase in fluorescence intensity in the present system can be explained as schematically shown in Figure 2-13.

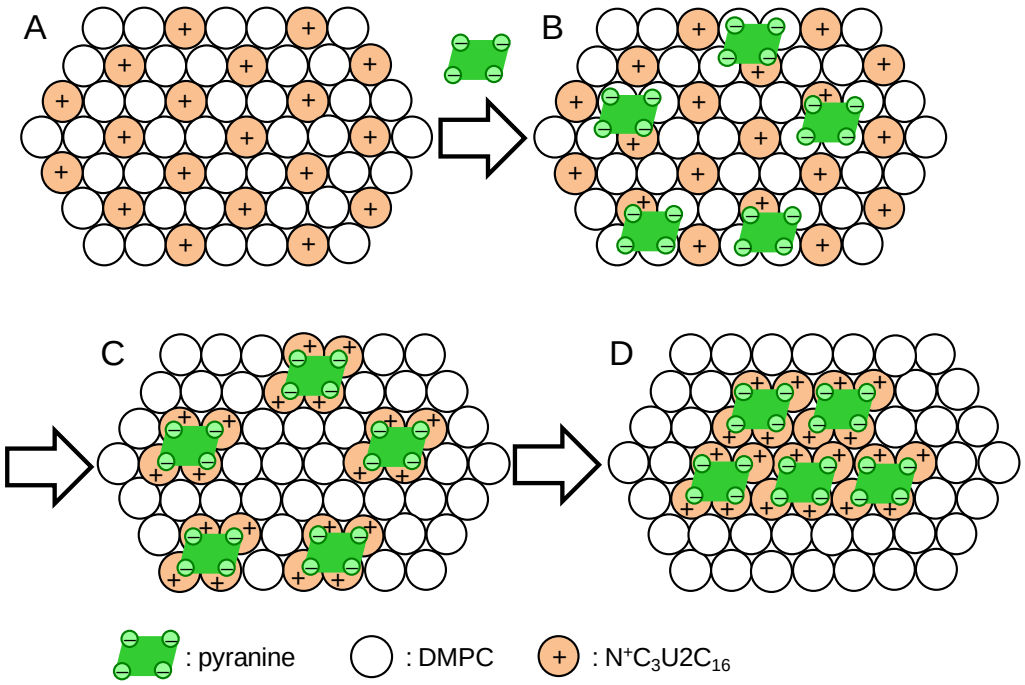

Figure 2-13. Schematic illustration of the signal binding and followed domain formation of liposomal membrane formed by DMPC and $N^{+}C_3U2C_{16}$ in a molar ratio of 7:3.

In the liposomal membrane, DMPC and $N^{+}C_3U2C_{16}$ distribute homogeneously in the absence of the chemical signal, presumably due to predominant electrostatic repulsion among the cationic polar head moieties in the latter lipid molecules (Figure 2-13 (A)). When tetraanionic pyranine approaches to the membrane surface through the electrostatic interactions, this molecule first binds to one cationic lipid head to form an ionic pair complex (Figure 2-13 (B)). After that, this 1:1 complex gathers additional cationic lipids through electroctatic interactions to form the complex composed of pyranine and cationic lipids in a stoichiometry of 1:4 (Figure 2-13 (C)). The second complexation process requires diffusion of cationic lipid molecules in the membrane. As for the 1:4 complexes in the membrane, the electrostatic repulsion among polar head groups is depressed and hydrogen bonding interactions among the urea moieties introduced into the cationic lipid molecule act effectively in the hydrophobic membrane

region. As a result, the 1:4 complexes gather to form the cationic lipid rich domain (Figure 2-13 (D)).

In the phase transition temperature range, the membrane fluidity is larger and smaller than these in the gel and the liquid crystalline state, respectively. In the gel state, the lateral diffusion of lipid molecules is much restricted to form the 1:4 complex. In contrast, the lateral diffusion is very fast in the liquid crystalline state, and the dynamic complex formation process is hard to be detected experimentally in a time scale of seconds. Thus, the dynamic process to form the 1:4 complex was observed as the time-dependent fluorescence intensity changes of pyranine only in the phase transition temperature range with moderate diffusion rate of lipid molecules in the liposomal membrane.

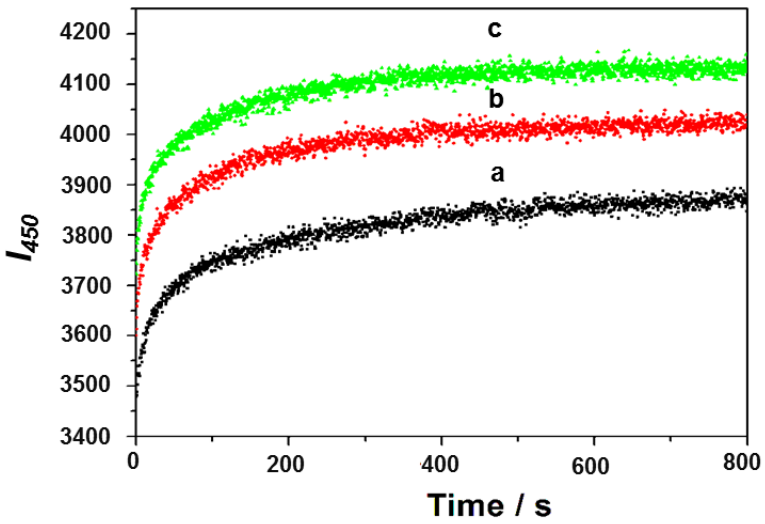

Figure 2-14. Dependences of lipid concentration on time course of fluorescence intensity of 1 μM pyranine upon addition of liposomal membrane formed by DMPC and $N^{+}C_3U2C_{16}$ in a molar ratio of 7:3 in aqueous solution at pH 10.3 and 26 ℃. Total lipid concentrations; 340, 544, and 680 μM for a, b, and c, respectively. λ_{ex}, 450 nm; λ_{em}, 510 nm.

Figure 2-14 shows the time courses of fluorescence intensity change of pyranine upon addition of different concentrations of liposomal membrane formed by DMPC and

$N^+C_3U2C_{16}$ in a molar ratio of 7:3 at pH 10.3 and 26 °C. The half-lives of fluorescence change were nearly constant to be 25 s for the different lipid concentrations. The results suggest that the kinetics of fluorescence intensity change was determined in the present system by the process of 1:4 complex formation and/or followed growth of membrane domain enriched by the signal-lipid complexes as schematically shown in Figure 2-13.

2.3.1.3 Factors influencing signal binding

In order to clarify physicochemical factors which influence in the signal binding to the liposomal membranes, the apparent acid dissociation constant (pK_a) for hydroxyl group on pyranine was evaluated under various conditions.

(a) pKa values of pyranine in the presence and absence of liposomal membrane

pH dependences of fluorescence intensity for pyranine at 510 nm in the presence and absence of the liposomal membrane formed by DMPC and $N^+C_3U2C_{16}$ in a molar ratio of 7:3 at 26 °C were shown in Figure 2-15 (A).

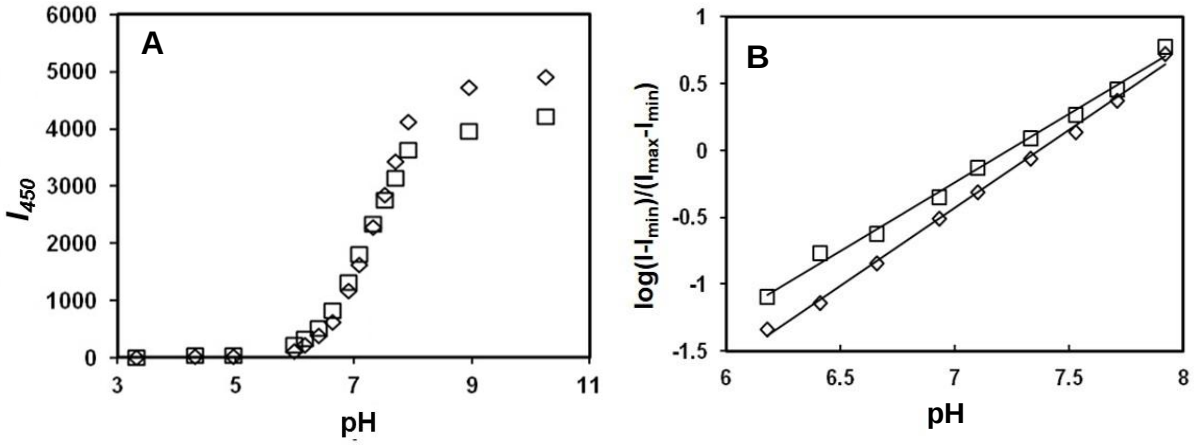

Figure 2-15. pH dependences of fluorescence intensity of 1 μM pyranine in the presence (◊) and absence (□) of liposomal membrane formed by DMPC and $N^+C_3U2C_{16}$ in a molar ratio of 7:3 in 5.0 mM Na_2HPO_4/citric acid buffer at 26 ℃ (A) and their linear plots to evaluate pK_a values (B). Total lipid concentration, 20 μM. λ_{ex}, 450 nm; λ_{em}, 510 nm.

The pK_a values were obtained from the linear plot, log $(I–I_{min})/(I_{max}–I_{min})$ vs pH,

where I, I_{max}, and I_{min} were fluorescence intensities at observed, highest, and lowest pH, respectively (Figure 2-15 (B)). In this linear plots, the pK_a values correspond to the pH when the value of vertical axis is zero. The observed pK_a values were 7.22 and 7.40 in the presence and absence of liposomal membrane, respectively. It has been reported that pyranine molecules located on a cationic membrane with positive zeta potential.[21] In general, local concentration of hydroxide ions increases on the cationic membrane surface to decrease the apparent pK_a values of chemical species. Thus, in the present system, the lower pK_a value in the presence of liposomal membrane than that without membrane reflects the binding of pyranine with the membrane surface through the electrostatic interactions.

(b) Effect of lipid composition on pK_a of pyranine

The acid dissociation behavior of pyranine in the presence of liposomal membranes with different lipid compositions was examined. pH dependences of fluorescence intensity for pyranine at 510 nm in the liposomal membrane formed by DMPC and $N^+C_3U2C_{16}$ in various molar ratios at 26 ^oC were shown in Figure 2-16 (A). The pK_a values obtained from the linear plot, log $(I-I_{min})/(I_{max}-I_{min})$ vs pH, as shown in Figure 2-16 (B) were listed in Table 2-1.

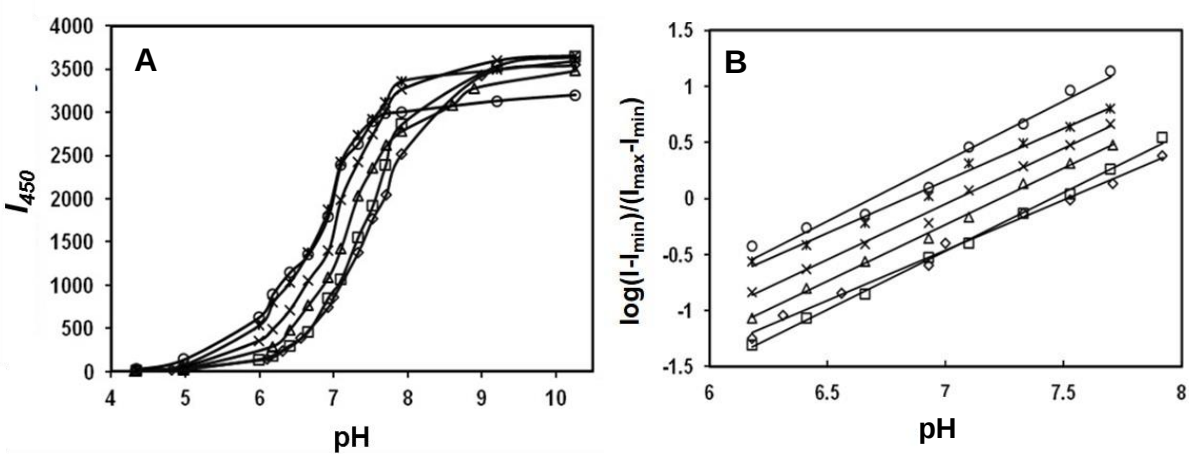

Figure 2-16. pH dependences of fluorescence intensity of 1 μM pyranine in the liposomal membrane formed by DMPC and $N^+C_3U2C_{16}$ in molar ratio of 10:0 (◊), 8:2 (□), 7:3 (△), 50:50 (×), 3:7 (＊), 0:10 (○) in 5.0 mM Na_2HPO_4/citric acid buffer at 26 ℃ (A) and their linear plots to evaluate pK_a values (B). Total lipid concentration, 40 μM. λ_{ex}, 450 nm; λ_{em}, 510 nm.

Table 2-1. The apparent pK_a values of pyranine in the liposomal membrane formed by DMPC and $N^+C_3U2C_{16}$ in various molar ratios at 26 ℃.

DMPC-$N^+C_3U2C_{16}$	Linear equation (Correlation constant)	pK_a
10:0	y=0.898x-6.748 (R^2=0.993)	7.44
8:2	y=1.045x-7.776 (R^2=0.997)	7.49
7:3	y=1.008x-7.288 (R^2=0.997)	7.22
5:5	y=0.996x-7.018 (R^2=0.995)	7.05
3:7	y=0.935x-6.387 (R^2=0.992)	6.83
0:10	y=1.069x-7.148 (R^2=0.995)	6.68

x, pH; y, log $(I-I_{min})/(I_{max}-I_{min})$.

The apparent pK_a values were increased with increasing the ratio of $N^+C_3U2C_{16}$ with DMPC in the membrane. The results reflect that anionic pyranine molecules were concentrated on the cationic membrane surface through the electrostatic interactions and that the higher ratio of cationic lipid to zwitter ionic phospholipid increase the local pH value on the membrane surface to decrease the apparent pK_a value of pyranine.

(c) Effect of temperature on pK_a of pyranine

The acid dissociation behavior of pyranine in the liposomal membranes was examined at different temperatures. Temperature effects on pH dependence of fluorescence intensity for pyranine at 510 nm in the liposomal membrane formed by DMPC and $N^+C_3U2C_{16}$ in a molar ratio of 7:3 at 10, 26, and 35 ^oC were shown in Figure 2-18 (A). The pK_a values obtained from the linear plot, log $(I-I_{min})/(I_{max}-I_{min})$ vs pH, as shown in Figure 2-17 (B) were listed in Table 2-2.

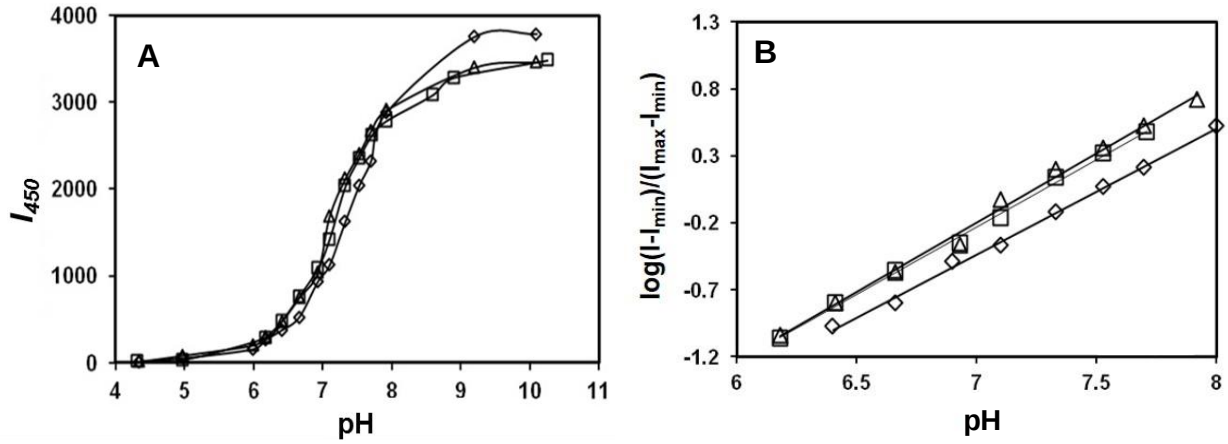

Figure 2-17. pH dependences of fluorescence intensity of 1 μM pyranine in the liposomal membrane formed by DMPC and $N^+C_3U2C_{16}$ in a molar ratio of 7:3 in 5.0 mM Na_2HPO_4/citric acid buffer at 10 (△), 26 (□), and 35 (◊) ℃ (A) and their linear plots to evaluate pK_a values (B). Total lipid concentration, 40 μM. λ_{ex}, 450 nm; λ_{em}, 510 nm.

Table 2-2. The apparent pK_a values of pyranine in the liposomal membrane formed by DMPC and $N^+C_3U2C_{16}$ in a molar ratio of 7:3 at 10, 26, and 35 ℃.

Temperature / ℃	Linear equation (Correlation constant)	pK_a
10	y=1.035x-7.441 (R^2=0.994)	7.19
26	y=1.008x-7.288 (R^2=0.997)	7.22
35	y=0.940x-7.107 (R^2=0.997)	7.56

x, pH; y, log $(I-I_{min})/(I_{max}-I_{min})$.

The apparent pK_a values were gradually increased with increasing the temperature of aqueous vesicular solution, and it seems that the change of pK_a values is larger than that of simple temperature effect inaqueous media. The bilayer membrane is in the gel and the liquid crystalline state at 10 and 35 ^{o}C, respectively, and in the phase transition temperature range at 26 ^{o}C. The results imply that the observed temperature dependence of pK_a values reflects the difference in phase state of liposomal membrane. In order to confirm this possibility, in the next part, the acid dissociation behavior of pyranine in the liposomal membranes composed of $N^{+}C_3U2C_{16}$ and phosphatidylcholines with different phase transition temperature at a constant temperature of 26 ^{o}C.

(d) Effect of phospholipid double-chain length on pK_a of pyranine

pH dependences of fluorescence intensity for pyranine at 510 nm in the liposomal membranes formed by DPPC, DMPC, or DLPC with $N^{+}C_3U2C_{16}$ in a molar ratio of 7:3 at 26 ^{o}C were shown in Figure 2-18 (A). The pK_a values obtained from the linear plot, log $(I-I_{min})/(I_{max}-I_{min})$ vs pH, as shown in Figure 2-18 (B) were listed in Table 2-3. The pK_a values were 7.15, 7.22, and 7.52 in the liposomal membranes formed by DPPC, DMPC, or DLPC with $N^{+}C_3U2C_{16}$, respectively.

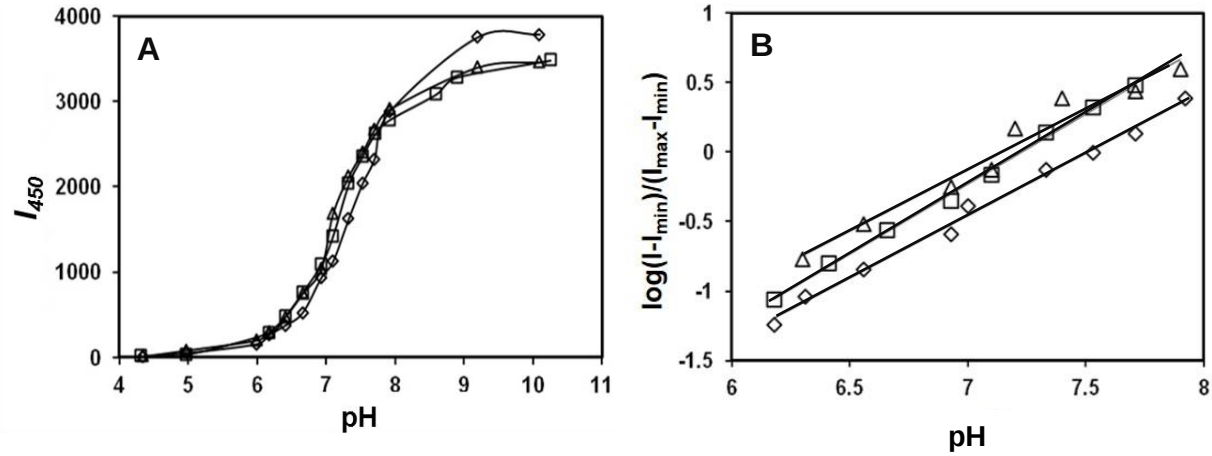

Figure 2-18. pH dependences of fluorescence intensity of 1 μM pyranine in the liposomal membrane formed by DPPC (△), DMPC (□), or DLPC (◊)with $N^+C_3U2C_{16}$ in a molar ratio of 7:3 in 5.0 mM Na_2HPO_4/citric acid buffer at 26 ℃ (A) and their linear plots to evaluate pK_a values (B). Total lipid concentration, 40 μM. λ_{ex}, 450 nm; λ_{em}, 510 nm.

Table 2-3. The apparent pK_a values of pyranine in the liposomal membrane formed by DPPC, DMPC, or DLPC with $N^+C_3U2C_{16}$ in a molar ratio of 7:3 at 26 ℃.

Phospholipid	Linear equation (Correlation constant)	pK_a
DPPC	y=0.885x-6.326 (R^2=0.963)	7.15
DMPC	y=1.008x-7.288 (R^2=0.997)	7.22
DLPC	y=0.898x-6.741 (R^2=0.981)	7.52

x, pH; y, log $(I-I_{min})/(I_{max}-I_{min})$.

These phospholipids having different double-chain length show the phase transition temperatures of 41, 24, -2 °C for DPPC, DMPC, and DLPC, respectively, in individual state. In the liposomal membranes formed by DPPC, DMPC, or DLPC with $N^+C_3U2C_{16}$ in a molar ratio of 7:3, the phase transition temperature were 40, 26, or 10 °C, respectively, as evaluated by differential scanning calorimerty (vide infra). Thus, at 26 °C, the liposomal membranes formed by DPPC, DMPC, or DLPC with $N^+C_3U2C_{16}$ are in a gel state, a transition state, or a liquid crystalline state, respectively. The observed

pK_a values in Table 2-2 and 2-3 are in good agreement with the same phase state. These results well support the above interpretation that the apparent pK_a values of pyranine in the presence of cationic liposomal membrane decrease in the order of liquid crystalline state, phase transition region, and gel state. This behavior presumably reflects the extent of phase separation in the mixed lipid membrane. That is, phase separation was enhanced in the gel state of liposomal membrane than in liquid crystalline state. Such phase separation induced the formation of cationic lipid rich domain with higher positive charge density, in which the microenvironmental pH increased to afford lower apparent pK_a value of pyranine on the membrane surface.

(e) Effect of ionic strength on pK_a of pyranine

In general, the electrostatic interactions in aqueous media are affected by ionic strength. In order to clarify that the present signal binging behavior toward liposomal membrane is governed mainly by the electrostatic interactions between anionic pyranine and cationic membrane surface, an effect of ionic strength on the pK_a value of pyranine in the presence of liposomal membrane was evaluated.

pH dependences of fluorescence intensity for pyranine at 510 nm in the liposomal membranes formed by DMPC and $N^+C_3U2C_{16}$ in a molar ratio of 7:3 at 26 ^oC were measured in the presence of potassium chloride with various concentration (Figure 2-19 (A)). The pK_a values obtained from the linear plot, log $(I-I_{min})/(I_{max}-I_{min})$ vs pH, as shown in Figure 2-19 (B) were listed in Table 2-4.

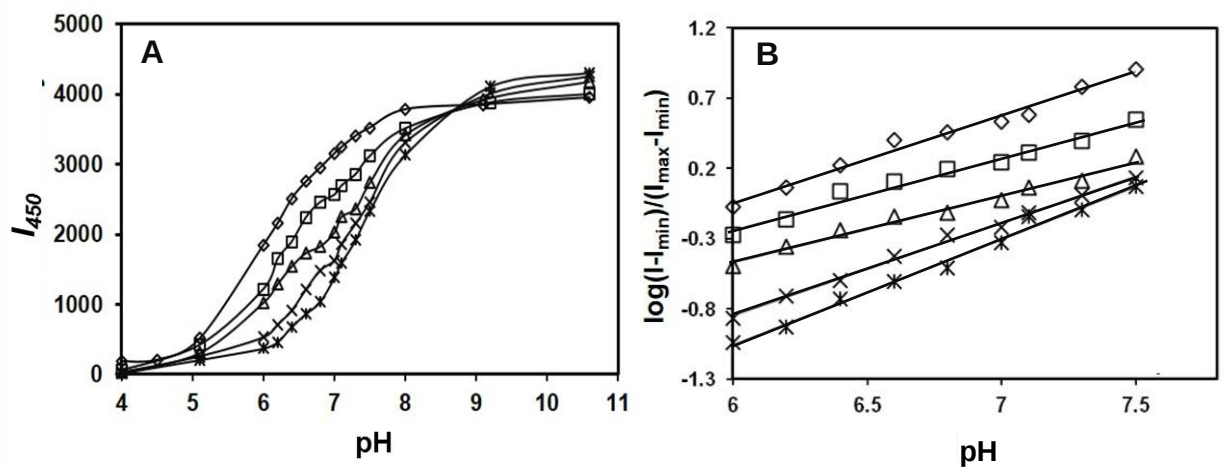

Figure 2-19. pH dependences of fluorescence intensity of 1 μM pyranine in the liposomal membrane formed by DMPC and $N^+C_3U2C_{16}$ in a molar ratio of 7:3 at 26 ℃ in the absence (◊) and presence of 1 (□), 2 (△), 3 (×). 5 (✻) mM potassium chloride (A) and their linear plots to evaluate pK_a values (B). Total lipid concentration, 40 μM. λ_{ex}, 450 nm; λ_{em}, 510 nm.

Table 2-4. The apparent pK_a values of pyranine in the liposomal membrane formed by DMPC and $N^+C_3U2C_{16}$ in a molar ratio of 7:3 at 26 ℃ and different ionic strength.

[KCl] / mM	Linear equation (Correlation constant)	pK_a
0	y=0.625x-3.804 (R^2=0.984)	6.08
1	y=0.511x-3.309 (R^2=0.980)	6.47
2	y=0.473x-3.303 (R^2=0.981)	6.99
3	y=0.659x-4.806 (R^2=0.996)	7.29
5	y=0.751x-5.565 (R^2=0.990)	7.41

x, pH; y, log $(I-I_{min})/(I_{max}-I_{min})$.

The pK_a value was 6.08 in the absence of potassium chloride. The value was gradually increased with increasing the salt concentration to reach to 7.41 at 5 mM potassium chloride, which is nearly equal to the pKa value in water (7.40). The results clearly indicate that electrostatic interaction is the predominant force between pyranine

and the liposomal membrane and that the pK_a value of pyranine in the presence of liposomal membrane has marked dependence on ionic strength.

2.3.2 Phase separation behavior induced by a chemical signal

2.3.2.1 Phase separation behavior evaluated by differential scanning calorimetry

The interaction of chemical signal to liposomal membranes would affect the phase transition of lipid bilayer phase, and such phase behavior can be evaluated by differential scanning calorimetry (DSC). The DSC thermograms for the liposomal membrane formed by DMPC and $N^+C_3U2C_{16}$ in a molar ratio of 7:3 in the presence and absence of pyranine were shown in Figure 2-20.

In the absence of chemical signal, a single endothermic peak corresponding to the phase transition from gel to liquid crystalline phase for the DMPC/$N^+C_3U2C_{16}$ binary lipid vesicles was appeared at 26.42 ℃ with enthalpy change of 19.4 kJ·mol^{-1} (Table 2-5). This indicates random and homogeneous packing of two kinds of lipid molecules in the membrane.[22] In the presence of 10 μM pyranine, the phase transition peak broadened and a new peak appeared as a shoulder at 26.69 ℃. Upon further addition of pyranine, the original and new transition peak decreased and increased with concomitant shift of peak temperature to lower and higher temperature range, respectively. At 35 μM pyranine concentration, the original transition peak nearly disappeared and a new peak with a peak temperature of 27.64 ℃ became to be predominant.

The results indicate that the mixing of DMPC and $N^+C_3U2C_{16}$ became heterogeneous upon addition of pyranine.[22] In other words, phase separation happened in the membrane. One phase with lower peak temperature corresponds to a DMPC-rich phase, while another one with higher peak temperature is assigned to a $N^+C_3U2C_{16}$-rich

phase.

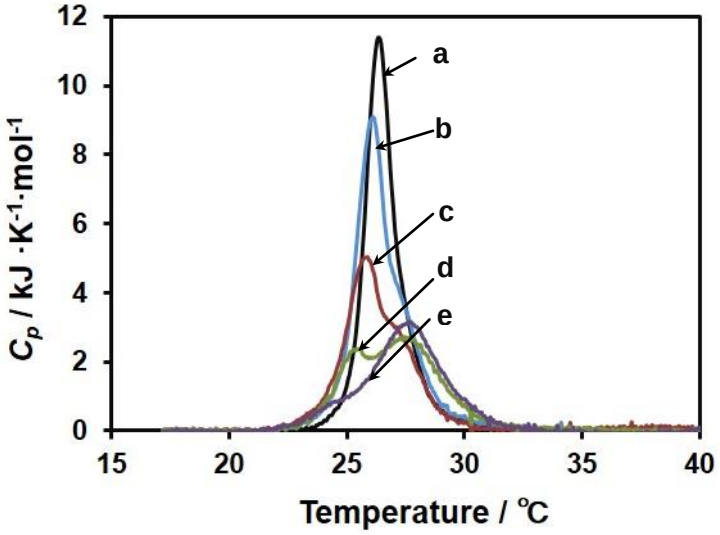

Figure 2-20. DSC thermograms of liposomal membrane formed by DMPC and $N^+C_3U2C_{16}$ in a molar ratio of 7:3 in 12 mM aqueous sucrose at pH 6.5 in the absence (a) and presence of 10 (b), 15 (c), 25 (d), and 35 (e) μM of pyranine. Total lipid concentrations, 0.5 mM. Scan rate, 0.5 ℃ min^{-1}.

Table 2-5. Phase transition parameters for the liposomal membrane formed by DMPC and $N^+C_3U2C_{16}$ in a molar ratio of 7:3 in 12 mM aqueous sucrose at pH 6.5 in the presence and absence of pyranine.

[Pyranine] / μM	T_{m1} / ℃	ΔH_1 / kJ mol^{-1}	$C.U._1$	T_{m2} / ℃	ΔH_2 / kJ mol^{-1}	$C.U._2$
0	26.42	19.4	87	——	——	——
10	25.95	12.4	148	26.69	8.11	123
15	25.58	6.23	255	26.87	8.54	103
25	25.14	2.95	527	27.56	9.99	80
35	24.40	1.20	877	27.64	11.42	71

In addition, the changes of DSC thermogram give us a good hint to evaluate the effect of pyranine to the lipid packing in the membrane. It has been reported that dehydration of phosphatidylcholines in liposomal membranes lead to an increase in phase transition temperature.[23] For example, the effect of a polymer, poly(2-ethylacrylic

acid), on the lipid packing in DPPC vesicles was evaluated by DSC.[24] In this system, by changing medium pH values, the polymer absorbed on the vesicular surface caused partial dehydration of head group of lipid, which gave rise to the increase in phase transition temperature.

In the present system, I have clarified by means of fluorescence spectroscopy that pyranine as a chemical signal interacted with $N^+C_3U2C_{16}$ to form the 1:4 complex on the surface of liposomal membrane (vide supra). In the absence of chemical signal, the cationic lipid molecule takes a cylindrical packing shape in the membrane to afford lipid bilayer structure. Upon the complex formation of pyranine with $N^+C_3U2C_{16}$, the distance among the cationic head groups of lipid would decrease due to formation of ion pair species of tetraanionic pyranine with four cationic lipids accompanying with dehydration of lipid head moieties, as schematically shown in Figure 2-21. As a result, the cationic lipid changes the molecular packing from the cylindrical to a conical shape. Such consideration can be supported by the finding that the distances among anionic sulfonate or phenolate groups are shorter than the effective diameter of hydrated lipid head moiety in bilayer membrane.[25] Accordingly, the dehydration of cationic lipids probably gives out the increase in phase transition temperature for the $N^+C_3U2C_{16}$-rich domain.

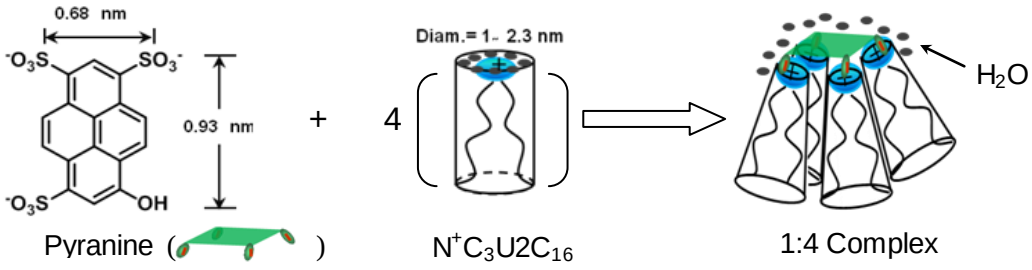

Figure 2-21. Schematic representation of the 1:4 complex formation of pyranine with $N^+C_3U2C_{16}$ accompanying with dehydration of lipid head groups.

Comparison of phase transition parameters listed in Table 2-5 gives us further insights to understand the phase behavior of liposomal membranes. Addition of pyranine decreased the enthalpy change (ΔH_1) of the DMPC-rich phase with the lower peak temperature (T_{m1}). The decrease of enthalpy change is due to the extrusion of $N^+C_3U2C_{16}$ lipid molecules from the DMPC-rich domain. While the increase in transition enthalpy change (ΔH_2) at the higher peak temperature (T_{m2}) upon addition of pyranine reflects the enhanced formation of $N^+C_3U2C_{16}$-rich domain.

The cooperativity for the phase transition of liposomal membranes can be discussed by comparing the cooperative unit (*C.U.*), defined as $\Delta H_{vh}/\Delta H$. Where, ΔH_{vh} and ΔH are van't Hoff enthalpy change and the observed phase transition enthalpy change, respectively. The *C.U.* value reflects the number of lipids simultaneously undergoing phase transition from the gel to liquid crystalline phase.[26]

Addition of pyranine to the liposomal membrane formed by DMPC and $N^+C_3U2C_{16}$ led to a significant increase in cooperative unit ($C.U._1$) for the DMPC-rich phase. This suggests that the percentage of DMPC in the DMPC-rich phase gradually increased as extrusion of $N^+C_3U2C_{16}$ from this phase upon addition of pyranine.[27] On contrary, cooperative unit ($C.U._2$) for the $N^+C_3U2C_{16}$-rich phase was decreased upon addition of pyranine. The result demonstrates that the $N^+C_3U2C_{16}$-rich phase becomes more heterogeneous upon addition of pyranine. In other words, enhancement of complex formation of pyranine with $N^+C_3U2C_{16}$ in the $N^+C_3U2C_{16}$-rich phase turns to the lipid packing of phase more heterogeneous.

Formation of the $N^+C_3U2C_{16}$-rich and the DMPC-rich phase is explained as follows. The predominant driving force for the phase separation in this system would be hydrogen bonding interactions among the cationic lipids. It is well known that hydrogen

bonding is one of the important noncovalent interactions in lipid membranes.[28] The cationic synthetic lipid, $N^+C_3U2C_{16}$, has a urea residue interposed between a polar head moiety and a hydrophobic double-chain segment. The urea group acts as an effective hydrogen bonding unit having both strong hydrogen donor and acceptor parts. On the other hand, DMPC is a glycerophospholipid having ester groups as a weak hydrogen acceptor. Thus, $N^+C_3U2C_{16}$ molecules have potential to form a lipid domain through self-aggregation in the DMPC membrane, if there is no repulsive interaction among the lipid molecules. However, the formation of phase separated lipid domains was not detected practically, judging from the thermogram of differential scanning calorimetry (Figure 2-20). The result indicates that the electrostatic repulsion among the polar head groups overcomes to the attractive hydrogen bonding interactions among urea residues in the absence of chemical signal.

Upon addition of pyranine, as a chemical signal, the complex of pyranine with cationic lipids formed in a 1:4 stoichiometry through the multipoint electrostatic interactions. The formation of signal-lipid complex enhances charge neutralization of lipid polar head. Thus, the decrease of electrostatic repulsion among the cationic head moieties reverses the force balance between the repulsive electrostatic interactions and the attractive hydrogen bonding interactions. This is another driving force for the phase separation to form individual lipid-rich domains.

The phase separation behavior observed in the present liposomal membrane is capable of being reasonable, judging from the related works reported previously. For example, multivalent ions such as calcium ions induced lateral phase separation in the outer layer of liposomal membrane through formation of ion complex with negatively charged lipids, such as phosphatidic acid or phosphatidylserine.[29] The phase separation

was initiated by the ion complex clustering through van der Waals attractive interactions.[30] Another example is that phase separation of two-component lipids began with the formation of a new phase, growth, and fusion of the phases to give the larger domains on the supported phospholipid bilayers.[31]

Such phase separation behavior can be understood from the line energy concept.[31] In the liposomal membrane, in which two phases coexist, there are boundaries between these phases. Line energy is ideally proportional to the boundary length. Globally, any phase-separated system tends to minimize the line energy by small phases coalescence, while it is opposed by reduction in entropy.[31 a] In the present liposomal membrane, a 1:4 complex is considered as a minimal phase, and there is a boundary around the small phase. The small lipid phases tend to minimize line energy through the phases coalescence. Therefore, the complexes fused each other to form a larger lipid phase with the shorter boundary length, as schematically shown in Figure 2-12.

In conclusion, the results evaluated by differential scanning calorimetry illustrated that pyranine binding on the liposomal membrane formed by DMPC and $N^{+}C_3U2C_{16}$ induced the phase separation to form the $N^{+}C_3U2C_{16}$-rich phase with lower cooperativity.

2.3.2.2 Effect of salt concentration on phase separation

In this part, the effect of salt concentration on the phase separation behavior of liposomal membrane formed by DMPC and $N^{+}C_3U2C_{16}$ as induced by pyranine was evaluated by DSC measurements.

As shown in Figure 2-22, the DSC thermogram showed two phase separated peaks induced by the presence of 25 μM pyranine. Two phase in the DSC thermogram gradually fuse to one phase with an increase in concentration of potassium chloride. The

phase transition parameters were listed in Table 2-6.

The increase in concentration of potassium chloride increased the phase transition enthalpy change (ΔH_1) of the DMPC-rich domain with the lower peak temperature (T_{m1}). While the enthalpy change (ΔH_2) of $N^+C_3U2C_{16}$-rich domain with the higher peak temperature (T_{m2}) decreased upon addition of potassium chloride. As for the cooperative unit, $C.U._1$ for the DMPC-rich domain and $C.U._2$ for the $N^+C_3U2C_{16}$-rich domain were decreased and increased, respectively, with the increase in concentration of potassium chloride. These results indicate that, the phase separated domains induced by binding of pyranine were diminished with potassium chloride to form the original homogeneous lipid phase, in which DMPC and $N^+C_3U2C_{16}$ were dispersed nearly homogeneously. In other words, the increase in salt concentration weakened the electrostatic interactions between pyranine and cationic lipid molecules to decrease the stability of 1:4 complex, which is the key species to form the $N^+C_3U2C_{16}$-rich domain. Sunamoto and his coworkers have reported that pyranine bound to cationic liposomal membrane composed of egg phosphatidylcholine can be replaced by anions, such as chloride and perchlorate, under the conditions that these anions bind to the cationic membrane much stronger than pyranine.[21]

In conclusion, it became apparent that the phase separation behavior of liposomal membrane formed by DMPC and $N^+C_3U2C_{16}$ as induced by pyranine was controlled by changing salt concentration.

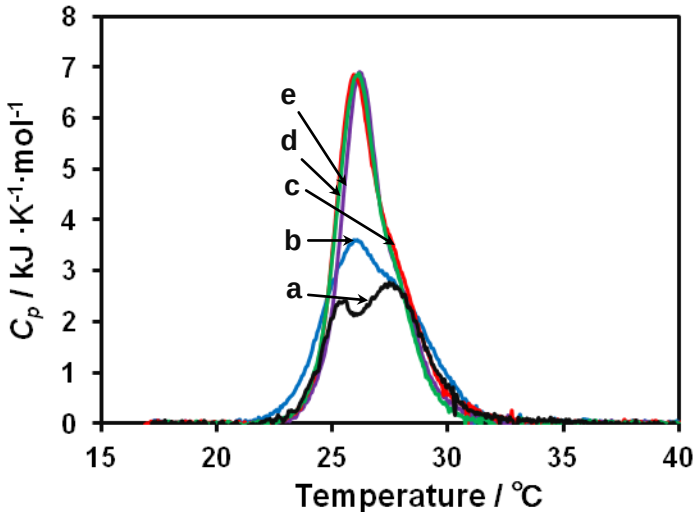

Figure 2-22. DSC thermograms of liposomal membrane formed by DMPC and $N^+C_3U2C_{16}$ in a molar ratio of 7:3 upon addition of 25 μM pyranine in 12 mM aqueous sucrose at pH 6.5 in the absence (a) and presence of 1 (b), 2 (c), 3 (d), and 5 (e) mM of potassium chloride. Total lipid concentrations, 0.5 mM. Scan rate, 0.5 ℃ min^{-1}.

Table 2-6. Phase transition parameters for the liposomal membrane formed by DMPC and $N^+C_3U2C_{16}$ in a molar ratio of 7:3 upon addition of 25 μM pyranine in 12 mM aqueous sucrose at pH 6.5 in the presence and absence of potassium chloride.

[KCl] / mM	T_{m1} / ℃	ΔH_1 / kJ mol^{-1}	$C.U._1$	T_{m2} / ℃	ΔH_2 / kJ mol^{-1}	$C.U._2$
0	25.14	2.95	527	27.56	10.0	80
1	25.53	7.2	133	27.54	9.6	73
2	25.65	9.9	161	27.45	8.8	99
3	25.93	10.8	131	27.4	8.2	112
5	26.03	12.1	111	27.33	7.5	110

2.3.2.3 Effect of lipid composition on phase separation

Here, phase separation behavior of the liposomal membrane formed by DMPC and $N^+C_3U2C_{16}$ in various molar ratios upon addition of pyranine was evaluated by DSC

measurements.

Figure 2-23 shows the effect of pyranine as a chemical signal on DSC thermograms for the liposomal membranes formed by DMPC and $N^+C_3U2C_{16}$ in molar ratios of 8:2, 7:3, 5:5, and 3:7. The phase transition parameters for these liposomal membranes were listed in Tables 2-7, 2-8, 2-9, and 2-10.

In the absence of chemical signal, each liposomal membrane has a single phase transition mainly. However, the cooperative unit ($C.U._1$) decreased from 106 to 37 with an increase in molar ratio of $N^+C_3U2C_{16}$ from 20 to 70%. It has been reported that the cooperative unit of liposomal membrane formed by single lipid component was decreased by mixing another lipid due to enhanced heterogeneity of membrane.[27b] The results imply that the present cationic lipid gives larger perturbation on the lipid packing in the membrane than the phospholipid.

Upon addition of pyranine, phase separation was observed for every liposomal membrane. An increase in concentration of pyranine decreased the phase transition enthalpy change (ΔH_1) of the DMPC-rich domain with the lower peak temperature (T_{m1}). While the enthalpy change (ΔH_2) of $N^+C_3U2C_{16}$-rich domain with higher peak temperature (T_{m2}) increased upon addition of pyranine. As for the cooperative unit, $C.U._1$ for the DMPC-rich domain and $C.U._2$ for the $N^+C_3U2C_{16}$-rich domain were increased and decreased, respectively, with the increase in concentration of pyranine.

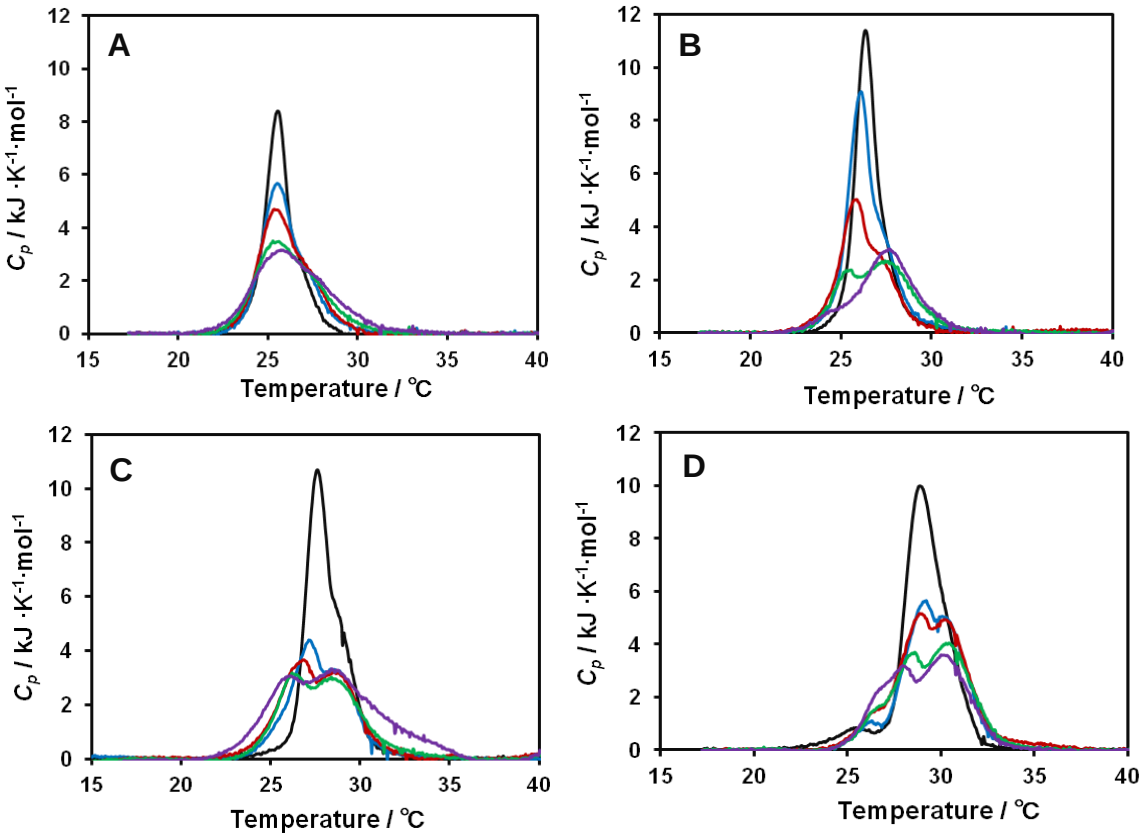

Figure 2-23. DSC thermograms of liposomal membrane formed by DMPC and $N^+C_3U2C_{16}$ in a molar ratio of 8:2 (A), 7:3 (B), 5:5 (C), and 3:7 (D) upon addition of pyranine in 12 mM aqueous sucrose at pH 6.5. Total lipid concentrations, 0.5 mM. Pyranine concentrations, 0, 10, 15, 25 and 35 μM (corresponding curves color respectively: dark, blue, red, green and purple) for each sample. Scan rate, 0.5 ℃ min^{-1}.

Table 2-7. Phase transition parameters for the liposomal membrane formed by DMPC and $N^+C_3U2C_{16}$ in a molar ratio of 8:2 upon addition of pyranine in 12 mM aqueous sucrose at pH 6.5.

[Pyranine] / μM	T_{m1} / ℃	ΔH_1/ kJ mol^{-1}	$C.U._1$	T_{m2} / ℃	ΔH_2 / kJ mol^{-1}	$C.U._2$
0	25.56	13.8	106	——	——	——
10	25.43	9.2	123	27.08	4.5	221
15	25.32	8.5	146	27.18	4.9	203
25	25.8	7.2	144	27.38	5.5	147
35	25.34	7.1	143	27.58	6.4	101

Table 2-8. Phase transition parameters for the liposomal membrane formed by DMPC and $N^+C_3U2C_{16}$ in a molar ratio of 7:3 upon addition of pyranine in 12 mM aqueous sucrose at pH 6.5.

[Pyranine] / μM	T_{m1} / ℃	ΔH_1 / kJ mol^{-1}	$C.U._1$	T_{m2} / ℃	ΔH_2 / kJ mol^{-1}	$C.U._2$
0	26.42	19.4	87	——	——	——
10	25.95	12.4	148	26.69	8.11	123
15	25.58	6.23	255	26.87	8.54	103
25	25.14	2.95	527	27.56	9.99	80
35	24.40	1.20	877	27.64	11.42	71

Table 2-9. Phase transition parameters for the liposomal membrane formed by DMPC and $N^+C_3U2C_{16}$ in a molar ratio of 5:5 upon addition of pyranine in 12 mM aqueous sucrose at pH 6.5.

[Pyranine] / μM	T_{m1} / ℃	ΔH_1 / kJ mol^{-1}	$C.U._1$	T_{m2} / ℃	ΔH_2 / kJ mol^{-1}	$C.U._2$
0	27.64	25.3	43	——	——	——
10	27.03	8.1	113	28.40	8.8	82
15	26.22	7.0	160	28.60	10.2	84
25	26.05	5.1	256	28.62	11.3	67
35	25.76	4.4	322	28.73	19.2	24

Table 2-10. Phase transition parameters for the liposomal membrane formed by DMPC and $N^+C_3U2C_{16}$ in a molar ratio of 3:7 upon addition of pyranine in 12 mM aqueous sucrose at pH 6.5.

[Pyranine] / μM	T_{m1} / ℃	ΔH_1 / kJ mol^{-1}	$C.U._1$	T_{m2} / ℃	ΔH_2 / kJ mol^{-1}	$C.U._2$
0	29.11	26.1	37	——	——	——
10	28.73	18.1	61	30.15	5.8	176
15	28.49	16.9	61	30.22	6.4	177
25	28.32	13.4	73	30.32	7.2	152
35	28.04	13.1	66	30.36	7.9	129

Effect of lipid composition on the phase separation behavior was reflected on the cooperative units. Figure 2-24 shows the relationship between the cooperative unit ($C.U._1$) for the DMPC-rich domain and pyranine concentration. The $C.U._1$ value for the liposomal membrane formed by DMPC to $N^+C_3U2C_{16}$ in a molar ratio of 7:3 drastically increased from 87 to 877, when concentration of pyranine increased from 0 to 35 μM.

On the other hand, the $C.U._1$ value increased in a range of 106-143 and 37-66 for the liposomal membrane formed by DMPC to $N^+C_3U2C_{16}$ in molar ratios of 8:2 and 3:7, respectively. The liposomal membrane formed by DMPC to $N^+C_3U2C_{16}$ in a molar ratio of 5:5 exhibited a moderate increase in $C.U._1$ value from 43 to 322. The difference in $C.U._1$ value change may reflect the extent of easiness for the phase separation to create the signal bound $N^+C_3U2C_{16}$-rich domain.

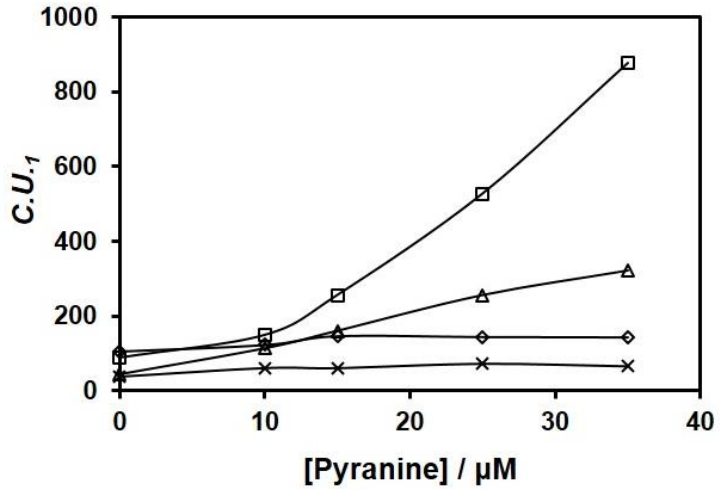

Figure 2-24. Dependences of cooperative unit ($C.U._1$) on pyranine concentration for the DMPC-rich phase in the liposomal membranes formed by DMPC and $N^+C_3U2C_{16}$ in a molar ratio of 8:2 (◊), 7:3 (□), 5:5 (△), and 3:7 (×) at pH 6.5. The data were taken from Tables 2-7, 2-8, 2-9, and 2-10.

2.3.2.4 Phase separation behavior evaluated by fluorescence microscopy

Interactions of pyranine as a chemical signal with liposomal membrane formed by a phospholipid and a cationic synthetic lipid were investigated by means of fluorescence

spectroscopy and differential scanning calorimetry. The results revealed that binding of the chemical signal onto the membrane surface through the multiple electrostatic interactions to induce the phase separation of liposomal membrane. In this part, the phase separation behavior was visualized directly by fluorescence microscopic observation.

Giant unilamellar vesicles (GUVs) formed by DMPC and $N^{+}C_3U2C_{16}$ in a molar ratio of 7:3 were prepared by electroformation method in 12 mM aqueous sucrose. The vesicular solution was placed on a temperature controlled sample stage of optical microscope. Aqueous stock solution of pyranine was injected into the vesicular solution by micro-syringe, and the fluorescence from pyranine molecules was monitored by a high sensitivity CCD camera. Time dependence of microscopic images was taken as snap shots and video mode.

Figure 2-25 shows time dependences of fluorescence microscopic images of GUV formed by DMPC and $N^{+}C_3U2C_{16}$ in a molar ratio of 7:3 upon addition of pyranine at different temperatures of 40, 26, and 18 ℃.

In the liquid crystalline state at 40 ℃, the vesicle was homogeneously stained with pyranine molecules with green fluorescence just after mixing, reflecting the binding of chemical signal on the membrane surface. However, the green vesicle promptly changed to the mottled one with high and low fluorescence intensity within 30 s. The results indicate that the vesicle contains pyranine rich and poor domains heterogeneously due to signal-induced phase separation. The former and latter domains presumably correspond to the $N^{+}C_3U2C_{16}$- and DMPC-rich domains as detected by differential scanning calorimetry.

In the phase transition temperature range at 26 ℃, the phase separation behavior

was also observed at a slower speed. The mottled vesicle stained with green color of pyranine was clearly observed after 2 min. A difference in the speed of phase separation reflects that the aggregation of 1:4 complex of pyranine with cationic lipids to form phase separated domains is slower in the phase transition temperature range than in liquid crystalline state, reflecting the difference in lateral diffusion of lipid molecules.

On the other hand, the signal-induced phase separation was not observed in the gel state of membrane, in which lateral diffusion of lipid molecules was practically frozen.

These results on the effect of thermotropic phase separation clarified by fluorescence microscopy are in good agreement with these observed by fluorescence spectroscopy mentioned above.

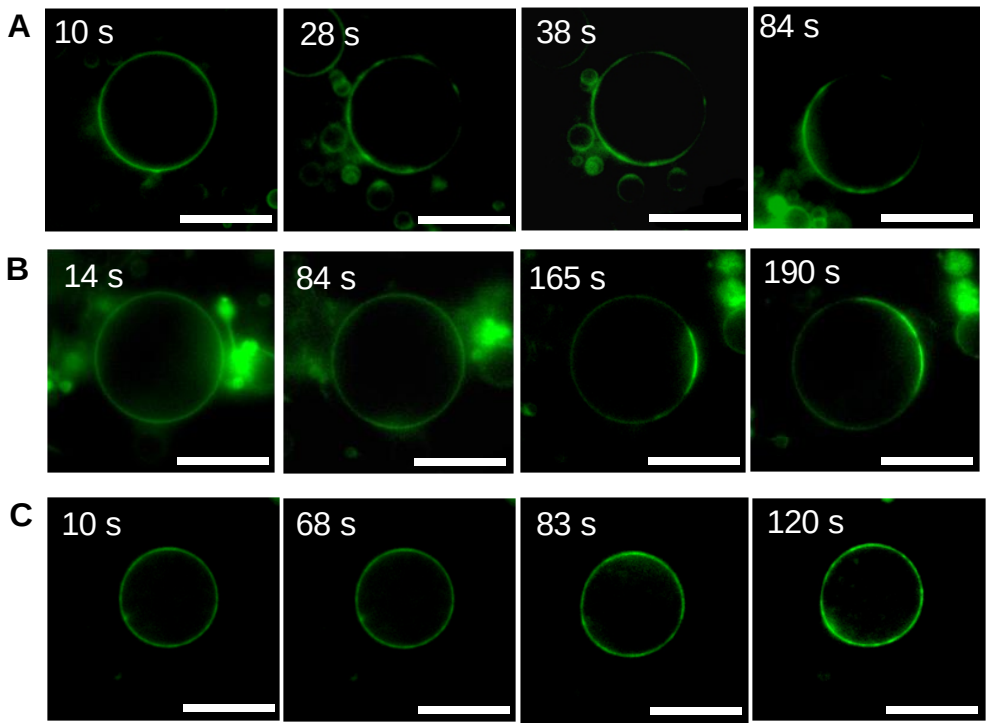

Figure 2-25. Time dependences of fluorescence microscopic images of giant vesicle formed by DMPC and $N^{+}C_3U2C_{16}$ in a molar ratio of 7:3 in 12 mM aqueous sucrose at 40 (A), 26 (B), and 18 ℃ (C) upon addition of 5 μM pyranine. Total lipid concentrations, 50 μM. Scale bars, 10 μm.

As for the effect of ionic strength on phase separation induced by signal binding, fluorescence spectroscopy and DSC measurement clarify that the increase in ionic strength significantly weakened the electrostatic interactions between pyranine and cationic vesicles to favor the miscibility of DMPC and $N^{+}C_3U2C_{16}$ even in the presence of chemical signal. Here, the effect of ionic strength on the phase separation behavior was also visualized by fluorescence microscopy.

As shown in Figure 2-26, the giant vesicle with phase separated lipid domains induced by signal binding was stained heterogeneously in the absence of inorganic salt. Upon addition of 2 mM potassium chloride into the vesicular solution, the heterogeneous fluorescence image gradually turned into homogeneous one. The results indicate that the two kinds of lipids in the liposomal membrane became miscible with the increase in ionic strength, since the stability of signal-cationic lipids complex, which induced the phase separation, was decreased.

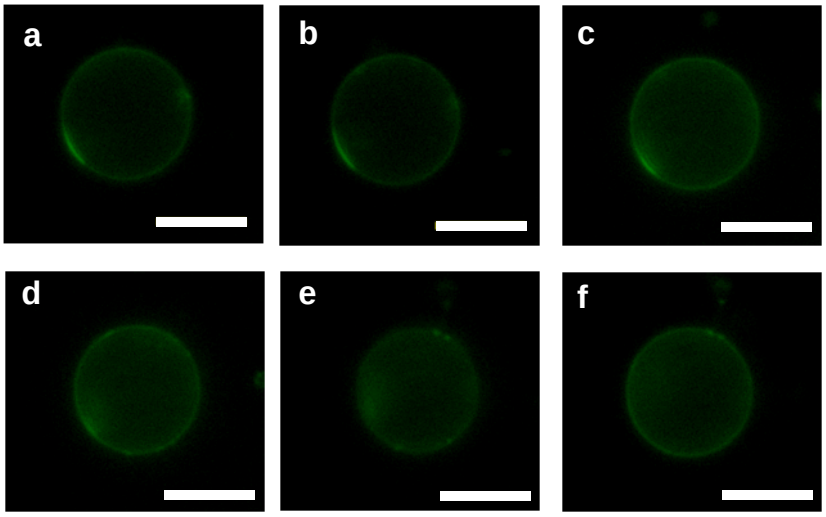

Figure 2-26. Time dependence of fluorescence microscopic image of giant vesicle formed by DMPC and $N^{+}C_3U2C_{16}$ in a molar ratio of 7:3 in 12 mM aqueous sucrose at 26 ℃ in the presence of 5 μM pyranine. Total lipid concentration, 50 μM. (a) is the image without salt, and (b), (c), (d), (e), and (f) are images after 10, 39, 61, 80, and 112 s upon addition of 2 mM potassium chloride. Scale bars, 10 μm.

The increase in concentration of pyranine relative to that of lipids affected the complex formation behavior between the chemical signal and the cationic lipids and the following membrane dynamics. When the concentration of pyranine was increased to 30 μM, the complex formation was enhanced and shrink of giant vesicle was observed in place of phase separation by means of fluorescence microscopy (Figure 2-27). Osmotic shrinkage of liposomal membranes is well-known phenomenon.[32] The increase in ionic strength outside vesicles caused the water permeability across the single bilayer membrane that is osmotically sensitive. After the shrinkage, the vesicles became to be spherical again.[32] In the present system, the observed shrinkage of liposomal membrane presumably comes from the difference of osmotic pressures in outer and inner aqueous phase of vesicle. After the shrinkage, the vesicle structure was still maintained.

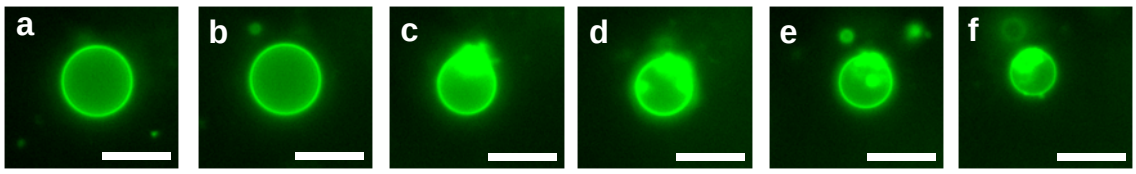

Figure 2-27. Time dependence of fluorescence microscopic image of giant vesicle formed by DMPC and $N^+C_3U2C_{16}$ in a molar ratio of 7:3 at 26 °C upon addition of pyranine. Total lipid concentration, 50 μM. (a) is the image immediately after addition of 10 μM pyranine. (b), (c), (d), (e), and (f) are images after 8, 18, 23, 40, and 63 s, respectively, upon further addition of 20 μM pyranine. Scale bars, 10 μm.

2.3.3 Budding and fission behavior evaluated by fluorescence microscopy

Interestingly, budding and followed fission of liposomal membrane were observed for the giant vesicles with phase separation. Figure 2-28 shows snap shots for time dependence of fluorescence microscopic image of giant vesicle formed by DMPC and $N^+C_3U2C_{16}$ in a molar ratio of 7:3 upon addition of pyranine. It should be noted that the

membrabne budding is arising from the region with higher fluorescence intensity, that is, $N^+C_3U2C_{16}$–rich domain. This is very important information to understand the mechanism of pyranine induced membrane division (vide infra).

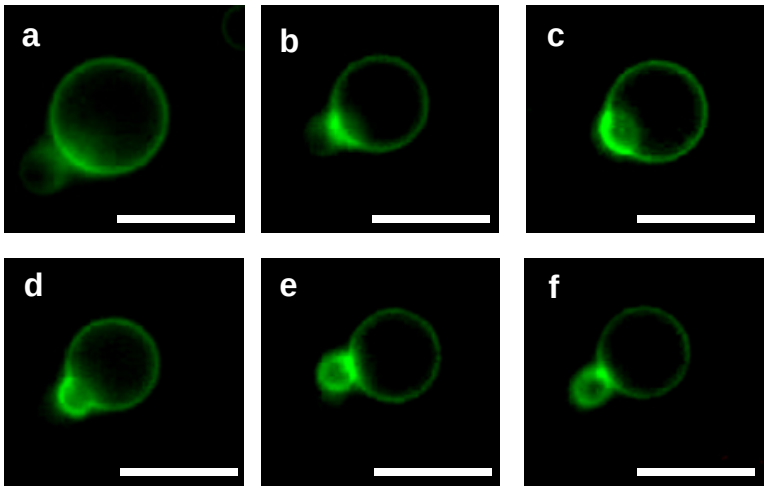

Figure 2-28. Time dependence of the budding process for giant vesicle formed by DMPC and $N^+C_3U2C_{16}$ in a molar ratio of 7:3 in 12 mM aqueous sucrose at 26 ℃ upon addition of 10 μM pyranine. (a), (b), (c), (d), (e) and (f) are images after 290, 330, 340, 346, 347, and 366 s, respectively, upon addition of pyranine. Scale bars, 10 μm.

The other examples of visualized membrane budding were shown in Figure 2-29. The giant vesicle, shown in Figure 2-29 (A), maintained its spherical shape without phase separation for 3 min upon addition of pyranine. The phase separation occurred after 3 min, and the pyranine-bound $N^+C_3U2C_{16}$–rich domain developed gradually with time to give large bright domain. The budding of vesicle observed after 4 min form the bright domain, and a relatively big daughter vesicle was produced.

In the case of giant vesicle, shown in Figure 2-29 (B), dynamic membrane behavior was basically analogous to the former vesicle. However, formation of phase separated domains was not so obvious than that of the former. Thus, two small daughter vesicles generated from the mother vesicle.

In the case of giant vesicle, shown in Figure 2-29 (C), the signal-induced phase

separation was clearly observed, but the size of bright domain was relatively small. As a result, a small daughter vesicle was produced from the mother vesicle.

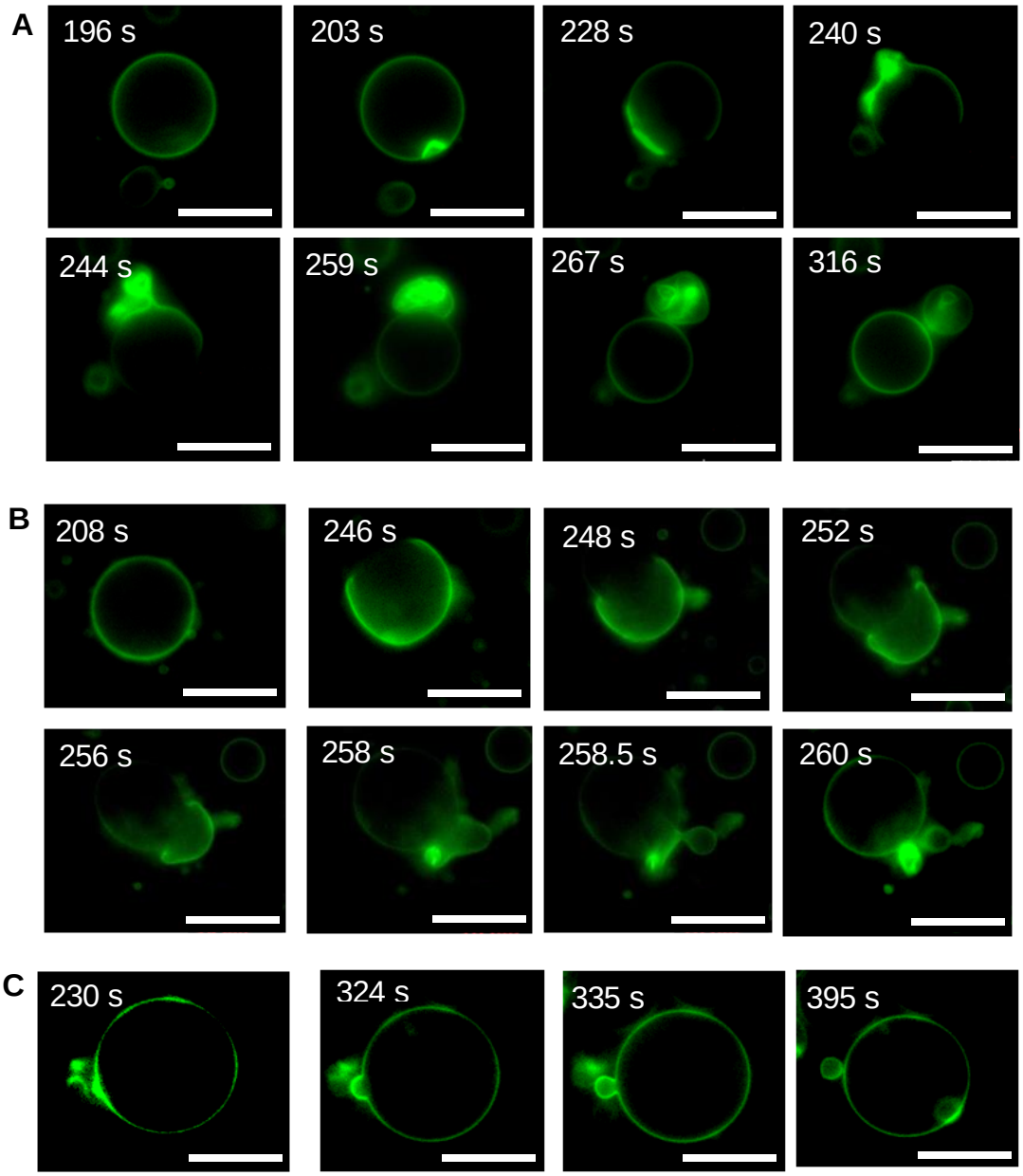

Figure 2-29. Time dependences of fluorescence microscopic images for giant vesicles formed by DMPC and $N^{+}C_3U2C_{16}$ in a molar ratio of 7:3 in 12 mM aqueous sucrose at 26 ^{o}C upon addition of 10 μM pyranine. (A), (B), and (C) represent that a big daughter vesicle, two small daughter vesicles, and a small daughter vesicle were generated from the mother vesicle, respectively. Scale bars, 10 μm.

The difference in membrane division behavior observed in Figure 2-29 may reflect

individuality characteristic to giant vesicles with micrometer size as cell membrane models.

As mentioned above, ionic strength significantly affects the signal binding to the membrane and followed phase separation behavior in the present liposomal membrane. Here, effect of ionic strength on membrane budding was evaluated by fluorescence microscopy. Figure 2-30 shows time dependence of fluorescence microscopic image of giant vesicle formed by DMPC and $N^{+}C_3U2C_{16}$ in a molar ratio of 7:3 in the presence of pyranine. Before addition of inorganic salt, the giant vesicle was in budding process. Upon addition of potassium chloride to the budding vesicular solution, the budded structure gradually went back to the original spherical shape with time. Accordingly, it became apparent that membrane budding behavior is capable of tuning by ionic strength.

Judging from the observation of membrane division process by optical microscopy, the daughter vesicles produced from the mother vesicles are so stable to keep their vesicular structures more than 1 hour without aggregation in the phase transition temperature range.

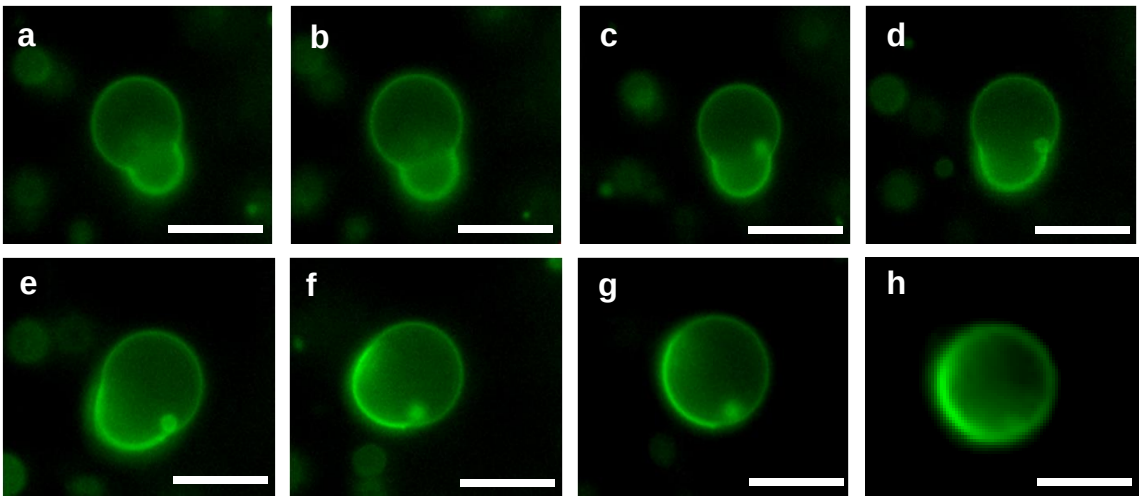

Figure 2-30. Time dependence of fluorescence microscopic image of giant vesicle formed by DMPC and $N^{+}C_3U2C_{16}$ in a molar ratio of 7:3 at 26 ℃ in the presence of 10 μM pyranine. Total lipid concentration, 50 μM. (a) is the image without salt, and (b), (c), (d), (e), (f), (g), and (h) are images after 5, 15, 50, 72, 105, 125, and 180 s upon addition of 2 mM potassium chloride. Scale bars, 10 μm.

2.3.4 Mechanism of membrane division induced by chemical signal

Based on the step-by-step investigation of the present membrane division system by means of fluorescence spectroscopy, differential scanning calorimetry, and fluorescence microscopy, a plausible mechanism of signal-induced membrane division is proposed here (Figure 2-31).

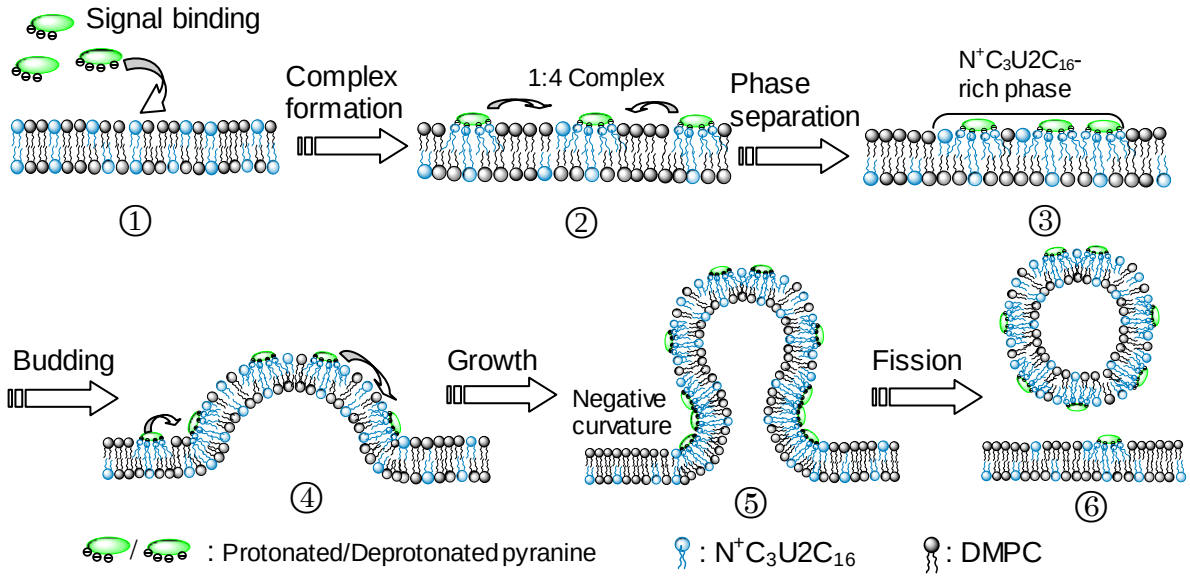

Figure 2-31. Mechanism of division of liposomal membrane formed by DMPC and $N^+C_3U2C_{16}$ induced by pyranine.

Asymmetric binding of pyranine on the membrane surface and appearance of $N^+C_3U2C_{16}$-rich domain in the outer leaflet of bilayer membrane afford that the two adjacent monolayers have a different lipid composition. Such asymmetric composition induces a positive spontaneous curvature towards the exterior that is denoted by C_{sp}.[33] According to Lipowsky's work,[34] the total energy (E) of a budding domain/phase as a function of budding curvature C is given by the following equation.

$$E = (LC - LC_{sp})^2 + \left(\frac{L}{\xi}\right)[1 - (\frac{LC}{2})^2]^{1/2} \qquad (2\text{-}12)$$

Where, ξ is a size-independent parameter reflecting the balance between two phases in the membrane. L is the diameter of the flat domain before budding. The parameters LC_{sp} and LC represent the spontaneous curvature and the budding structure, respectively. Hence budding energy E can be moderated by controlling the asymmetric composition that affects C_{sp}, and changing physical properties ξ of the two phases such

as membrane rigidity or the line tension at the interface of the two phases.

According to the above discussion, in this study, pyranine binding behavior and followi phase separation directly affect the asymmetry and the diameter of the $N^+C_3U2C_{16}$-rich phase. On these grounds, the systematic analysis was performed to clarify factors influencing the pyranine binding and followed phase separation performed. The results give us a good hint how to control the asymmetric composition and the dynamic membrane behavior in molecular level. For example, changing of ionic strength in aqueous solution significantly weakened the electrostatic interactions between pyranine and cationic vesicles, and favored the miscibility of DMPC and $N^+C_3U2C_{16}$ even in the presence of pyranine. Hence, the ionic strength change directly affects the asymmetric composition between outer and inner leaflet. Furthermore, ionic strength can adjust the dynamic process including the signal binding, phase separation, and budding.

In general, the spontaneous curvature formation effect has been used to explain membrane budding behavior or related membrane morphological changes. However, recent work claimed that asymmetric binding of external agent, or a kind of enzyme, phospholipase A2, that increases the spontaneous curvature of bilayer membrane, is not sufficient for membrane budding.[35] Therefore, it should be considered that the self-assembly formation of the 1:4 complex has another effect, besides the role in inducing spontaneous curvature, which induces the budding and fission behavior.

Budding growth process requires the formation of transient structure with negative curvature at the fission neck, and followed fission process is induced by destabilization of the neck.[34] Reported results have showed that the presence of lipids favoring formation of such negative curvature at the neck promotes the fission behavior.[33,36,37]

In this work, we have emphasized that the 1:4 complex formation of pyranine with cationic lipids caused the dehydration of head group of $N^+C_3U2C_{16}$, leading the lipid packing from the cylindrical to the conical shape. In general, the lipids with conical shape, such as phosphatidylethanolamine, facilitate formation of membrane structures with negative curvature.[37] Hence, it is possible that the 1:4 complex including the conical shape of $N^+C_3U2C_{16}$ are preferably concentrated in the neck region, stabilizing the thermodynamically unstable neck structure to afford membrane fission. Fluorescence microscopic images of captured vesicles with budding structure support this consideration (Figure 2-32).

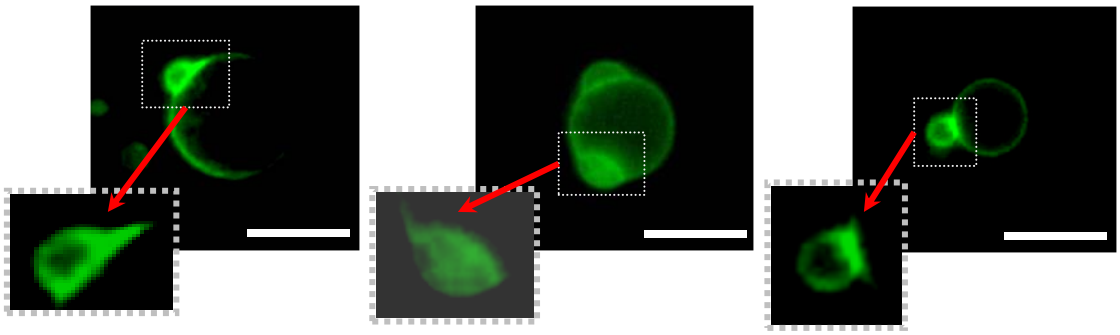

Figure 2-32. Fluorescence microscopic images of representative budding vesicles with negative surface curvature formed by DMPC and $N^+C_3U2C_{16}$ in a molar ratio of 7:3 upon addition of pyranine. The negative curvature regions are highlighted and zoomed. Scale bars, 10 μm.

2.4 Conclusions

In this chapter, I investigated the division behavior of artificial bilayer membrane composed of a zwitterionic phospholipid, DMPC, and a cationic synthetic lipid, $N^{+}C_3U2C_{16}$, induced by a fluorescent chemical signal, pyranine. This is a good model system to investigate the mechanism of dynamic membrane behavior in detail, since the whole process can be analyzed by separating into the following unit processses as schematically shown in Figure 2-31; (1) signal binding to membrane, (2) phase separation of membrane, and (3) membrane budding and followed fission.

As for the first unit process, the signal binding behavior on the membrane surface was analyzed thermodynamically and kinetically by using fluorescence spectroscopy. A few factors, such as charge density of membrane surface, membrane phase state and medium ionic strength, significantly affect the signal binding behavior. The tetraanionic signal molecule binds to the cationic lipid in a stoichiometry of 1:4 through the multipoint electrostatic interactions. The resulting lateral relocation of cationic lipid molecules was evaluated by monitoring time-course of fluorescence intensity. When the membrane was in the phase transition state from the gel to liquid-crystalline phase, the dynamics of signal binding process was easily observed in a time scale of seconds. As for the second unit process, the phase separation behavior followed by signal binding was characterized by differential scanning calorimetry. The results showed that the signal binding induced the phase separation of membrane to form two domains composed of cationic lipid-rich and phospholipid-rich domain. As for the final budding and fission process, the dynamic membrane morphological changes were observed in detail by fluorescence microscopy in both static and video mode.

Accordingly, the present dynamic membrane behavior, including signal binding,

phase separation and budding and followed fission, were systematically analyzed and the mechanism of membrane division induced by a chemical signal was proposed. On these grounds, I also demonstrated that phase separation and budding are adjustable by changing the ionic strength.

There are several published works on non-biological liposomal division, however, almost of them have reported on results based on optical microscopy and discussion trying physical interpretation without additional experimental evidences. As compared with these previous works, the present study has three major advantages. First, the step-by-step analysis of present fission system can tell us what kinds of factors affect the dynamic membrane processes. Second, the step-by-step analysis provides a useful guidepost how to adjust the dynamic process. For example, change of ionic strength made the budding vesicles to back to the original shape. Third, pyranine as a fission trigger is a good molecular probe to monitor the dynamic membrane processes using fluorescence microscopy.

2.5 References.

(1) Meer, G. V.; Sprong, H. *Curr. Opin. Cell Biol.* **2004,** *16*, 373-378.

(2) Melissa, A. E.; Smith, C.; Owen, D. *Nature Rev. Mol. Cell Biol.* **2006,** 32-44.

(3) Springer, S.; Spang, A.; Schekman, R. *Cell* **1999**, *97*, 145-148.

(4) Menger, F. M.; Balachander, N. *J. Am. Chem. Soc.* **1992-12***4*, 5862-5863.

(5) Kaler, E. W.; Murthy, A. K.; Rodriguez, B. E.; Zasadzinski, J. A. N. *Science* **1989**, *245*, 1371-1374.

(6) Hanczyc, M. M.; Fujikawa, S. M.; Szostak, J. W. *Science* **2003**, *302*, 618-622.

(7) Takakura, K.; Sugawara, T. *Langmuir* **2004,** *20*, 3832-3834,

(8) Nomura, F.; Nagata, M.; Inaba, T.; Hiramatsu, H.; Hotani, H.; Takiguchi, K. *Proc. Natl. Acad. Sci. U.S.A.* **2001,** *98*, 2340-2345.

(9) Hotani, H.; Nomura, F.; Suzuki, Y. *Curr. Opin. Colloid Interface Sci.* **1999,** *4*, 358-368.

(10) Wang, Z. H.; Yashuhara, K.; Ito, H.; Mukai, M.; Kikuchi, J. *Chem. Lett.* **2010,** *39*, 54-55.

(11) Angelova, M. I.; Sol éau, S.; M él éard, P.; Faucon, J. F.; Bothorel, P. *Prog Colloid Polym Sci.* **1992,** *89*, 127-131.

(12) Nomura, T.; Escabi-Perez, J. R.; Sunamoto, J.; Fendler, J. H. *J. Am.* Chem. *Soc.***1980,** *102*, 1484-1488.

(13) Kano, K.; Fendler, J. H. *Biochim. Biophys. Acta.* ***1*978,** *509*, 289-299.

(14) Kondo, H.; Miwa, I.; Sunamoto, J. *J. Phys. Chem.* **1982,** *86*, 4826-4831.

(15) Smith, K. K.; Kaufmann, K. J.; Huppert, D.; Gutman, M. *Chem. Phys. Lett.*, **1979,** *64*, 522-527.

(16) Pan, B.; Chakraborty, R.; Bergiund, K. A. *J. Cryst. Growth* **1993,** *130*, 587-599.

(17) (a) Barrash-Shiftan, N.; Brina, B.; Pines, E. *J. Phys. Org. Chem.* **1998,** *11*, 743-746; (b) Tran-Thi, T.-H.; Prayer, C.; Millie, P.; Uznanski, P.; Hynes, J. T. *J. Phys. Chem. A* **2002,** *106*, 2244-2255.

(18) Yilmaz, Y.; Uysal, N.; Gelir, A.; Guney, O.; Demet, K.; Gogebakan, A. S.; Oner, A. *Spectrochim. Acta, Part A* **2009,** *72*, 332-338.

(19) Evingu, G. A.; Aktas, D. K.; Pekcan, O. *Phase Transitions,* **2009,** *82*, 53-65.

(20) Evigur, **A. G.**; Pekcan, O.; O. *Adv. Polym. Tech.* **2013,** *32*, E231-E240.

(21) Montal, M.; Gitler, C. *Bioenergetics* **1973**, *4*, 363-382.

(22) Nomuna, T.; Sunamoto, J. *Bull. Chem. Soc. Jpn.* **1981,** *54*, 1239-1240.

(23) Chapman, D.; Williams, R. M.; Ladbrooke, B. D. *Chem. Phys. Lipids* **1967,** *1*, 445-475.

(24) Schroeder, U. K. O.; Tirrell, D. A. *Macromolecules* **1989,** *22*, 765-769.

(25) (a) Osamu T.; Masumi V.; Akira S.; Hiroo N. *Bull. Chem. Soc. Jpn.* **2007,** *80*, 1723-1730; (b) Huang, C.; Mason, J. T. *Proc. Natl. Acad. Sci. USA*, **1978,** *75*, 308-310.

(26) Johann, C.; Garidel, P.; Mennicke, L.; Blume, A. *Biophysical J.* **1996,** *71*, 3215-3228.

(27) Wiener, J. R.; Wagner, R. R.; Freire, E. *Biochemistry* **1983,** *22*, 6117-6123.

(28) (a) Katagiri, K.; Hashizume, M.; Ariga, K.; Terashima, T.; Kikuchi, J. *Chem. Eur. J.* **2007,** *13*, 5272-5281; (b) Hashizume, M.; Saeki, I.; Otsuki, M.; Kikuchi, J. *J. Sol-Gel Sci. Techn.* **2006,** *40*, 227-232; (c) Katagiri, K.; Hamasaki, R.; Ariga, K.; Kikuchi, J. *Langmuir* **2002,** *18*, 6709-6711.

(29) Agafonov, A. V.; Gritsenko, E. N.; Shlyapnikova, E. A.; Kharakoz, D. P.; Belosludtseva, N. V.; Lezhnev, E. I.; Saris, N. L.; Mironova, G. D. *J. Membrane*

Biol. **2007,** *215*, 57-68.

(30) (a) Binder, W. H.; Barragan, V.; Menger, F. M. *Angew. Chem. Int. Ed*. **2003**, *42*, 5802-5827; (b) Jogensen, K.; Sperotto, M. M.; Mouritsen, O. G.; Ipsen, J. H.; Zuckermann, M. J. *Biochim. Biophys. Acta* **1993**, *1152*, 135-145.

(31) (a) Nielsen, L. K.; Balashev, K.; Callisen, T. H; Jornholm, B. T. *Biophys. J*. **2002,** *83*, 2617–2624; (b) Ohnishi, S.; Ito, T. *Biochemistry*, **1974,** *13*, 881-887.

(32) Reeves, J. P.; Dowben, R. M. *J. Cell Physiol*. **1969,** *73*, 49-60.

(33) Staneva, G.; Seigneuret, M.; Koumanov, K.; Trugnan, G.;Angelova, M. I. *Chem. Phys. Lipids* **2005,** *136*, 55-66.

(34) Lipowsky, R. *Biophys. J*. **1993,** *64*, 1133-1138.

(35) Staneva, G.; Miglena, I.; Koumanov, A. K. *Chem. Phys. Lipids* **2004**, *129*, 53-62.

(36) Kozlovsky, Y.; Kozlov, M. M. *Biophys. J*. **2003,** *85*, 85-96.

(37) Chen, C. M.; Higgs, P. G.; Mac-Kintosh, F. C. *Phys. Rev. Lett*. **1997,** *79*, 1579-1582.

Chapter 3: Synthetic cell division system: Effect of nonbilayer forming lipid on division of liposomal membranes

3.1 Introduction

Biological membranes are constructed with various kinds of lipid mixture containing bilayer- and nonbilayer-forming lipids. Pure nonbilayer-forming lipids, such as phosphatidylehanolamine (PE) and monogalactosyldiacylglycerol (MGDG), form nonbilayer structure, or inverted hexagonal phase (H_{II}). The mixture of bilayer- and nonbilayer-forming lipids usually takes bilayer phase in biological membranes.[1] The H_{II} phase was first recognized by X-ray diffraction[2] and then detected by ^{31}P-NMR.[3] Nonbilayer phases sometimes appear in liposomal membranes upon heating above physiological temperature, dehydration of lipid head group, or being treated with divalent cations.[4] Up to the present time, much attention has been paid to construct the nonbilayer structures, and various nonbilayer-forming lipid molecules have been developed to study physicochemical properties governing the phase transition from the bilayer to the nonbilayer phase.[5]

Recent studies have suggested that biological functions such as cell fusion and division are relative to the formation of nonbilayer structures.[6] For example, a nonbilayer forming lipid, phosphatidylethanolamine, is a dominant lipid component of most living organisms, and this lipid facilitates rapid trans-bilayer movement leading to membrane fusion, which has been confirmed in model membrane studies.[7] In practice, the nonbilayer structures have been observed at the jointing point of apposed membrane during fusion process by freeze-fracture transmission electron microscopy[8] and ^{31}P-NMR measurements[3].

Much effort has also been devoted to clarify the intermediate state during the membrane fusion process. It is strongly suggested that the membrane fusion requires participation of nonblilayer-forming lipids and that the bilayer lipid arrangement changes into transient nonbilayer configuration at the intermediate stage of fusion. The membrane fusion includes three sequential stages; (a) the membrane adhesion, (b) the jointing and (c) fission of fusing membranes as shown in Figure 3-1.[9] It is proposed that the apposed membrane forms polar contact points in the adhesion stage, which requires local dehydration to decrease the hydration force.[10] Hydration force provides significant repulsive pressure between the interacting membranes to prevent vesicles approaching each other.[11] The dehydration behavior is also important to adopt nonbilayer structures. Thus, some kinds of nonbilayer-forming lipids, such as PE and MGDG, are known to enhance the fusion of liposomes.[12]

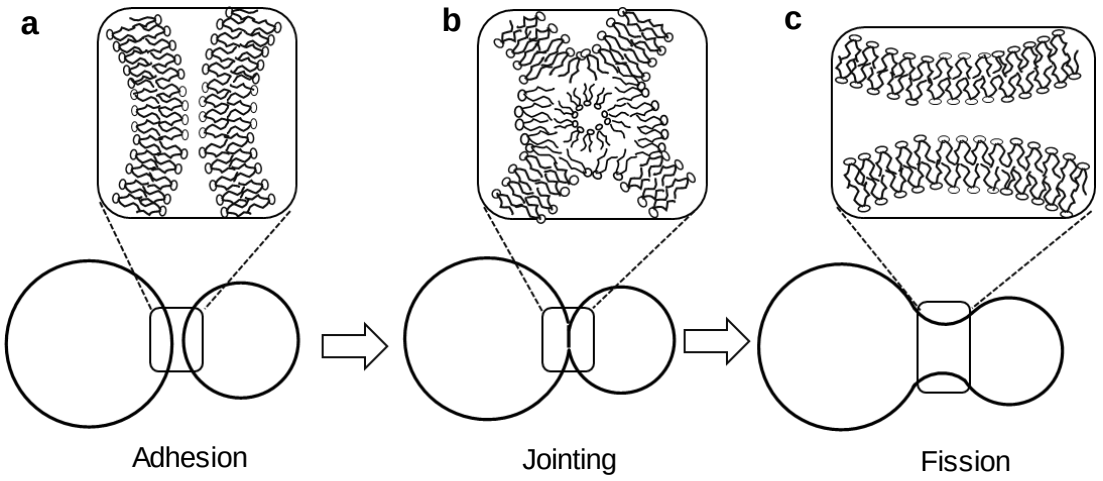

Figure 3-1. Drawings of membrane fusion intermediates due to the presence of nonbilayer forming lipids.[9]

Inspired by the fusion mechanism, membrane division, the reverse process of fusion, is also expected to undergo via the same intermediate states. The difference is that apposed membranes for division and fusion are located in same and different vesicles,

respectively. Such assumption was suggested for biological membrane division of Chinese hamster ovary cells.[13] In this study, phosphatidylethanolamine lipids were locally concentrated at the cleavage furrow during the late telophase of cytokinesis. The result suggests that redistribution of nonbilayer forming lipids play a pivotal role in mediating a coordinate movement between the contacting part and residual plasma membrane to achieve successful cell division.[13] However, there are few reports on the roles of nonbilayer structures or nonbilayer-forming lipids in division of artificial membranes.

In this study, a synthetic peptide lipid having quinoyl group as a polar head moiety, QC_5AlaC_{14}, which forms nonbilayer structure,[14] was employed to evaluate the participation of nonbilayer forming lipid in synthetic cell division. Giant vesicles composed of a bilayer forming phospholipid (DMPC) and a nonbilayer forming lipid (QC_5AlaC_{14}) underwent membrane division, when the binary membrane was in the transition state from gel to liquid-crystalline phase. On the other hand, membrane division behavior was not observed for liposome in the absence of nonbilayer forming lipid.

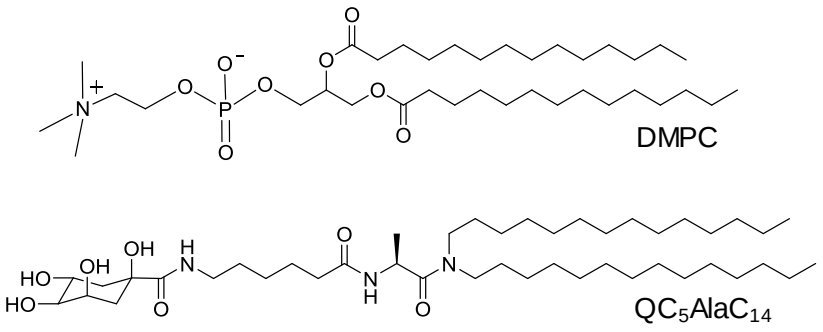

Chart 3-1. Srtuctures of bilayer and nonbiayer forming lipid.

The results suggested a possibility of the presence of nonbilayer structure as a transient intermediate structure in the membrane division process as schematically shown in Figure 3-2, which would be similar to the reverse-fusion behavior.

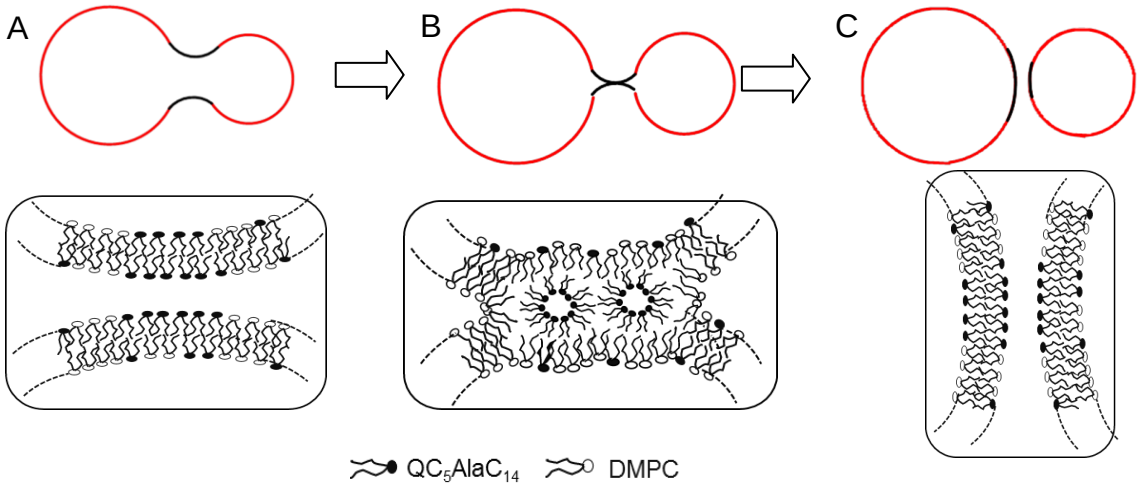

Figure 3-2. Proposed mechanism of division of liposomal membrane formed by a phospholipid and a nonbilayer forming lipid through formation of transient nonbilayer structures.

In order to evaluate the presence of intermediate nonbilayer structures in membrane fusion, fluorescence leakage experiments have been previously proposed.[37] This technique was also applied to the present membrane division system for evaluating intermediate structures in the membrane jointing region.

3.2 Experimental section

3.2.1 Materials and methods

Materials

Unless otherwise stated, all reagents and chemicals were obtained commercially and used without further purification. The nonionic peptide lipid, QC_5AlaC_{14}, and tetraacetylquinoyl chloride were synthesized according to the previously reported procedures as shown in Scheme 3-1. Ditetradecylamine was prepared by the reaction of

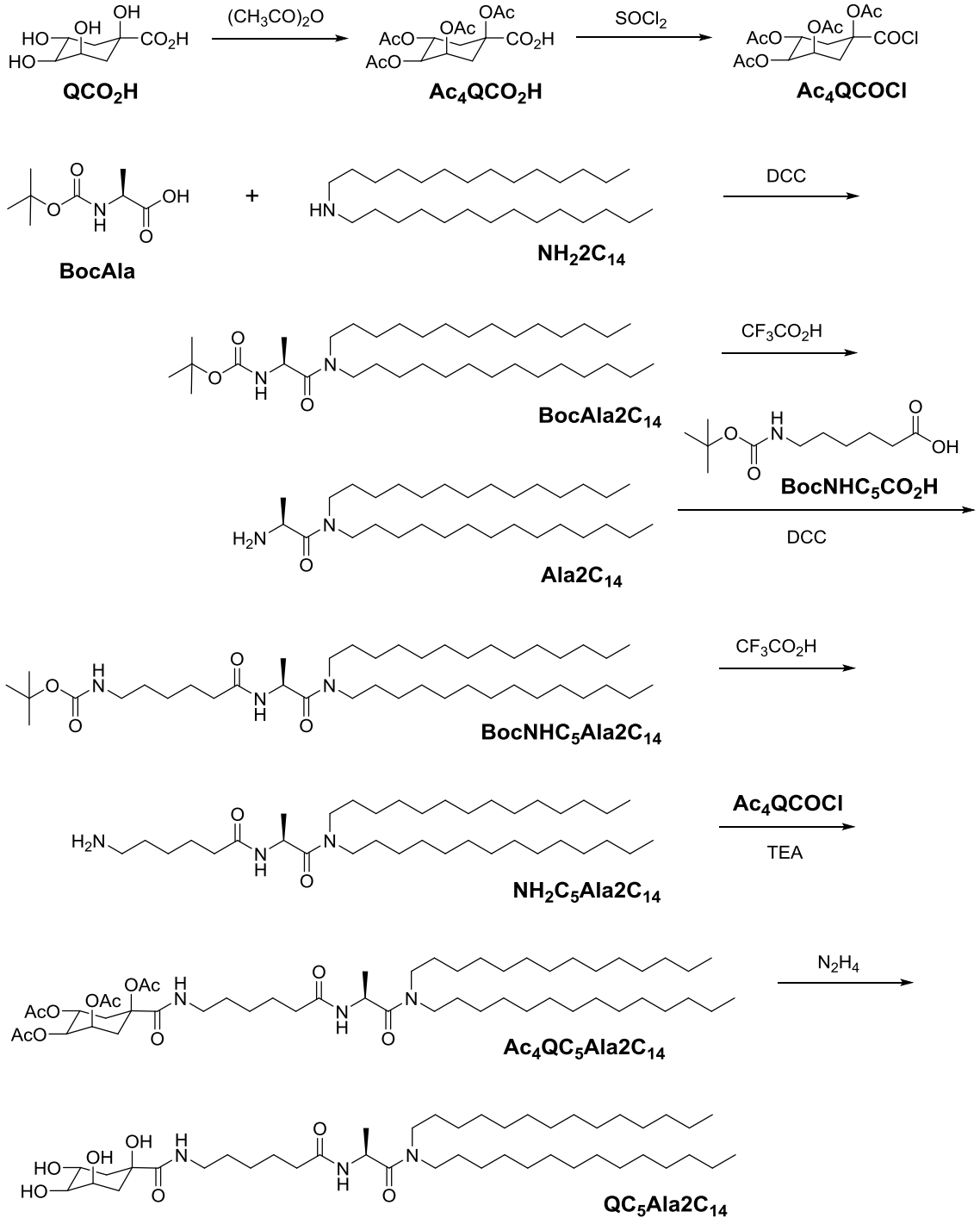
(CH3CO)2O
SOCl2
QCO2H
Ac4QCO2H
Ac4QCOCl
BocAla
NH2C14
DCC
CF3CO2H
BocAla2C14
BocNHC5CO2H
Ala2C14
DCC
CF3CO2H
BocNHC5Ala2C14
Ac4QCOCl
TEA
NH2C5Ala2C14
N2H4
Ac4QC5Ala2C14
QC5Ala2C14

Scheme 3-1

tetradecylamine with 1-bromotetradecane in the presence of sodium carbonate and purified by recrystallization from hexane. 1,2-Dimyristoyl-*sn*-glycero-3-phosphocholine (DMPC, lyophilized powder) was purchased from Avanti Polar Lipids. Quinic acid was commercially obtained from Tokyo Chemical Industry CO., LTD. *N*-(t-Butoxycarbonyl)-L-alanine was obtained from Peptide Institute. Trifluoroacetic acid (TFA) was purchased from Sigma-Aldrich. 8-Aminonaphthalene-1,3,6-trisulfonic acid disodium salt (ANTS) and *p*-xylenebispyridinium bromide (DPX) were purchased from Invitrogen. 1,2-Dihexadecanoyl-*sn*-glycero-3-phosphoethanolamine-*N*-(lissamine rhodamine B sulfonyl) ammonium salt (Rh-DPPE) was obtained from Avanti Polar Lipids.

Measurements

High performance liquid chromatography (HPLC) used for purification was a JAI Model instrument (Japan Analytical Instruments) equipped with JAIGEL-H-P columns. ^{1}H–NMR spectra were recorded on a JEOL JNM-EPC600NK spectrometer. Mass spectra were conducted by a JEOL JMS-700 spectrometer.

The gel to liquid-crystalline phase transition of liposomes was evaluated using a ultra high sensitive differential scanning calorimeter (VP-DSC, MicroCal Inc.). Fluorescence spectra were recorded on a HITACHI F-7000 spectrofluorometer. The optical microscopic observations were carried out using an Olympus IX71 epifluorescence microscope, and the fluorescent images were recorded using andigital camera C11440. Cryogenic transmission electron microscopy (TEM, JEM-3100FEF; JEOL) was performed using an acceleration voltage of 300 kV.

Leakage measurements of fluorescent ANTS encapsulated into liposomal membrane were done in the presence of DPX as a fluorescence quencher distributed inside of

vesicle. 1mM aqueous LUV (0.7 ml) formed by DMPC and QC_5AlaC_{14} in a molar ratio of 3:1 was diluted to 3 ml after gel filtration chromatography (Sepharose Cl-4B). The total lipid concentration of collected fraction (0.5 ml) was 0.23 mM. This fraction was diluted to 2 ml by 100 mM aqueous NaCl. The final lipid concentration was 58 μM. Fluorescence spectra were taken under following conditions; slit width for excitation and emission of 5 and 10 nm, respectively; excitation and excitation wavelength of 360 and 500 nm, respectively. The leakage of ANTS was calculated as $(F\text{-}F_0)/F_{max}$, where F, F_0, and F_{max} were fluorescence intensities at measured, initial, and final time, respectively. The F_{max} value corresponds to 100% leakage upon addition of 0.5% aqueous Triton X-100 to disrupt the liposomal membrane.

For quantitative characterization of GUVs morphologies, I introduced a distortion index (D), a measure of deviation from the spherical shape. The distortion index was defined as equation 3-1, where l and S were perimeter and area of GUVs on 2D images, respectively, analyzed using a software, ImageJ.

$$D = (l^2 / S) - 4\pi \qquad (3\text{-}1)$$

3.2.2 Synthesis of nonbilayer forming nonionic peptide lipid

Tetraacetylquinic acid (Ac_4QCO_2H)

Quinic acid (5.0 g, 20 mmol) was dissolved in pyridine (10 ml) at 70 ℃. After cooling down to 0 ℃, the solution was added into acetic anhydride (5.0 ml, 53 mmol). The reaction mixture was stirred at room temperature for 22 h. Then saturated aqueous NaCl including HCl was added to the reaction mixture, and the product was extracted with chloroform. The crude product was recrystallized three-time from isopropylalcohol and petroleum ether to give Ac_4QCO_2H as white solid. Yield, 5.3 g (74%).

^{1}H-NMR ($CDCl_3$, 400MHz, TMS): δ/ppm 1.95 (1H, dd, J =13.4, 10.8 Hz,

axial-*H*-6), 2.05 (9H, s, OAc), 2.14 (3H, s, *OAc*-1), 2.38 (1H, dd, *J* = 15.6, 3.8 Hz, axcial-*H*-2), 2.64 (2H, tt, *J* = 24.5, 6.9 Hz, equatorial-*H*-2, equatorial-*H*-6), 5.03 (1H, dd, *J* = 9.9, 3.3 Hz, axial-*H*-4), 5.45 (1H, td, *J* = 10.1, 4.3 Hz, axcial-*H*-5), 5.58 (1H, q, *J* = 3.5 Hz, equatorial-*H*-3).

Tetraacetylquinoly chloride (Ac$_4$QCOCl)

Tetraacetylquinic acid (1.5 g, 4.2 mmol) was dissolved in benzene (4 ml) at 80 ℃, and thionyl chloride (0.8 ml, 10 mmol) was added to the mixture. The reaction mixture was stirred at 80 ℃ for 3 h. The solvent was removed under reduced pressure and the crude product was recrystallized from diethyl ether and petroleum ether to give Ac$_4$QCOCl as white solid. Yield, 1.2 g (77%).

^{1}H-NMR ($CDCl_3$, 400MHz, TMS): δ/ppm 1.99 (1H, dd, *J* = 13.7, 10.1 Hz, axial-*H*-6), 2.05 (6H, s, OAc), 2.20 (3H, s, OAc-1), 2.45 (1H, dd, *J* = 15.7, 3.3 Hz, axcial-*H*-2), 2.641 (2H, tt, *J* = 14.4, 5.4, 2.4 Hz, equatorial-*H*-2, equatorial-*H*-6), 5.00-5.06 (1H, m, *J* = 8.2, 2.3 Hz, axial-*H*-4), 5.42 (1H, ddd, *J* = 19.7, 10.2, 4.3 Hz, axcial-*H*-5), 5.57 (1H, q, *J* = 4.0 Hz, equatorial-*H*-3).

N,N-Ditetradecyl-N$^{\alpha}$-(t-butoxycarbonyl)-L- alaninamide (BocAla2C$_{14}$)

N,N'-Dicyclohexylcarbodiimide (2.4 g, 12 mmol) was added to *N*-(t-butoxycarbonyl)-L-alanine (2.2 g, 12 mmol) in dry dichloromethane (50 ml) at 0 ℃ for 15 min. *N,N*-Ditertadecylamine (4.7 g, 12 mmol)) in dry dichloromethane (30 ml) was added dropwise into the mixture, and stirred at 0 ℃ for 30 min, then at room temperature for 15 h. The precipitated *N,N'*-dicyclohexylurea (DCUrea) was removed by filtration and solvent was evaporated under reduced pressure. The residue was dissolved in ethyl acetate at 4 ℃ for overnight. After removal of insoluble DCUrea by filtration, solvent was evaporated under reduced pressure. The crude product was

purified by column of silica gel using ethyl acetate-hexane (1:9 v/v) as eluant to give BocAla2C_{14} as colorless oil. Yield, 4.3 g (63%).

^{1}H-NMR ($CDCl_3$, 400MHz, TMS): δ/ppm 0.88 [6H, t, J = 6.6 Hz, $(CH_2)_{13}CH_3$], 1.28 [47H, m, J = 8.1 Hz, $CH_2(CH_2)_{11}CH_3$, $CH(CH_3)$], 1.43 [9H, s, $(CH_3)_3C$], 3.11-3.18 [1H, m, $CH_2(CH_2)_{13}CH_3$], 3.24 [2H, J = 7.5 Hz, $CH_2(CH_2)_{13}CH_3$], 3.41-3.48 [1H, m, $CH_2(CH_2)_{13}CH_3$], 4.53-4.60 [1H, m, CH_3CHCO], 5.46 [1 H, d, J = 7.7 Hz, OCONH].

N,N-Ditetradecyl-N$^{\alpha}$-(6-(t-butoxycarbonylamino)hexanoyl)-L-alaninamide (BocNHC$_5$Ala2C$_{14}$)

Trifluoroacetic acid (5.2 g, 44 mmol) was added to BocAla2C_{14} (1.9 g, 3.2 mmol) in dry dichloromethane (8 ml) and the mixture was stirred at room temperature for 2 h. After evaporation of solvent, the residue was dissolved in chloroform (20 ml) and washed with 5% aqueous $NaHCO_3$ (30 ml x 3). Evaporation of solvent gave Ala2C_{14} as colorless oil. Yield, 1.2 g (79%). Elimination of t-butoxycarbonyl group was confirmed by ^{1}H-NMR.

N,N'-Dicyclohexylcarbodiimide (0.74 g, 3.2 mmol) was added to N-(t-butoxycarbonyl)-L-alanine (0.72 g, 2.9 mmol) in dry dichloromethane (50 ml) at 0 ℃ for 15 min. N,N-Ditertadecylamine (4.7 g, 12 mmol)) in dry dichloromethane (30 ml) was added dropwise into the mixture, and stirred at 0 ℃ for 15 min, followed by addition of the amine (Ala2C_{14}) (1.7 g, 3.2 mmol). The mixture was stirred for 3 h at 0 ℃ and for 14 h at room temperature. The precipitated *N,N'*-dicyclohexylurea (DCUrea) was removed by filtration and solvent was evaporated under reduced pressure. The residue was dissolved in ethyl acetate (32 ml). The solution was then washed with 10% aqueous citric acid (10 ml x 2), water (50 ml), 4% aqueous sodium hydrogen carbonate (10 ml x 2), and water (10 ml x 2) in this sequence. After being dried over

sodium sulfate, the solution was evaporated to dryness in vacuum. The residue was chromatographed on a column of silica gel using ethyl acetate as an eluant. A white solid ($BocNHC_5Ala2C_{14}$), yield, 2.0 g (85%).

^{1}H-NMR ($CDCl_3$, 400MHz, TMS): δ/ppm 0.88 [6 H, t, J = 6.6 Hz $(CH_2)_{13}CH_3$], 1.29 [47 H, m, J = 12.3 Hz, $CH_2(CH_2)_{11}CH_3$, $CH(CH_3)$], 1.44 [9 H, s, $(CH_3)_3C$], 1.49 [4H, d, J = 6.6 Hz, $CH_2(CH_2)(CH_2)_{11}$], 2.19 [2 H, t, J = 7.5 Hz CH_2CONH], 3.11 [3 H, d, J = 6.6 Hz, $NCH_2(CH_2)_{12}$, $CONHCH_2$], 3.20-3.28 [2 H, m, J = 6.6 Hz, $NCH_2(CH_2)_{12}$], 3.46-3.53 [1 H, m, $NCH_2(CH_2)_{12}$], 4.56 [1 H, d, CH_2CONH], 4.83 [1H, t, J = 7.0 Hz, $(CH_3)_3CH$], 6.51 [l H, d, J = 7.3 Hz $OCONH$].

N,N-Ditetradecyl-N$^{\alpha}$-(6-(tetraacetylquinoyl)hexanoyl)-L-alaninamide ($AcQC_5AlaC_{14}$)

Trifluoroacetic acid (15 g, 130 mmol) was added to $BocNHC_5Ala2C_{14}$ (3.9 g, 5.6 mmol) in dry dichloromethane (37 ml) and the mixture was stirred at room temperature for 2 h. After evaporation of solvent, the residue was dissolved in chloroform (37 ml) and washed with 5% aqueous $NaHCO_3$ (50 ml x 3). Evaporation of solvent gave $NH_2C_5Ala2C_{14}$ as pale brown oil. Yield, 3.0 g (91%). Elimination of t-butoxylcarbonyl group was confirmed by ^{1}H -NMR.

$NH_2C_5Ala2C_{14}$ (1.5 g, 2.3 mmol) was dissolved in dry dichloromethane (11 ml) and cooled to 0 ℃. Triethylamine (2.5 g, 17 mmol) was added to the solution. To this mixture, tetraacetylquinoyl chloride (0.92 g, 2.5 mmol) in dry dichloromethane (5 ml) was added dropwise at 0 ℃ for 5 min. The mixture was stirred at room temperature for 3 h. The reaction mixture was washed with 10% aqueous citric acid (14 ml x 2) and 5% aqueous $NaHCO_3$ (14 ml x 3) in this sequence and dried with Na_2SO_4. The crude product was purified by HPLC to give $AcQC_5AlaC_{14}$ as pale brown viscous oil. Yield, 0.83 g (36%).

^{1}H-NMR ($CDCl_3$, 400MHz, TMS): δ/ppm 0.88 [6 H, t, J = 6.6 Hz $(CH_2)_{13}CH_3$], 1.29 [51 H, m, J = 12.4 Hz, $CH_2(CH_2)_{12}CH_3$, $CH(CH_3)$], 1.54 [6 H, dd, J = 32.8, 25.4 Hz, $HNCH_2(CH_2)_3CH_2CO$], 2.04 [12 H, m, $OCOCH_3$], 2.16 [2 H, dd, J = 19.8, 14.6 Hz, CH_2CONH], 3.07-3.53 [6 H, m, $CONHCH_2$, $NCH_2(CH_2)_{12}CH_3$], 4.79-5.06 [4 H, m, $CH(CH_3)$], 5.98 [l H, t, J = 5.3 Hz, $CONHCH_2$], 6.54 [l H, d, J = 7.3Hz, $OCNHCH(CH_3)$.

N,N-Ditetradecyl-N$^{\alpha}$-(6-quinoylhexanoyl)-L-alaninamide (QC_5AlaC_{14})

Hydrazine monohydrate (0.76 g, 17 mmol)) was added to $AcQC_5Ala2C_{14}$ (0.83 g, 0.83 mmol) in 85% ethanol solution (8 ml) and refluxed for 1 h. The reaction mixture was cooled to room temperature, added into cold water (80 ml), and extracted by chloroform (60 ml x 4). The crude product was purified by HPLC to give QC_5AlaC_{14} as white solid. Yield, 160 mg (23%).

^{1}H-NMR ($CDCl_3$, 400MHz, TMS): δ/ppm 0.88 [6 H, t, J = 6.4 Hz, $(CH_2)_{13}CH_3$], 1.29 [51 H, m, J = 12.4 Hz, $CH_2(CH_2)_{12}CH_3$, $CH(CH_3)$], 1.54 [6 H, dd, J = 30.8, 24.6 Hz, $HNCH_2(CH_2)_3CH_2CO$], 2.18 [2 H, dd, J = 15.9, 8.6 Hz, CH_2CONH], 3.04-3.55 [l 0 H, m, $CONHCH_2$ $NCH_2(CH_2)_{12}CH_3$, $CH_2CH(OCOCH_3)$], 4.76-4.99 [4 H, m, $CH(CH_3)$], 6.55 [l H, d, J = 7.0 Hz, $OCNHCH(CH_3)$.], 7.06 [1H, s, $CONHCH_2$].

HRMS (TFA-Na^+, *m/z*, matrix: m-NBA): calcd for $C_{29}H_{82}N_3O$ ($[M+Na]^+$), 790.6388; found, 790.6285.

3.2.3. Preparation of bilayer and nonbilayer aggregates

Preparation of giant unilamellar vesicles by electroformation method

Giant unilamellar vesicles (GUVs) composed of DMPC and QC_5AlaC_{14} in a molar ration of 3:1 was prepared by electroformation method which was described in the last chapter. Lipid mixture in 1 mM chloroform (10 μl) was spread and dried on a

conductive indium-tin oxide (ITO) coated glass slide at room temperature to give a lipid film. Then the film was kept under reduced pressure for 1 h to remove the solvent completely. The lipid film was rehydrated in 12 mM sucrose solution (200 μl) in a chamber. GUVs were allowed to grow on a temperature-controlled microscope stage for 20 min at 40 ℃ under a sine voltage (850 mV, 10 Hz).

Preparation of large unilamellar vesicles

Large unilamellar vesicles (LUVs) used for fluorescence spectroscopy were prepared as follows. Stock solutions of 10 mM DMPC in chloroform (75 μl) and 10 mM QC_5Ala2C_{14} in chloroform (25 μl) were placed in a round-bottom flask and the solvent was evaporated and dried under reduced pressure for 3 h to give a thin lipid film. 12 mM aqueous sucrose (1 ml) was gently added to the lipid film, and the mixture was incubated on a water bath for 30 min at 40 ℃ for swelling the lipid layer. Then the mixture was shaken by vortex mixer for 5 min to afford multi-walled vesicles. After 5 times repeating of freeze-and-thaw cycle at -196 and 40 ℃ for aqueous dispersion, the resulting aqueous vesicles were passed through a lipid vesicle extruder (LiposoFast miniextruder from Avestin) with a membrane having 100 nm diameter pore size for 21 times to form LUVs. LUVs containing ANTS/DPX were prepared in the similar manner. ANTS/DPX unencapsulated into LUVs was removed on a column of Sepharose-Cl-4B using 100 mM NaCl as eluant.

Preparation of nonbilayer aggregates

10 mM QC_5AlaC_{14} in chloroform (0.4 ml) was placed in a 5 ml round-bottom flask and the solvent was evaporated and dried under reduced pressure for at 3 h to give a thin film. Pure water (1 ml) was added and the mixture was shaken by vortex mixer with glass beads at room temperature for 40 min to give milky-like aqueous dispersion.

3.3 Reuslts and discussion

3.3.1 Nonbilayer structure observed by transmission electron microscopy

3.3.1.1 Structural characterization of nonbilayer structure

In this work, I characterized the nonbilayer structure composed of inverted micellar aggregates with aqueous internal compartments formed by nonionic peptide lipid, QC_5AlaC_{14}, by means of transmission electron microscopy (TEM) and TEM tomography.

The nonbilayer structure formed by QC_5AlaC_{14} in aqueous media has been characterized in our group by means of negative-staining TEM[15] and small angle X-ray diffraction measurements.[16] In general, the former method might produce some ambiguity regarding the aggregate structure in aqueous media, as the specimen must be examined after complete removal of the water phase in the presence of heavy metal staining ions. Meanwhile, the latter method might be unfavorable for dilute aqueous samples due to limited sensitivity.

The aggregate structure of QC_5AlaC_{14} in dilute aqueous media was evaluated by cryogenic TEM, an imaging technique which faithfully reflects aggregate structure in dilute aqueous solution without staining.[17] Cryogenic TEM imaging of a 4 mM aqueous dispersion of nonionic peptide lipid was well consistent with the cross-sectional view of a nonbilayer structure previously proposed here (Figures 3-3 (A) and 3-3 (C), respectively). The repeating distance of inner aqueous compartments was measured at ~11 nm, comparable to the corresponding value (10 nm) for the 22% lipid/water mixture (w/w) evaluated by small angle X-ray diffraction measurements.[16]

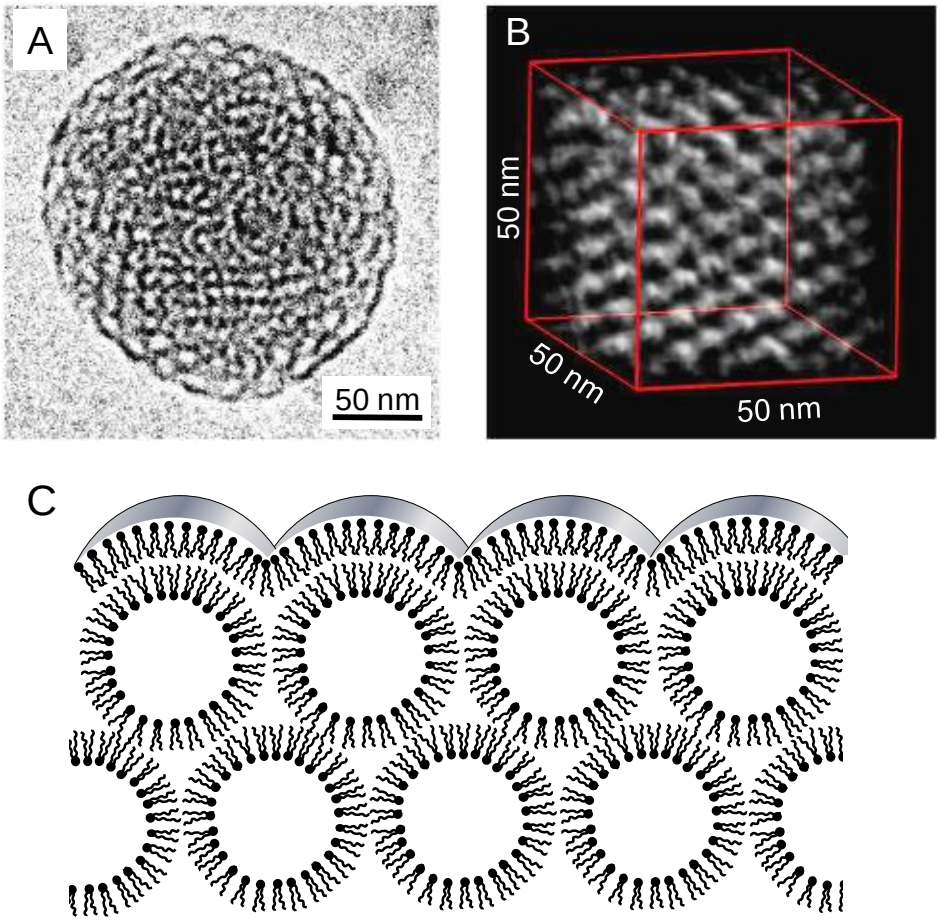

Figure 3-3. TEM images of nonbilayer structure formed by QC_5AlaC_{14}, taken in cryogenic (A) and negative staining tomographic modes (B), and a schematic illustration of a nonbilayer structure (C).

The three-dimensional imaging of nonbilayer structures was also accomplished by means of TEM tomography.[17] Because of constructive restrictions of the TEM instrument (JEOL JEM-3100FEF, JEOL, Ltd., Tokyo, Japan) used here, tomographic images were taken for the dried specimen negatively stained with phosphotungstic acid. An image of the three-dimensional lipid layer network of nonbilayer structures was reconstituted from 121 images accumulated by tilting the sample stage in 1 °increments from −60 ° to +60 ° (Figure 3-3 B). The nonbilayer structure formed by this nonionic peptide lipid would have been stabilized through multiple hydrogen-bonding

interactions among the polar head moieties and amino acid residues of individual lipid molecules in the lipid assembly.

3.3.1.2 Nonbilayer structure in liposomal membrane

It has been reported that phosphatidylcholine, a bilayer forming lipid, favors formation of bilayer structure even in the presence of phosphatidylethanolamine, which is one of the nonbilayer forming lipids.[18] The stabilization of bilayer structure in the mixed lipids system was the result of phase preference by these lipids mixing rather than the specific interactions between these lipids.[19]

In this section, I evaluated aggregate structure of mixed lipids system composed of QC_5AlaC_{14} and DMPC, whether the system adopted bilayer structure without specific interactions between these lipids. Figure 3-4 shows the aggregate morphology of mixture of DMPC and QC_5AlaC_{14} in a molar ratio of 3:1, as observed by cryogenic TEM.

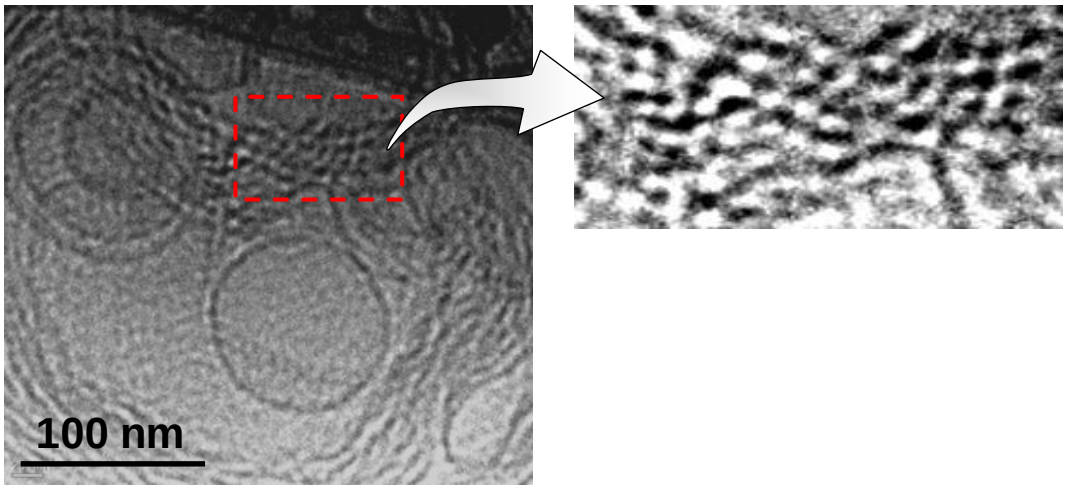

Figure 3-4. Cryogenic TEM images of aggregate structure composed of DMPC and QC_5AlaC_{14} in a molar ratio of 3:1 in aqueous media. Total lipid concentration, 4 mM. Right image is the zoomed nonbilayer structure observed in left image.

The images showed that the predominant structure is bilayer membrane with dark striped patterns. Interestingly, the nonbilayer structure with small aqueous compartments was also observed in the microscopic image. The nonbilayer structure presumably comes from phase separated QC_5AlaC_{14}. I calculated the repeating distance of small aqueous compartments to be 10.6 ± 1.6 nm. The repeating distance was very close to that, 11.1 ± 0.8 nm, of nonbilayer structure formed by pure QC_5AlaC_{14} in aqueous media. This indicates that the hydrogen bonding interactions among polar head moieties of QC_5AlaC_{14} would be effective in DMPC membrane matrix to afford nearly completely phase separated domain of nonbilayer forming lipid in part. The results strongly implies that the nonbilayer structure participate as an intermediate in the present liposomal division, if the dynamic membrane process proceeds.

3.3.2. Phase transition behavior evaluated by differential scanning calorimetry

It has been generally suggested that phase separation in lipid membranes is important for inducing liposomal membrane budding.[20] Thus, phase separation behavior in the liposomal membranes formed by phospholipid (DMPC) in the presence of nonbilayer forming lipid (QC_5AlaC_{14}) was examined by differential scanning calorimetry (DSC). DSC thermogram of an aqueous dispersion of QC_5AlaC_{14} and DMPC in a 1:3 molar ratio revealed two phase transitions from gel to liquid-crystalline phase in a temperature range of 15–25 ℃ with phase transition temperatures (T_m) of 17.3 and 21.4 ℃ and an enthalpy changes (ΔH) of 16.6 and 5.6 kJ mol^{-1}, respectively (Figure 3-5). The corresponding phase transition parameters for the individual lipids were 1.9 ℃ and 9.6 kJ mol^{-1} for QC_5AlaC_{14}[21] and 24.2 ℃ and 22.7 kJ mol^{-1} for DMPC[22]. Completely isolated domains of individual lipids were not detected by DSC measurements in this mixed-lipid system, indicating that the molecular assembly

formed by QC_5AlaC_{14} and DMPC consisted of two phase-separated lipid domains with different mixing ratios, probably these domains would be assigned to a nonbilayer forming lipid-rich and a phospholipid-rich domain with lower and higher phase transition temperature, respectively.

In general, two kinds of lipids having marked difference in phase transition temperature easily form phase separated domains under the phase transition temperature of mixed lipid membrane.[23] In this work, the solution temperature was decreased to 12 ℃, after preparation of vesicles at 40 ℃. During the cooling process, the gel sate composed of locally concentrated DMPC should first appear to form the DMPC-rich gel phase. Along with further decrease in temperature, QC_5AlaC_{14} lipid molecules aggregate together to form hydrogen bonding networks among the quinic acid moieties and the amino acid residues, respectively. The aggregation behavior resulted in formation of QC_5AlaC_{14}-rich domain with lower phase transition temperature. The presence of QC_5AlaC_{14}-rich phase was also supported by cryo-TEM observation. Such phase separation behavior provides us a hint to understand the temperature-dependent morphological changes in this system.

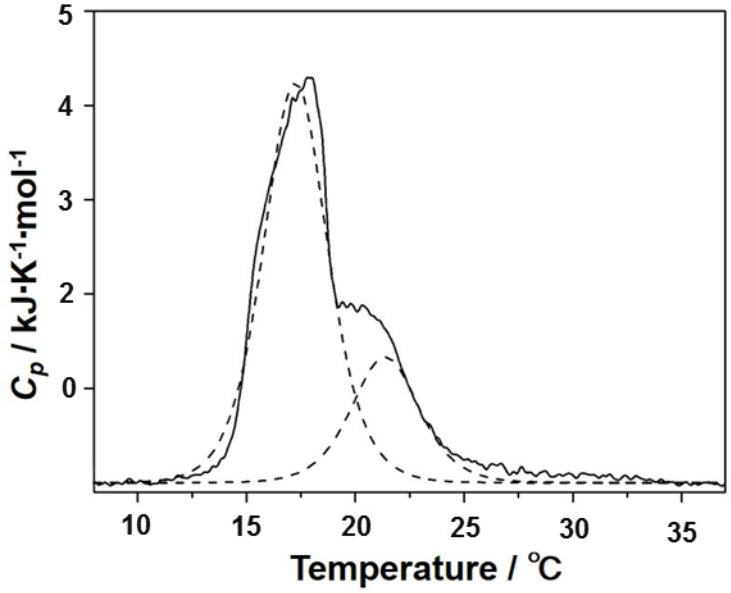

Figure 3-5. DSC thermogram of giant unilamellar vesicles composed of DMPC and QC_5AlaC_{14} in a molar ratio of 3:1. Total lipid concentration, 0.5 mM. Scan rate, 0.5 ℃/min.

3.3.3. Dynamic morphological changes evaluated by optical microscopy

3.3.3.1 Morphological changes induced by nonbilayer forming lipids

Here, the nonbilayer forming lipid, QC_5AlaC_{14}, mixed with bilayer forming lipid, DMPC, was used to fabricate the giant unilamellar vesicles (GUVs) to observe the dynamic membrane morphology. GUVs formed by QC_5AlaC_{14} and DMPC in a molar ratio of 1:3 were observed by phase contrast optical microscopy as shown in Figure 3-6. Interestingly, when the binary vesicles were incubated at 18 ℃ within the temperature range of phase transition from 15 to 25 ℃, the spherical shape of GUVs gradually transformed into prolate shape. In contrast, the pure DMPC vesicles didn't show obvious shape deformation at 24 ℃, the phase transition temperature for DMPC vesicles. Therefore, the nonbilayer forming lipid dramatically affected the morphological stability of GUVs leading to the deformation of binary vesicles.

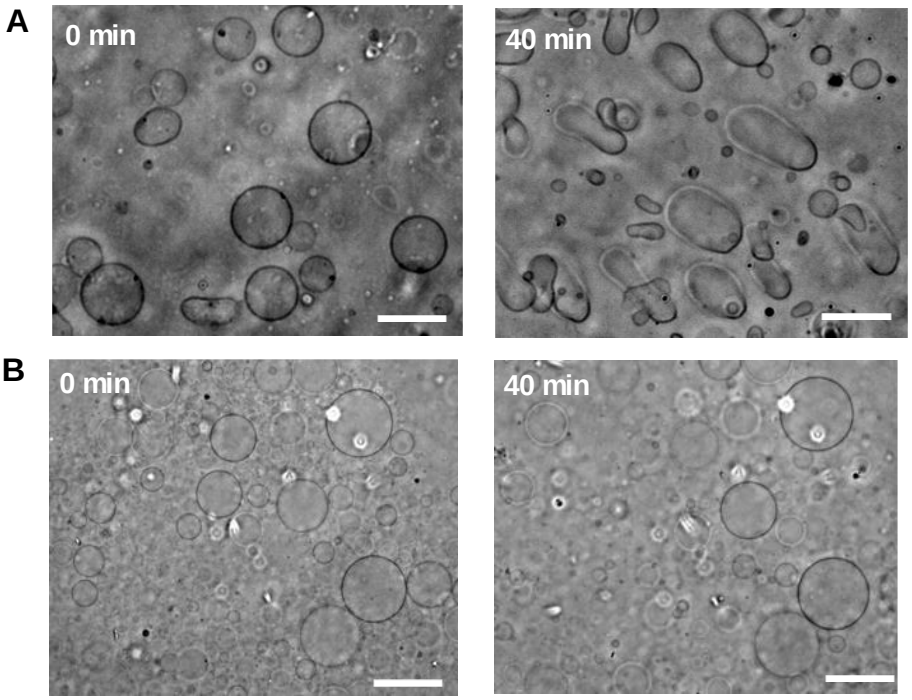

Figure 3-6. Phase contrast optical microscopic images of GUVs composed of DMPC/QC_5AlaC_{14} (3:1) at 18 ℃ (A) and DMPC at 24 ℃ (B), prepared by electrofomation method in 12 mM aqueous sucrose at 34 ℃ for 30 min. Total lipid concentrations, 50 μM. Scale bars, 10 μm.

Time-course of morphological changes of GUV containing nonbilayer forming lipid monitored at 18 ℃ for 60 min was tracked to reveal as snap shots in Figure 3-7. The occurrence of such prolate shape should be intimately related to the membrane division behavior.[25] To characterize the vesicle deformation quantitatively, distortion index (*D*) parameter describing the deviation from spherical shape, has been introduced.[24] Time-curse of distortion index analyzed for the giant vesicles was shown in Figure 3-8. The distortion index at 18 ℃ was gradually increased with time and saturated after 40 min. The results indicates that the GUVs formed by QC_5AlaC_{14} and DMPC in a molar ratio of 1:3, taking spherical shape in the liquid crystalline state above the phase transition temperature, changed their structures to prolate shape, reflecting the phase separation as detected by differential scanning calorimetry.

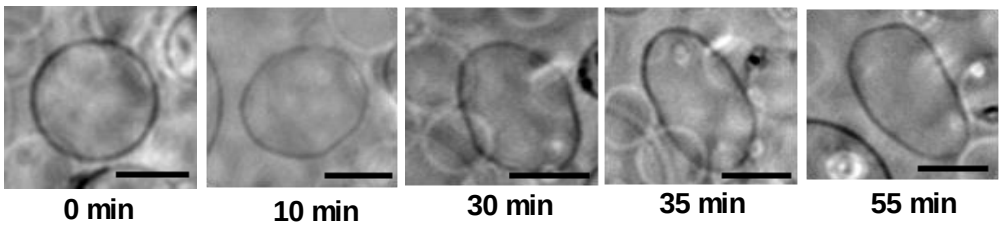

Figure 3-7. Phase contrast optical microscopic images for GUV composed of DMPC/QC_5AlaC_{14} (3:1) incubated at 18 ℃. Times indicate that after cooling the vesicles to 18 ℃, which was prepared at 40 ℃. Scale bars, 5 μm.

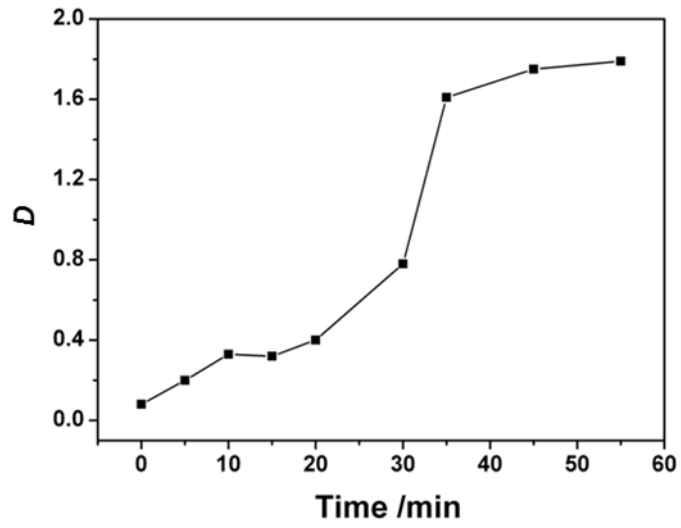

Figure 3-8. Time-course of distortion index for GUVs composed of DMPC/QC_5AlaC_{14} (3:1) incubated at 18 ℃.

From the physical point of view, the transition between different shapes of liposomal membranes can be explained by curvature stress.[26] When the monolayer of liposomal membrane contains nonbilayer forming lipids, the curvature of monolayer trends to be adjusted. When nonbilayer forming lipids present in the two opposite monolayers of bilayer structure, the two monolayers are forced to adopt a structure with zero curvature as schematically shown in Figure 3-9, leading to a bilayers with two frustrated monolayer containing stored curvature stress.[27] Such curvature stress energy would be relaxed by forming a zero or negative curvature phase[28] or by coupling with other membrane.[29] The curvature stress describes the overall property of vesicle,[30] and

also can be moderated in different ways. For example, the increase in curvature stress of bilayer membrane can be explained by either a decrease in the area of lipid head group or an increase in hydrocarbon chain unsaturation.[31]

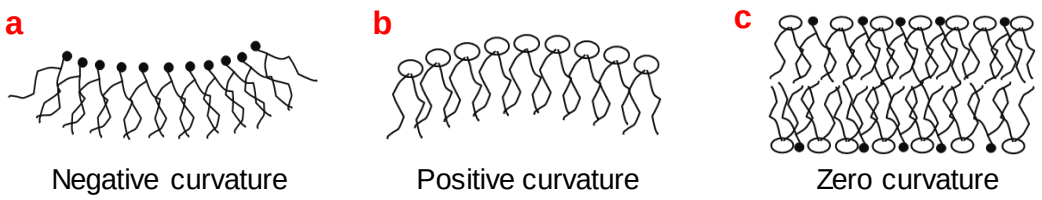

Figure 3-9. Schematic representation of different membrane curvatures. Negative curvature formed by nonbilayer forming lipids with smaller head groups (a), positive curvature formed by bilayer forming lipids with conical shape (b), and zero curvature forced by mixture of nonbilayer and bilayer forming lipids (c).

The nonbilayer forming lipid, QC_5AlaC_{14}, aggregates to form the negative curvature structure constructing the inverted cubic phase.[16] DSC result tells us that the phase separation happened in and below the phase transition temperature range. So the binary lipid membrane at 18 ℃ experienced the phase separation into QC_5AlaC_{14}- and DMPC-rich phase. In the QC_5AlaC_{14}-rich domain, dehydration of polar head moiety in nonbilayer forming lipid through multiple intermolecular hydrogen bonding interactions causes the volume of head group smaller than that of bilayer forming lipids. Therefore, the QC_5AlaC_{14}-rich phase affected the membrane curvature stress leading to fluctuated bilayers containing stored curvature stress. The spherical shape of vesicle then changed to release the curvature stress. As a result, the spherical vesicular shape gradually transferred into the prolate shape with zero curvature. To confirm this idea, the membrane deformation behavior was evaluated at different temperatures.

3.3.3.2 Temperature effect of morphological changes

Time dependence of aggregate morphology for GUVs formed by QC_5AlaC_{14} and DMPC in a molar ratio of 1:3 was observed above the phase transition temperature at 34 ℃ by phase contrast optical microscopy. At this temperature, the membrane takes liquid crystalline phase in which there is increased head group mobility and water penetration into the interfacial region of lipid bilayer.[32] The microscopic images showed that the morphological changes were not so drastic. That is, few elliptical shapes were observed, and most of the vesicles adopt the spherical shape (Figure 3-10).

The result is contrastive to that observed in the phase transition temperature range at 18 ℃. GUV morphologies were quantitatively characterized by calculating the distortion index (*D*). The time dependence of distortion index was evaluated for vesicles formed by QC_5AlaC_{14} and DMPC in a molar ratio of 1:3 at 18 and 34 ℃ (Figure 3-11). The GUV distortion index at 18 ℃ was found to gradually increase with time, whereas the corresponding value at 34 ℃ was essentially time independent.

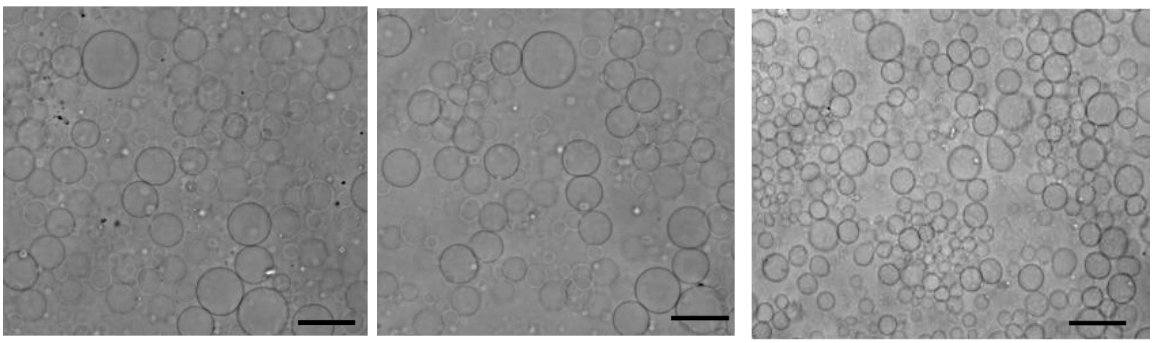

Figure 3-10. Phase contrast optical microscopic images for GUV composed of DMPC/QC_5AlaC_{14} (3:1) incubated at 34 ℃. Times indicate that after cooling the vesicles to 34 ℃, which was prepared at 40 ℃. Scale bars, 10 μm.

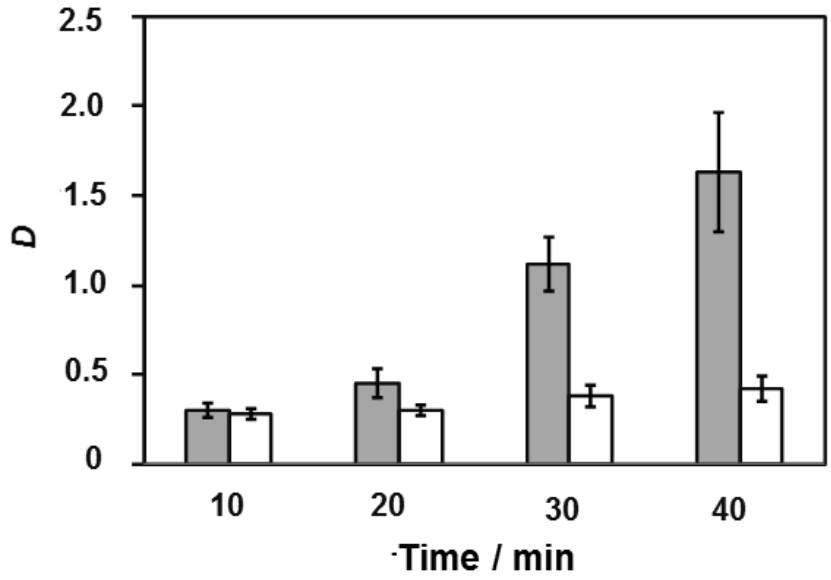

Figure 3-11. Time dependence of distortion index (*D*) for the giant vesicles formed by DMPC and QC_5AlaC_{14} in 1:3 molar ratio, having $D \geq 0.2$ and $l \geq 22$ μm with standard errors, at 18 (gray bar) and 34 ℃ (white bar), respectively. At least 15 vesicles were examined under each conditions. Total lipid concentration, 50 μM.

These observed dynamic changes in vesicular shapes probably reflected time- and temperature-dependent phase separation behavior of mixed lipid membranes formed by these two lipids. That is, in the liquid crystalline state of GUVs, these lipids were dispersed with relatively high uniformity, due to sufficient lateral diffusion of lipid molecules in the fluid membrane phase. In a phase-transition temperature range, however, phase separation proceeded to form QC_5AlaC_{14} rich domains, which could be assigned as domains with lower T_m values (Figure 3-5). In this domain, dehydration on the membrane surface was enhanced through hydrogen-bonding interactions among polar head moieties of QC_5AlaC_{14} which thus stabilized the elliptical membrane surface at a lower curvature. Thus, the observed deformation of GUVs from spherical to elliptical shapes can be understood as having been caused by the formation of two kinds of lipid domains through phase separation.

Previously, Crowe and his co-workers proposed that gel to liquid-crystalline phase transition of phosphlipids facilitates the local concentration of phosphatidylethanolamine, the nonbilayer forming lipid, to favor the formation of H_{II} phase in bilayer membrane.[33] It was also reported that the nonbilayer forming lipid redistribution takes place in biomembranes to aggregate together forming the nonbilayer phase during cooling process from growth temperature to phase transition temperature.[34] These findings in biomembrane and its model membrane system suggest that the QC_5AlaC_{14} lipid molecules locally aggregate in the phase transition of mixed membrane much more effectively than in the liquid crystalline state. The resulting appearance of QC_5AlaC_{14} rich domain in the phase transition temperature range would induce the morphological changes of liposomal giant vesicles.

3.3.4 Membrane division behavior evaluated by optical microscopy

3.3.4.1 Phase contrast images of division

It is very interesting that some of the vesicles with elliptical shape processed fission behavior as shown in Figure 3-12. The elliptical vesicles gradually became to dumbbell shape to divide into two spherical daughter vesicles (Figure 3-12. (A)-(C)). The vesicles also experienced the pear shape as the intermediate structure (Figure 3-12. (D)), peeling off an elongated vesicle from a spherical vesicle.

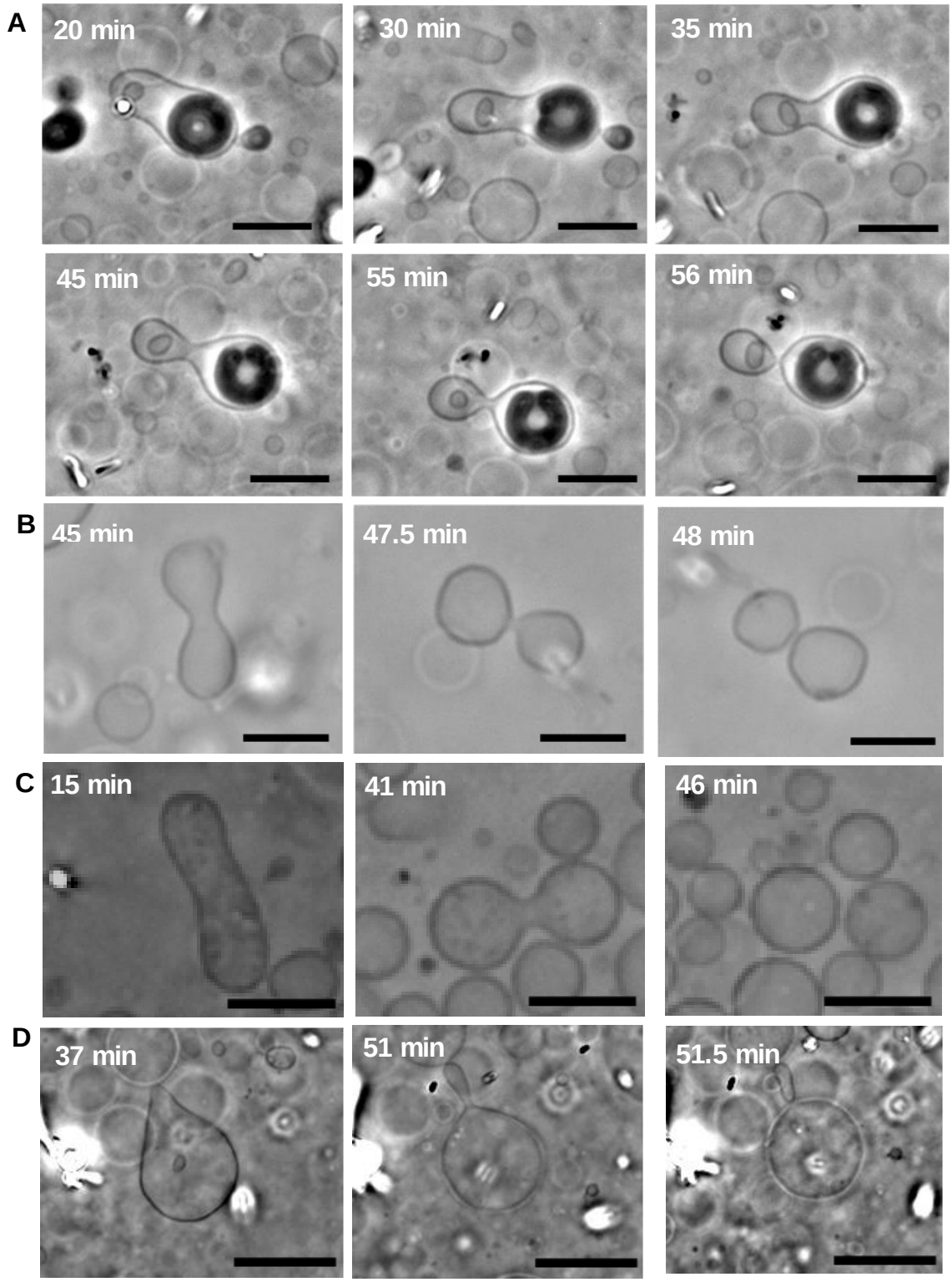

Figure 3-12. Phase contrast optical microscopic images for GUVs composed of DMPC/QC_5AlaC_{14} (3:1) incubated at 18 ℃. A, B, C, and D are time-dependent snapshots for different GUVs. Times indicate that after cooling the vesicles to 18 ℃, which was prepared at 40 ℃. Scale bars, 10 μm.

The present morphological changes would be explained by considering the membrane curvature effects as follows. Firstly, the membrane region with zero curvature gradually transforms into the structure with negative curvature. This behavior comes from the increase in percentage of QC_5AlaC_{14} lipid molecules in the local membrane region with zero curvature probably through time-dependent dynamic membrane fluctuation. The increase in local concentration of nonbilayer forming lipid further enhances the formation of more fluctuated bilayer domain with stored curvature stress. Such fluctuated bilayer adopts negative curvature to relax the curvature stress, which shorted the distance between opposing bilayers with the similar stored curvature stress.

The attachment of opposing two bilayers closely approaching each other is essentially required for the vesicle fission. It has been proposed that devision of bilayer vesicles, the reverse process of membrane division, experienced the initial stage of adhesion of opposing bilayers from different vesicles followed by jointing and fission stages of lipid membrane, especially focusing on hydration force.[9] Hence, the mechanism of membrane division also should be understood from the viewpoint of hydration force by referring that of membrane fusion.

Upon decreasing the distance between opposing two bilayers in a vesicle, repulsive hydration force on the membrane prevents their approach. The hydration force is predominant, if two hydration shells formed on the membrane surface are in the contact distance. For example, when the distance between opposing two bilayers was decreased within 2 nm, such force is greater than the electrostatic repulsion between two charged bilayers.[35] In the presence of nonbilayer forming lipid, QC_5AlaC_{14}, hydrogen bonding interactions among lipid polar head moieties enhance the dehydration of membrane

surface to decrease the hydration force. Thus, in the QC_5AlaC_{14}-rich domain, the dehydration of hydrophilic interface facilitates the attachment of opposing two bilayers.

In the second stage, intermixing of lipid molecules takes place at the bilayer attachment region. Formation of nonbilayer structure such as inverted miceller aggregates may stabilize the intermediate structure in this membrane region, since I have confirmed that the lipid aggregates formed by QC_5AlaC_{14} takes the inverted cubic phase compose of inverted micelles in the presence and absence of DMPC, by means of cryogenic TEM observations (*vide supra*).

In the final stage of membrane division, the mother vesicle gives rise to two daughter having independent aqueous components. During the second stage, the two vesicles are connected by a narrow stalk composed of inverted micelles, which is a high-energy interstitial hydrocarbon region at the narrow neck.[36]

Thus this is the final process to decrease the free energy for the meta-stable membrane intermediate, merging outer monolayer membranes and giving the followed vesicle fission.

3.3.4.2 Fluorescence images of division

Fluorescence optical microscopy was used for the present dynamic membrane process in order to get further information on the mechanism of membrane division. Rh-DPPE, a phospholipid having a fluorescent rhodamine dye in the head moiety, was employed as a fluorescent lipid probe to monitor the division of giant vesicles formed by DMPC and QC_5AlaC_{14} in a molar ratio of 3:1. This fluorescent probe is expected to stain the DMPC rich domain rather than the QC_5AlaC_{14} rich domain, judging from the molecular structural analogy. As shown in Figure 3-13, Rh-DPPE stained the lipid bilayer in red.

In Figure 3-13, the membrane region, in which the opposing two bilayers were closely approaching, was less stained in red than the other region. The results strongly suggest that the former region is QC_5AlaC_{14} rich domain reflecting lower distribution of Rh-DPPE molecules than DMPC rich domain.

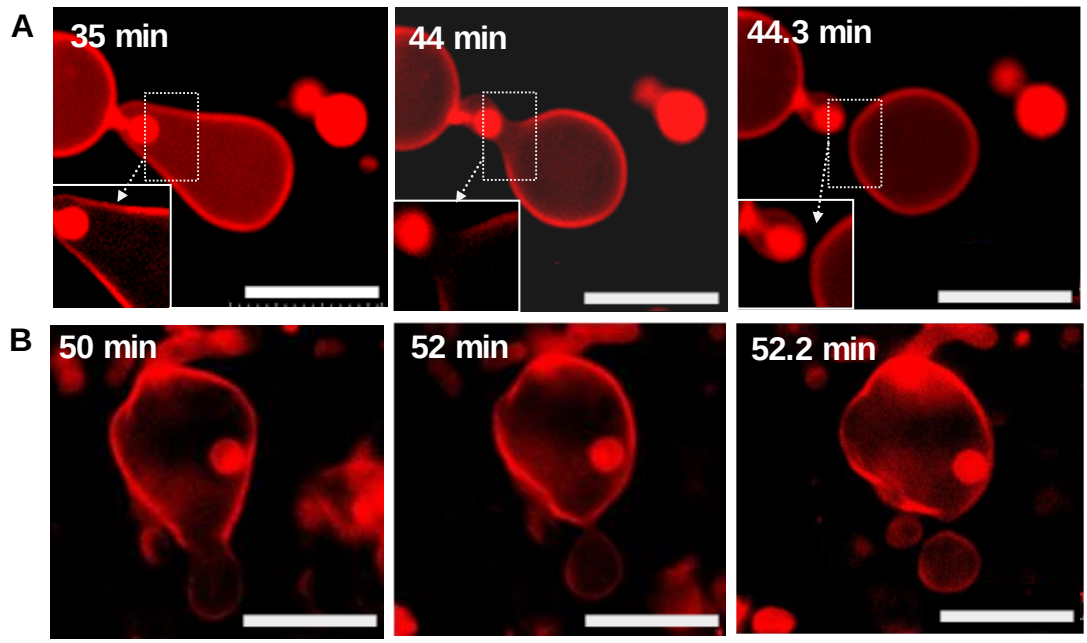

Figure 3-13. Fluorescence optical microscopic images for GUVs composed of DMPC/QC_5AlaC_{14} (3:1) incubated at 18 ℃ in the presence of 0.1 mol% Rh-DPPE. (A) and (B) are time-dependent snapshots for different GUVs. Times indicate that after cooling the vesicles to 18 ℃, which was prepared at 40 ℃. Scale bars, 10 μm.

3.3.5 Participation of nonbilayer structure in membrane division as evaluated by fluorescence spectroscopy

In order to get an additional evidence on participation of nonbilayer forming lipid in the present membrane division system, leakage behavior of a water-soluble fluorescent probe, ANTS, encapsulated in liposomal membrane was evaluated by fluorescence spectroscopy.

Previously, this fluorescent probe has been used to evaluate the formation of

intermediate nonbilayer structure during fusion of liposomal membranes.[37] ANTS does not show self-quenching fluorescence behavior, since there is no significant overlap between its excitation and emission spectra.[38] In addition, DPX acts as an effective quencher for ANTS through classical Förster type resonance energy transfer.[38] Thus, a pair of fluorescence markers involving ANTS and DPX has been used for quantitative assay of liposomal fusion process containing phasphatidylethanolamine.[37] ANTS and DPX are once released from the vesicles into bulk aqueous phase, the quenching is completely relieved due to dilution of these quenching pair. Thus, the fluorescence quenching keeps during fusion of vesicles, if the fusion proceeds through simple mixing of inner aqueous phases of each vesicle, without forming intermediate nonbilayer structure. On the other hand, the fluorescence quenching is relieved, if nonbilayer structure with inverted micelles is present as intermediate in the fusion process.

In this work, I employed this technique to evaluate the formation of nonbilayer structure during the division of liposomal membranes. Time-dependences of encapsulated ANTS/DPX leakage for the vesicles formed by DMPC and QC_5AlaC_{14} in a molar ratio of 3:1 at different temperatures were shown in Figure 3-14 (A). When the membrane was in the phase transition temperature range at 18 ℃, the leakage gradually increased with time and saturated after 60 min. The time scale of leakage is comparable to that for the membrane division observed by optical microscopy. The results strongly imply that nonbilayer aggregate composed of inverted micelles having inner aqueous compartments probably formed as the transient intermediate structure of liposomal division process. In the liquid crystalline state at 34 ℃, however, the leakage was much slower than that at 18 ℃, suggesting that liposomal division did not proceed effectively due to the difficult formation of nonbilayer structure.

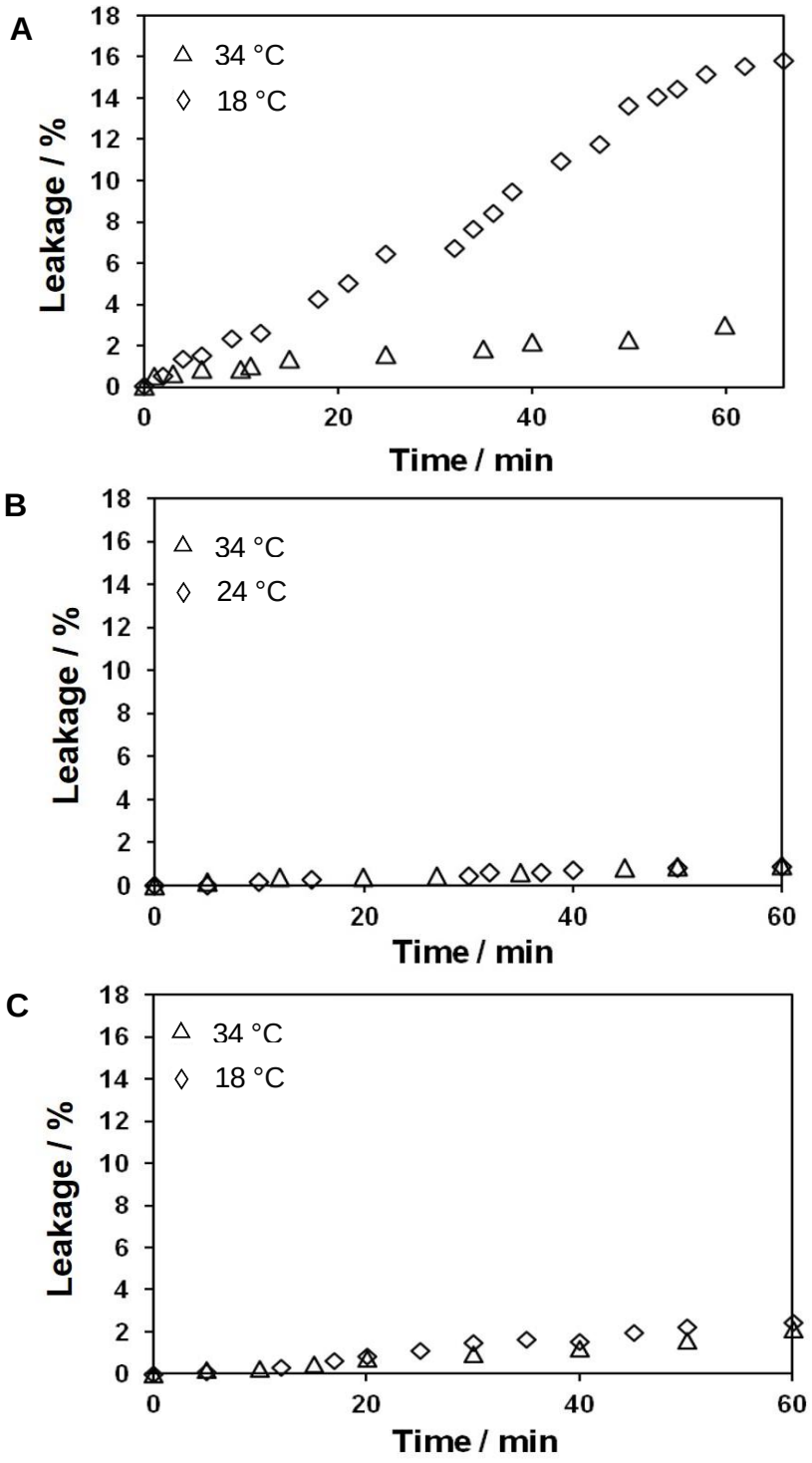

Figure 3-14. Time dependences on leakage of ANTS/DPX encapsulated in liposomal membranes. A, DMPC/QC_5AlaC_{14} (3/1); B, DMPC; C, DMPC/DLPC (3/1). Concentrations: total lipid, 58 μM; ANTS, DPX, and NaCl in the inner aqueous phase of vesicles are 12.5 mM, 45 mM, and 22.5 mM, respectively; NaCl in bulk aqueous phase, 100 mM. λ_{ex}, 360 nm; λ_{em}, 500 nm.

Figure 3-14 (B) shows the time dependence of leakage from DMPC vesicle in the absence of nonbilayer forming lipid as control experiments. The bilayer membrane formed by DMPC has phase transition from gel to liquid crystalline phase at 24 ℃. Less than 1% leakage was observed for 60 min both in the phase transition temperaturerange and in the liquid crystalline state. The behavior reflects that there is no morphological change of DMPC vesicle in this time scale, and that ANTS and DPX both having good water-solubility cannot leak from the vesicles.

As another control experiment, the leakage behavior of ANTS/DPX from liposomal membrane was monitored for DMPC vesicles containing DLPC, bilayer forming lipid, in place of nonbilayer forming QC_5AlaC_{14}. The leakage less than 3% for 60 min was observed at 18 and 34 ℃ (Figure 3-14 (C)). While bilayer membrane was formed by DLPC (the phase transition at −2 ℃), the mixed liposome composed of DMPC and DLPC in a molar ratio exhibits the phase transition in the analogous temperature range of that formed by DMPC and QC_5AlaC_{14} as shown in Figure 3-15. The liposomal membrane formed by DMPC and DLPC also shows phase separation to give DMPC- and DLPC-rich domain, however, the presence of nonbilayer structure as intermediate in the membrane division was not suggested from the leakage experiments both in the phase transition temperature range and in the liquid crystalline state. A little higher leakage for the DMPC/DLPC system than the pure DMPC one may reflect the difference in lipid packing in both bilayer membranes.[39]

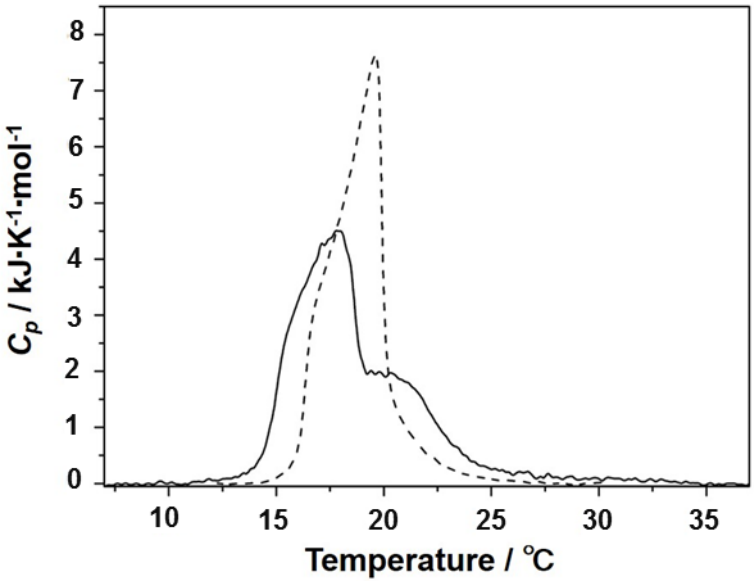

Figure 3-15. DSC thermograms of giant unilamellar vesicles formed by DMPC/QC_5AlaC_{14} (3/1) (solid line) and DMPC/DLPC (3/1) (dashed line). Total lipid concentrations, 0.5 mM. Scan rate, 0.5 ℃/min.

Accordingly, effective leakage of encapsulated ANTS/DPX from liposomal membrane was observed only for the DMPC vesicles containing the nonbilayer forming lipid in the phase transition temperature range. It has been reported that the fusion of liposomal membranes formed by phosphatidylserine or phosphatidic acid in the presence of nonbilayer forming phosphatidylethanolamine was induced by calcium ions, and that the formation of nonbilayer structure was suggested by the similar leakage experiments of fluorescence probe.[40] The results given by the present fluorescence spectroscopic measurements strongly suggest that the nonbilayer forming lipid, QC_5AlaC_{14}, participates the formation of nonbilayer aggregates as a transient intermediate structure during the division of liposomal membranes.

As for the participation of nonbilayer structure in dynamic membrane behavior, a mechanism of exocytotic release of Chromafin granule from the liposomal membrane formed by phosphatidylethanolamine and phosphatidylserine induced by calcium ions

has been proposed.[41] In this system, the formation of inverted micelle was suggested as intermediate structure in the flip-flop processes of bilayer membrane.[42] The solvates captured in the aqueous core of micelle as carrier transported through the hydrophobic region, and the solvates were released into opposite bulk phase as shown in Figure 3-16.

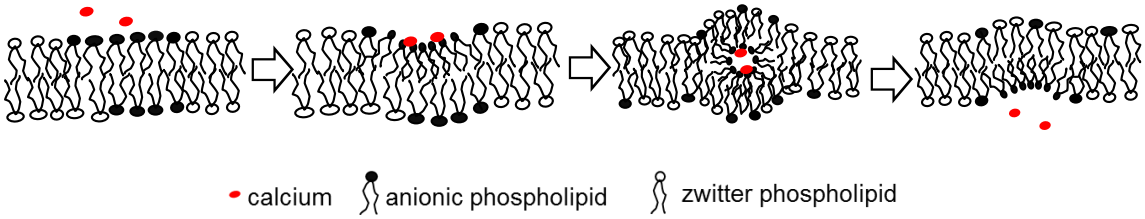

Figure 3-16. Schematic illustration of facilitated transport of calcium ions via formation of an intermediate inverted micelle encapsulating solvates. The head groups of negatively charged phospholipid interact with calcium ions to form the inverted micelle.[41]

On these grounds, the enhanced leakage of ANTS/DPX observed in the liposomal membrane formed by DMPC and QC_5AlaC_{14} can be understood by the formation of inverted micellar aggregates as intermediate structure during the membrane division, due to the similarity of presence of nonbilayer forming lipid. It should be noted that the nonbilayer structure was derived from multiple hydrogen bonding interactions among polar head moieties in the liposomal membranes containing QC_5AlaC_{14}, whereas the multipoint electrostatic interactions of anionic polar head moieties with calcium ions induce to form the nonbilayer structure in the liposomal membranes containing phosphatidylethanolamine.

3.4 Conclusions

In this chapter, the nonbilayer structure formed by nonionic peptide lipid having quinoyl moiety, QC_5AlaC_{14}, was first characterized by cryogenic TEM and TEM tomography. The microscopic images observed by cryogenic TEM revealed the aggregate structure in dilute aqueous solution without staining. In addition, its three-dimensional structure was visualized by negatively stained TEM tomography. The results clearly indicate the formation of inverted cubic phase with small aqueous compartments. The repeating distance between the aqueous compartment, or the diameter of inverted micelles, as evaluated by cryogenic TEM was 11 nm, which was in good agreement with the value analyzed by small angle X-ray diffraction measurements for the same aqueous lipid in high concentrations.

On these grounds, I clarified the synthetic cell division behavior for the liposomal membranes formed by bilayer forming phospholipid, DMPC, in the presence and absence of nonbilayer forming lipid, QC_5AlaC_{14}. Phase contrast optical microscopic observation indicated that membrane division of giant unilamellar vesicles formed by DMPC and QC_5AlaC_{14} in a molar ratio of 7:3 proceeded in the temperature range of the gel to liquid-crystalline phase transition. The membrane division was temperature sensitive and including the dynamic membrane processes; the morphological change from spherical to elliptical shape, further transformation to gourd-like constricted shape, and followed fission of mother vesicle to give daughter vesicles. In contrast, membrane division was not observed in the absence of nonbilayer forming lipid.

The present division was induced by formation of QC_5AlaC_{14}-rich domain in the liposomal membrane, which was clarified from the phase transition behavior by means of differential scanning calorimetriy and fluorescence microscopy using a fluorescent

lipid probe. In addition, participation of nonbilayer structure with inverted micellar aggregates as intermediate structure during the membrane division process was strongly suggested from the leakage experiments using a couple of water-soluble fluorescent probe and its quencher, which was encapsulated into the inner aqueous phase of liposomal membranes.

In conclusion, I developed the division of liposomal membranes induced by a nonbilayer forming peptide lipid. To the best of my knowledge, this is the first example of artificially designed synthetic cell division concerning the nonbilayer structures.

3.5 References

(1) (a) Cullis P. R.; Hope M. J.; Tilcock C. P. S. *Chem. Phys. Lipids* **1986,** *40*, 127-144; (b) Tenchov, B.; Koynova, R. *Eur. Biophys J.* **2012,** *41*, 841-850.

(2) Uzzati, V.; Reiss-Husson, F. *J. Cell Biol.***1962,** *12*, 207-219.

(3) Cullis, P. R.; de Kruijff, B. D. *Biochim. Biophys. Acta* **1979,** *559*, 399-420.

(4) (a) Rilfors, L.; Lindblom, G. *Colloids Surf., B* **2002,** *26*, 112-124; (b) Koynova, R.; Mac-Donald, R. C. *Biochim Biophys Acta Biomemb*. **2007,** *1768*, 2373-2382; (c) Mariani, P.; Rivas, E.; Luzzati, V.; Delacroix, H. *Biochemistry* **1990,** *29*, 6799-6810.

(5) Epand, R. M. *Chem. Phys. Lipids* **1996,** *81*, 101-104.

(6) (a) Kuzmin P. I.; Zimmerberg, J.; Chizmadzhev, Y. A; Cohen, F. S. *Proc Natl Acad Sci USA* **2001,** *98*, 7235-7240; (b) de Kruijff, B. D. *Curr. Opin. Chem. Biol.* **1997,** *1* 564-569.

(7) Ellens, H.; Siegel, D. P.; Alford, D.; Yeagle, P. L.; Boni, L., Lis, L. J., Quinn, P. J. Bentz, J. *Biochemistry* **1989,** *28*, 3692-3703.

(8) (a) Deamer, D. W.; Leonard, R.; Tardieu, A.; Branton, D. *Biochim. Biophys. Acta* **1970,** *219*, 47-60; (b) Verkleij, A. J.; Mombers, C.; Gerritsen, W. J.; Leunissen-Bijvelt, L.; Cullis, P. R. *Biochim. Biophys. Acta*, **1979,** *555*, 358-361.

(9) Arie, J.; Verkleij, J. *Biochim. Biophys. Acta* **1984,** *779*, 43-63.

(10) Knutton, S. *J. Cell Sci.* **1979,** *36*, 61-72.

(11) (a) Rand, R. P. *Ann. Rev. Biophys. Bioeng.* **1981,** *10*, 277-314; (b) Le-Neveu, D.; Rand, R. P.; Parsegian, V. A. *Nature* **1976,** *259*, 601-603.

(12) (a) Ellens, H.; Bentz, J.; Szoka, F. C. *Biochemistry*, **1986,** *25***,** 4141-4147; (b) Verkleij, A. J.; Mombers, C.; Gerritsen, W. J.; Leunissen-Bijvelt, J.; Cullis, P. R.

Biochim. Biophys. Acta **1979,** *555*, 358-361; (c) Verkleij, A. J.; Van-Echteld, C. J. A.; Gerritsen, W. J.; Cullis, P. R.; de Kruijff, B. D. *Biochim. Biophys. Acta* **1980,** *600*, 620-624.

(13) Emoto, K.; Kobayashi, T.; Yamaji, A.; Aizawa, H.; Yahra, I.; Inoue, K.; Umeda, M. *Proc. Natl. Acad. Sci. USA,* **1996,** *93*, 12867-12872.

(14) Murakami, Y.; Kikuchi, J.; Takaki, T.; Uchimura, K. *Chem. Lett.* **1986,** 325-328.

(15) Murakami, Y.; Nakano, A.; Kikuchi, J.; Takaki, T. *Chem. Lett.* **1983,** 1891-1894.

(16) Murakami, Y.; Kikuchi, J.; Takaki, T.; Uchimura, K. *Bull. Chem. Soc. Jpn.* **1987,** *60*, 1469-1479.

(17) Kikuchi, J.; Yasuhara, K. in *Supramolecular Chemistry from Molecules to Nanomaterials*, eds. by P. A. Gale, J. W. Steed, John Wiley & Sons, Chichester, 2012, *Vol. 2,* pp. 633-645.

(18) (a) Cullis, P. R.; Hope, M. J.; Tilcock, C. P. S. *Chem Phys Lipids* **1986,** *40*, 127-144. (b) Webb, M. S.; Hui, S. W.; Steponkus, P. L. *Biochim Biophys Acta* **1993,** *1145*, 93-104.

(19) Tilcock, C. P. S. *Chem. Phys. Lipids* **1986,** *40*, 109-125.

(20) (a) Staneva, G.; Seigneuret, M.; Koumanov, K.; Trugnan, G.; Angelova, M. I.; *Chem. Phys. Lipids*, **2005**, *136*, 55-56. (b) Hamada, T.; Miura, Y.; Ishii, K.; Araki, S.; Yosikawa, K.; Vestergaard, M.; Takagi, M. *J. Phys. Chem. B,* **2007**, *111*, 10853-10857. (c) Andes-Koback, M.; Keating, C. D. *J. Am. Chem. Soc.*, **2011**, *133*, 9545-9555.

(21) Murakami, Y.; Kikuchi, J.; Takaki, T.; Uchimura, K.; Nakano, A. *J. Am. Chem. Soc.* **1985,** *107*, 2161-2167.

(22) Wang, Z. H.; Yashuhara, K.; Ito, H.; Mukai, M.; Kikuchi, J. *Chem. Lett.* **2010,** *39*,

54-55.

(23) Seeger, H. M.; Fidorra, M.; Heiburg, T. *Macromol. Symp*. **2005,** *219*, 85-96.

(24) Tomita, T.; Sugawara, T.; Wakamoto, Y. *Langmuir*, **2011,** *27*, 10106–10112.

(25) Seifert, U.; Berndl, K.; Lipowsky, R. *Phys. Rev. A: At. Mol. Opt. Phys.* **1992,** *44*, 1182-1202.

(26) (a) Svetina, S.; Zeks, B. *Biomed. Biochim. Acta* **1983**, *42*, 86-91; (b) Svetina, S.; Zeks, B. *Eur. Biophys. J.* **1989,** *17*, 101-107.

(27) Hui, S. W.; Sen, A. *Proc. Natl. Acad. Sci. U. S. A.* **1989,** *86*, 5825- 5829.

(28) Janes, N. *Chem. Phys. Lipids* **1996,** *81*, 133-150.

(29) Ep, R. M.; Epand, R.F. *Biophys. J.* **1994,** *66*, 1450-1456.

(30) Keller, S. L.; Bezrukov, S. M.; Gruner, S. M.; Tate, M. W.; Parsegian, V. A. *Biophys. J.* **1993,** *65*, 23-27.

(31) Booth, P. J. *Biochim. Biophys. Acta* **2003,** *1610*, 51-56.

(32) (a) David G. C.; Henry H. M. *Biophys. J.* **1982,** *38*, 175-184; (b) Lewis, B. A.; Das-Gupta, ***S.*** K.; Griffin, R. G. *Biochemistry* **1984,** *23*, 1988-1993.

(33) Crowe, J. H.; Crowe, L.M. in *Biological Membranes*, ed. by Chapman, D., Academic Press, London, **1984,** *Vol. 5*, pp. 57-103.

(34) Quinn, P. J. *Cryobiogogy* **1985,** *22*, 128-146.

(35) Rand, R. P. *Ann. Rev. Biophys. Bioeng.* **1981,** *10*, 277-314.

(36) Kinoshita, K.; Li, S. J.; Yamazaki, M. *Eur. Biophys. J.* **2001**, *30*, 207-220.

(37) Bentz, J.; Szoka, F. C. *Biochemistry* **1984,** *23*, 1532-1538.

(38) (a) Leire, C.; Wunderlich, B.; Myles, V. M.; Schneider, M. F. *Biophys. Chem.* **2009,** *143*, 106-109; (b) Inaoka, Y.; Yamazaki, M. *Langmuir* **2007,** *23*, 720-728.

(39) (a) Weinstein, J. H.; Yoshikama, S.; Henkart, P.; Blumenthal, R.; Hagins, W. **A.** *Science* **1997,** *195,* 489-492; (b) Wilschut, J.; Papahadjopoulos, D. *Nature* **1979,**

281, 690-692.

(40) Cullis, P. R.; de Kruijff, B. D.; Hope, M. J.; Nayar, R.; Schmid, S. L. *Can. J. Biochem.* **1980,** *58*, 1091-1100.

(41) Cullis, P. R.; de Kruijff, B. D. *Biochim. Biophys. Acta* **1978,** *507*, 207-218.

(42) Ellens, H.; Bentz, J.; Szoka, F. C. *Biochemistry* **1986,** *25*, 4141-4147.

Chapter 4: General conclusions and future perspective

In this work, two novel synthetic cell division systems were developed. First system provides us a guidepost how to design membrane division system induced by a hydrophilic chemical signal. Second system gives us a first successful example to demonstrate participation of nonbilayer structure in artificial membrane division. In this thesis, the results were summarized as follows.

In Chapter 2, I clarified the division behavior of artificial bilayer membrane composed of a zwitterionic phospholipid and a cationic synthetic lipid induced by a fluorescent chemical signal, pyranine. This is a good model system to investigate the mechanism of dynamic membrane behavior in detail, since the whole process can analyse by separating into the following unit processses; (1) signal binding to membrane, (2) phase separation of membrane, and (3) membrane budding and followed fission.

As for the first unit process, the signal binding behavior on the membrane surface was analyzed thermodynamically and kinetically by using fluorescence spectroscopy. A few factors, such as charge density of membrane surface, membrane phase state and medium ionic strength, significantly affect the signal binding behavior. The tetraanionic signal molecule binds to the cationic lipid in a stoichiometry of 1:4 through the multipoint electrostatic interactions. The resulting lateral relocation of cationic lipid molecules was evaluated by monitoring time-course of fluorescence intensity. When the membrane was in phase transition state from gel to liquid-crystalline phase, the signal binding process was kinetically observed in a time scale of seconds, and the reaction rate for signal binding to membrane surface was calculated to be the first order for

signal species. As for the second unit process, the phase separation behavior followed by the signal binding was characterized by differential scanning calorimetry. The results showed that the signal binding induced the phase separation of membrane to form two domains composed of cationic lipid-rich and phospholipid-rich domain. As for the final budding and fission process, the dynamic membrane morphological changes were observed in detail by fluorescence microscopy in both static and video mode.

Accordingly, the present dynamic membrane behavior, including the signal binding, phase separation and budding and followed fission, were systematically analyzed and the mechanism of membrane division induced by a chemical signal was proposed. On these grounds, I also demonstrated that phase separation and budding are adjustable by changing the ionic strength.

In Chapter 3, I demonstrated a new membrane division behavior concerning nonbilayer structure. As a nonbilayer forming lipid, nonionic peptide lipid having a quinoyl moiety at the polar head moiety was employed. Firstly, nonbilayer structure formed by the nonionic peptide lipid was characterized by transmission electron microscopy (TEM). The latest TEM techniques, cryogenic TEM and TEM tomography, were applied for structural characterization of nonbilayer structure. The cryogenic TEM observation for frozen and dilute aqueous sample without staining clearly revealed the nonbilayer structure composed of inverted cubic phase with small aqueous compartments, which has been previously suggested by negative staining TEM image for the completely dried sample in the presence of heavy metal ions as a stain and small angle X-ray diffraction measurements for aqueous sample in extremely high concentration. In addition, the nonbilayer structure was further confirmed by three-dimensional image derived from TEM tomography. In the presence of the

nonbilayer forming lipid in liposomal membrane formed by phopholipid, dynamic membrane division was specifically observed by optical microscopy in phase contrast and fluorescence mode. Differential scanning calorimetric measurements clarified that the membrane division was induced by formation of phase separated domains in membrane, probably nonbilayer forming lipid-rich and phspholipid-rich domain. In addition, I found that the membrane division behavior was sensitive to temperature, which influenced in the phase state of lipid membrane. On these ground, the mechanism of present membrane division system concerning nonbilayer forming lipid was proposed.

Two kinds of membrane division systems developed in this work strongly suggest us a guidepost how to design synthetic cell division systems in general. Firstly, I have clarified that active division of liposomal membranes formed by a phospholipid and a bilayer-forming synthetic lipid proceeded upon addition of a hydrophilic chemical signal. Vesicle division was induced by the chemical signal binding to membrane surfaces through the multiple electrostatic interactions, followed by phase separation to form lipid domains favorable for vesicle budding. Secondly, I have revealed that phase-separated domain formation for membrane division was achieved by the coexistence of a nonbilayer-forming with a bilayer-forming lipid. On these grounds, a guideline is proposed such that synthetic division of a mother vesicle to generate daughter vesicles could be purposely designed if lipid domains are formed that are favorable for budding of the mother vesicles.

Finally, I would like to discuss on the possibilities of application of synthetic cell division. Recently, a new communication paradigm, “molecular communication,” has been proposed in the interdisciplinary research area covering information and

communication technology (ICT), biological sciences, and materials science (Figure 4-1).[1,2] The research aim is to establish the next-generation ICT, inspired by biological processes such as signal transduction and membrane trafficking.

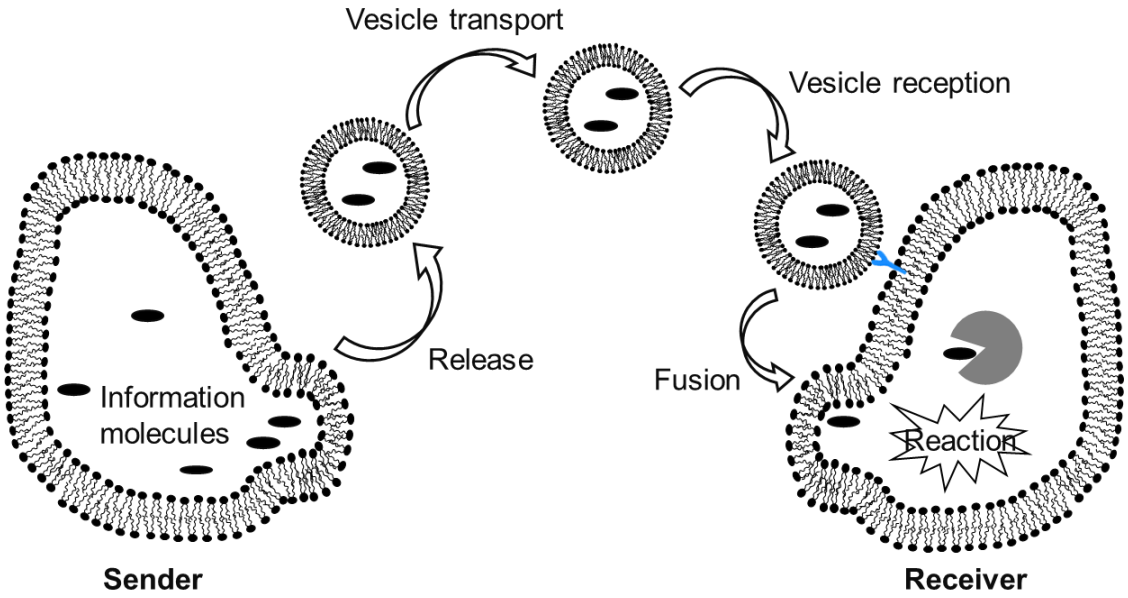

Figure 4-1. Molecular communication architecture that includes the key system components, i.e., senders, molecular communication interfaces, molecular propagation systems, and receivers.

Along these lines, our research group has been developing the components of a molecular communication system using artificial cell membranes.[3-8] The system is composed of the following sequential dynamic processes; (1) sending of information molecules capsule in lipid vesicles from a sender formed by artificial cell membrane through membrane division, (2) selective propagation of molecular information from the sender to a target receiver formed by artificial cell membrane, and (3) receiving of information molecules to the receiver through membrane fusion and followed decoding of molecular information. In order to establish the basic unit technologies for molecular communication, universal design for morphological control of artificial cell membranes including membrane division and fusion is essentially necessary. I believe that the

results of my work would make a great contribution to realize the molecular communication as a new information and communication technology in near future.

References

(1) Hiyama, S.; Moritani, Y. *Nano Communication Networks* **2010,** *1*, 20-30.

(2) Nakano, T.; Eckford, A. W.; Haraguchi, T. *Molecular Communication*, Cambridge University Press, New York, **2013**.

(3) Mukai, M.; Maruo, K.; Kikuchi, J.; Sasaki, Y.; Hiyama, S.; Moritani, Y.; Tsuda, T. *Supramol. Chem.* **2009**, *21*, 284-291.

(4) Wang, Z.; Yasuhara, K.; Ito, H.; Mukai, M.; Kikuchi, J. *Chem. Lett.* **2010**, *39*, 54-55.

(5) Sasaki, Y.; Shioyama, Y.; Tian, W.-J.; Kikuchi, J.; Hiyama, S.; Moritani, Y.; Tsuda, T. *Biotechnol. Bioeng.* **2010**, *105*, 37-43.

(6) Sasaki, Y.; Mukai, M.; Kawasaki, A.; Yasuhara, K.; Kikuchi, J. *Org. Biomol. Chem.* **2011**, *9*, 2397-2402.

(7) Yasuhara, K.; Wang, Z.-H.; Ishikawa, T.; Kikuchi, J.; Sasaki, Y.; Hiyama, S.; Moritani, Y.; Tsuda, T. *Supramol. Chem.* **2011**, *23*, 218-225.

(8) Mukai, M.; Maruo, K.; Sasaki, Y.; Kikuchi, J. *Chem. Eur. J.* **2012**, *18*, 3258-3263.

Acknowledgments

I deeply appreciate my supervisor, Prof. Jun-ichi Kikuchi, Graduate School of Materials Science, Nara Institute of Science and Technology, for his excellent supervision, versatile and helpful supports throughout this thesis. I am also thankful to Prof. Tsuyoshi Kawai, Prof. Kiyomi Kakiuchi, and Associate Prof. Takashi Matsuo, Graduate School of Materials Science, Nara Institute of Science and Technology, for their valuable comments and suggestions in many interesting points and perspectives, and great effort in completion of this thesis.

I am very grateful to Assistant Prof. Kazuma Yasuhara and Assistant Prof. Keishiro Tahara, Graduate School of Materials Science, Nara Institute of Science and Technology, for their useful suggestions and supports of my work.

Many thanks to Ms. Sakiko Fujita, Technician of Graduate School of Materials Science, Nara Institute of Science and Technology, for her great help and excellent skill in interpreting the cryogenic TEM and TEM tomography.

I am thankful to Ms. Yurika Fujita, Secretary of Prof. Kikuchi Research Group, for her supports in daily life.

I would like to convey many thanks to all the staff, including the former colleagues, of the Biomimetic Materials Science Laboratory for their help, cooperation and supports for my study.

Finally, I gratefully acknowledge my family and my friends for their supports, especially in hard time, they share all difficulties with me and help me to overcome them.

List of publications

Publications originated from this study were listed as follows.

1. **Synthetic Cell Division System: Roles of a Chemical Signal Which Induce Division of Lipid Bilayer Vesicles**

   Fei Hao, Kazuma Yasuhara, Qian Zhang, Xi-Ming Song, and Jun-ichi Kikuchi,

   Journal of the American Chemical Society, to be submitted.

2. **Synthetic Cell Division System: Effect of a Nonbilayer Forming Lipid on Division of Liposomal Membranes**

   Fei Hao, Keishiro Tahara, and Jun-ichi Kikuchi,

   Chemistry Letters, **2014,** *43*, 811-813.

Related works

1. **Fabrication of an Amino Acid Interlinked Redox Enzyme/gold Nanoparticle/Graphene Hybrid system for Electrochemical Biosensing**

   Qian Zhang, Fei Hao, Ling Zhang, Daliang Liu, Hui Mao, Francis Verproot, and Xi-Ming Song,

   Science of Advanced Materials, **2014,** *6*, 1068-1073.

2. **Fabrication of a Biocompatible and Conductive Platform Based on a Single-Stranded DNA/Graphene Nanocomposite for Direct Electrochemistry and Electrocatalysis**

   Qian Zhang, Yun Qiao, Fei Hao, Lin Zhang, Shuyao Wu, Ying Li, Jinghong Li, and Xi-Ming Song,

   Chemistry-A Eurpean Journal, **2010**, *16*, 8133-8139.